SITING WIND TURBINES TO MINIMIZE RAPTOR COLLISIONS AT SAND HILL REPOWERING PROJECT, ALTAMONT PASS WIND RESOURCE AREA

K. Shawn Smallwood and Lee Neher

10 August 2018

EXECUTIVE SUMMARY

Map-based collision hazard models were prepared as a set of tools to help guide the careful siting of proposed new wind turbines as part of the repowering effort at Sand Hill in the eastern Alameda County portion of the Altamont Pass Wind Resource Area (APWRA). Similar collision hazard models were prepared for the Tres Vaqueros and Vasco Winds repowering projects in Contra Costa County and for the Patterson Pass, Golden Hills, Golden Hills North, Summit Winds repowering projects in Alameda County, as well as for an earlier version of the Sand Hill repowering project. After three years of fatality monitoring following construction, it was found that the repowering of Vasco Winds reduced fatalities of raptors as well as all birds as a group. Our newest set of models for Sand Hill benefit from the lessons learned at Vasco Winds, as well as from many additional data collected through 2015 and the emergence of dependent variables and predictor variables that we believe result in superior collision hazard models. The new models were derived from an additional four years of fatality monitoring data, including monitoring with much shorter fatality search intervals at repowered, modern wind turbines as well as at some old-generation wind turbines. And like the models developed for Sand Hill and Golden Hills North, the golden eagle collision hazard model was partly derived from GPS/GSM telemetry data transmitted by golden eagles (*Aquila chrysaetos*) flying within the APWRA.

Our collision hazard model for golden eagle was derived from 121,259 GPS/GSM telemetry positions within the APWRA, from thousands of behavior records made during visual scans across many stations in the APWRA 2012 through 2015, and from fatality rates at monitored wind turbines from 1998 through 2015. Our collision hazard models for red-tailed hawk (*Buteo jamaicensis*) and American kestrel (*Falco sparverius*) were derived from thousands of behavior records and from estimates of fatality rates at wind turbines. Our collision hazard model for burrowing owl (*Athene cunicularia*) was derived from estimates of fatality rates at wind turbines and what we learned about the distribution of burrowing owls in the APWRA after 5 years of monitoring of nest and refuge burrows among 46 randomly located sampling plots.

Based on the data used to generate the models, our models performed very well at predicting increasing fatality rates with increasing hazard class. Our model predictions were usually, but not always, consistent with Smallwood's on-site assessments of collision hazard at each proposed wind turbine site. With short-distance relocations of some turbines, we believe that 24 of the proposed turbine sites will be relatively safe for raptors, so long as grading for turbine pads avoids leaving cut slopes or berms in the prevailing upwind direction from the turbines. We predict 14 of the proposed sites would be considerably more hazardous to raptors due to existing terrain conditions at those sites. If wind turbines in this project can be located well outside of ridge saddles, ravines, canyons and breaks in slope, and if grading for turbine pads can be minimized, then we predict fatality rates will lessen for golden eagles, red-tailed hawks, American kestrels, and burrowing owls relative to the same capacity of old-generation wind turbines being replaced. Given the airspace that will be opened up to safe flight traffic, we believe the golden eagle and red-tailed hawk fatality rates will lessen relative to the old turbines. American kestrel fatalities will likely lessen due to the elimination of the many small wind turbines that not only caused collision fatalities but also entrapped kestrels in hollow tubes of the lattice towers and within the turbine machinery. Burrowing owl fatalities also should lessen, but the high concentration of burrowing owls in the project area will mean that fatality reductions will not be as great at this project site as compared to other repowering projects in the APWRA. Based on our experience with the repowering of Buena Vista, Vasco Winds and Golden Hills, the fatality rates of bats might increase over those experienced at the old-generation wind turbines formerly operating at Sand Hill. In our micro-siting assessment and recommendations, we offer no assessment of macro-siting or project size.

INTRODUCTION

S-Power plans to install up to 33 wind turbines as part of its Sand Hill repowering project in the Alameda County portion of the Altamont Pass Wind Resource Area ("APWRA"), California. Careful siting of wind turbines is one of the principal measures available to minimize raptor fatalities caused by collisions with the turbines (Smallwood and Thelander 2004, Smallwood and Karas 2009, Smallwood and Neher 20010a,b, Smallwood et al. 2017). Project-level siting is referred to as macro-siting and within-project siting as micro-siting. The objective of micro-siting is to carefully site new wind turbines to minimize the frequencies at which raptors of various species encounter the wind turbines while flying, but most especially while performing specific types of flight behaviors, such as golden eagles chasing or fleeing other birds or flying low across ridge-like topographic features, or red-tailed hawks or American kestrels hovering or kiting in deflected updrafts. In this study we developed simple Fuzzy Logic (FL) models

(Tanaka 1997) of raptor activity quantified from behavior data collected across the APWRA between 13 November 2012 and 29 October 2015, and at behavior studies performed at Rooney Ranch and Sand Hill sites between 30 April 2012 and 5 March 2015 and Patterson Pass between 15 October 2013 and 24 September 2014. The behaviors used in the modeling effort were derived from the results of Smallwood et al. (2009b), and an example application of the FL modeling approach can be seen in Smallwood et al. (2009a, 2017).

The Fuzzy Logic approach is a rule-based system useful with noisy, zero-dominated data sets. It is often applied to events occurring within classes that are assumed to have graduated rather than sharp boundaries (Tanaka 1997). The rules consist of assigning likelihood values of an event occurring, which in the case of this study would be the likelihood of a bird performing a specific behavior within a cell of an analytical grid laid over the project area. Likelihood values can range 0 to 1 for each predictor variable, depending on how far a value of the predictor variable differs from the mean where the event has been recorded. The magnitude of each deviation from the mean is assessed by the analyst based on error levels, data distribution, and the analyst's knowledge of the system. In our case, the events were of birds flying over terrain characterized by suites of slope conditions, or of fatalities at wind turbines associated with specific slope conditions.

Our study goal was to accurately predict the locations where golden eagles, red-tailed hawks, American kestrels and burrowing owls are most likely to perform flight behaviors putting these species at greater risk of collision with wind turbines, so that new wind turbines can be sited to avoid these locations to the degree reasonably feasible. Achieving this goal depended on our understanding of how these species use terrain and wind, and how they perceive and react to wind turbines. It also depended on understanding patterns of fatality rates in the APWRA, so we also developed fatality rate models for golden eagle, red-tailed hawk, American kestrel, and burrowing owl. Our model results were interpreted in tandem with Smallwood's familiarity with conditions associated with proposed wind turbine locations. By carefully siting the wind turbines to minimize collision risk, the Sand Hill project should prove safer to raptors than the wind turbines being replaced, so long as grading for turbine pads avoids leaving cut slopes or berms in the prevailing wind direction from the turbines. The Sand Hill micro-siting also benefits from what was learned at the Vasco Winds repowering project, which was micro-sited using a similar approach and monitored for collision fatalities for three years (Brown et al. 2013, 2014, 2016). Additional experience was gained at the post-repowered Golden Hills, Buena Vista, and Diablo Winds projects.

Our map-based models are intended to help guide micro-siting; they do not bear on macro-siting. The models are only as predictive as our understanding of wind turbine collisions and our ability to measure terrain features bearing on collision risk. Although research and monitoring efforts in the APWRA have set the pace worldwide (Orloff and Flannery 1992, Smallwood and Thelander 2008, Smallwood et al. 2009b,c, Brown et al. 2016, ICF International 2016, Smallwood 2016a,b, 2017a,b, Smallwood and Neher 2017a), there remains considerable uncertainty over collision mechanisms. Certain behavior patterns correlate with collision fatality rates (Smallwood et al. 2009b, 2016a,b), but correlations are often confounded by the unmeasured, unobserved factors. And whereas we know that collision risk is influenced by interactions between landscape and wind, wind turbine micro-siting cannot be guided by anything more detailed than measurable

terrain features and prevailing wind directions. Assuming that the prevailing wind directions are primarily from the southwest and secondarily from the northwest, and assuming that the avian behavior and fatality data reflect these prevailing wind directions, we weighted terrain features for collision risk based on whether wind turbines would be sited on or atop these features. However, when the wind shifts directions to the northeast or from the southeast, as examples, then the birds shift their activity patterns and collision risks also change. There is no way for us to micro-site wind turbines to minimize risk posed by all wind directions.

As another example of the limitations of our models, we examined the locations of golden eagle model prediction failures – sites of existing or past wind turbine sites where collision risk was predicted lowest but where fatality rates were relatively high. A pattern that quickly emerged from these sites was their occurrence on steeply declining ridge features, which is a terrain condition that we have not measured and could not incorporate into a model. We measured slope (elevation change relative to distance change) within analytical grid cells and across entire slope faces from valley bottom to ridge crest, but we did not measure slope along ridge features because this measurement did not occur to us until examining the model prediction failures. Of course, any remaining model prediction failures would likely lead us to additional as-yet-unmeasured terrain features. Our models express our current understanding and ability to measure collision factors, and should be interpreted in combination with expert opinion.

Assumptions and limitations aside, we feel that this iteration of collision hazard models in the APWRA qualifies as our best and most predictive, especially after revising our burrowing owl fatality model (reported herein). It is important to remember that the models are most effectively used as foils against expert judgement. It is also important to remember that all wind turbine locations pose collision risk to volant wildlife. Our aim is to avoid terrain settings that pose disproportionately greater collision risk to four focal species, including golden eagle, red-tailed hawk, American kestrel and burrowing owl. Attempting to optimize micro-siting to minimize impacts to these focal species could increase the risk for other bird species (Smallwood and Neher 2017b), and possibly for bats. It is also important to understand that our modeling approach is based on the assumption that wind turbines would not be installed on relatively low-lying terrain. Past research in the APWRA revealed terrain features, including low-lying areas, as more hazardous to raptors. General micro-siting guidelines were generated (Alameda County SRC 2007, 2010, Smallwood and Estep 2010), validated (Smallwood 2010a,b) and later incorporated into Alameda County's Programmatic Environmental Impact Report prepared for wind energy repowering. Our models will often predict low collision risk in low-lying areas only because we targeted our models to the higher terrain typically sought by wind companies in the APWRA.

In most cases we recommend siting the new wind turbines as far as reasonably feasible from hazard classes 3 and 4, but we also recommend considering expert input on micro-siting to account for factors not considered in the models. As a general rule, we recommend not siting wind turbines in relatively low terrain, or in ridge saddles, breaks in slope or on terrain located east (prevailing downwind) of major ridge saddles or breaks in slope. Herein are recommended changes to the initial wind turbine layout based on model predictions, expert judgment applied to on-site inspections, and fatality histories accumulated from fatality monitoring at old-generation wind turbines nearest the proposed installation sites. Two caveats are necessary for the Sand Hill

portion of the project. One is that burrowing owls in the APWRA have been most numerous on the Sand Hill area, and fatality rates have been high there. Any wind turbines installed at Sand Hill will carry considerable collision risk for burrowing owls regardless of micro-siting efforts. Second, the layout extended into an area we previously did not regard as part of the APWRA, and therefore we had not prepared terrain measurements or model extensions into that area. To assess collision risk of wind turbines proposed outside our modeling area, we relied solely on the expert judgement of Smallwood upon his site visits.

We further note that we had prepared collision hazard models for a previously planned, but abandoned, repowering project at Sand Hill (Smallwood and Neher 2016). That project was planned by a different company than the project considered herein.

METHODS

On-site Assessments

One of us (Smallwood) visited the proposed repowering project area to assess the collision hazard associated with proposed wind turbine sites. Smallwood visited the sites proposed in the initial layout in December 2017. He rated collision hazard on a scale of 0 to 10 using criteria adopted by the Alameda County Scientific Review Committee in 2007/2008 and 2010 (Alameda County SRC 2007, 2010), but modified in two ways. One modification was not lumping all ratings less than 7 into the same hazard level. Another was not considering turbine operability, which varied greatly among old-generation turbines but not among proposed wind turbine sites.

Predictive Models

Multiple types of data were needed to develop collision hazard models. For developing collision hazard models of golden eagle, red-tailed hawk, and American kestrel, flight behavior data were collected and then related to terrain. For golden eagles, we also made use of GPS/GSM telemetry data collected from 18 golden eagles fitted with transmitters and flying over portions of the Altamont Pass Wind Resource Area (Bell and Nowell 2015, Smallwood et al. 2017a). For all four raptor species, we estimated fatality rates among individual wind turbines monitored throughout the APWRA and over various time periods since 1998. And of course the terrain needed to be measured, and this was done using imagery, digital elevation models, and geoprocessing steps to bring objectivity to decisions about where a slope transitions from trending towards concavity to trending towards convexity, as an example. All of these data and the steps used to integrate them are covered in the following paragraphs. We begin with the biological survey data before describing the development of our digital elevation model (DEM) and terrain measurements, but we present the methods used for processing the GPS/GSM telemetry data until after the section on terrain measurements because we relied on our terrain measurements to screen the telemetry data for inclusion in the analysis.

Behavior data

Culminating 14 years of behavior surveys and utilization surveys in the APWRA (Smallwood et al. 2004, 2005, 2009b,c; Smallwood 2013), a new methodology was developed for behavior

monitoring to benefit the development of wind turbine collision hazard models (Smallwood 2016a,b). The earlier behavior surveys recorded avian behaviors that were unmapped (Smallwood and Thelander 2004, 2005; Smallwood et al. 2009b), so no spatial analysis was possible. The mapping of bird locations emerged in 2002 and continued through 2007 (Smallwood and Thelander 2005, Smallwood et al. 2009c) and 2011 (ICF International 2011), but the 2002 approach was integrated with utilization surveys that were focused primarily on counting birds to estimate relative abundance. For most observers this mixing of objectives impinged on both objectives – on both the counting of birds and the mapping of their behavior patterns. On-the-minute mapping of bird locations and behaviors yielded only crude spatial patterns for only a few site-repetitive behaviors such as perching, kiting and hovering. After comparing use rates to fatality rates and seeing no significant spatial or inter-annual relationships between the two rates, it was decided to focus more on the behavior patterns to predict collision hazards. New methods were formulated to map flight behaviors.

We gathered behavior data from 15 observation stations at Sand Hill, 9 stations in Patterson Pass, and 36 stations across the rest of the APWRA, the latter of which were funded by NextEra as mitigation for the Vasco Winds repowering project (Figure 1). Of the 36 stations funded by NextEra as mitigation, 21 were selected from those that had been ranked from 1st through 30th in order of the number of first observations per hour per km^3 of visible airspace out to the maximum survey radius at each station during use surveys performed by the Alameda County Avian Monitor from 2005 through 2009. To these 21 stations we added another 15 to Vasco Caves Regional Preserve, Northern Territories, Vasco Winds Energy Project, and the Buena Vista Wind Energy Project in Contra Costa County, where the Alameda County Avian Monitor had little coverage. The 15 stations at Sand Hill were optimized to observe how golden eagles and other raptors behave in the airspace around Ogin's before-after, control-impact (BACI) experimental treatment plots designed to test the avian safety of a new wind turbine model that was ultimately not installed.

Behavior sessions at Sand Hill lasted 30 minutes each, and elsewhere they lasted 1 hour each, including on some stations located on Sand Hill. Between 30 April 2012 and 5 March 2015 there were 2,002 surveys completed for 1,001 hours (126,084 birds tracked). The maximum survey radius depended on the printed map image extent and how far the observer felt comfortable estimating the bird's spatial location and height above ground. Map extents rarely permitted survey distances of >300 m. One of us (Smallwood) recorded all of the behavior data within Patterson Pass, and additional behavior data were collected at NextEra mitigation sites by Smallwood, Erika Walther, Elizabeth Leyvas, Skye Standish, Brian Karas, and Harvey Wilson.

The 9 Patterson Pass stations were surveyed 167 times (167 hours) from 15 October 2013 to 24 September 2014 (5,712 birds tracked). The 36 NextEra mitigation stations were surveyed 928 times (928 hours) from 13 November 2012 through 29 October 2015 (27,552 birds tracked). Between all three studies, 2,096 hours of behavior surveys (159,348 birds tracked) provided the data used for developing collision hazard models reported herein.

Each bird was recorded onto image-based maps of the survey area as point features connected by vector lines depicting the bird's flight path (Figures 2-5). Height above ground, behavior, and time into the session was recorded into Tascam digital voice recorders fitted with windjammers

designed to reduce noise buffeting by high winds. Point features were recorded as often as the observer could record attribute data into the voice recorder. One objective of the behavior sessions was to obtain high quality flight paths and summaries of flight behaviors of individual birds using the surveyed airspace, and it was notably not to count birds, although it was likely that just as many raptors were recorded as would have been counted based on the use survey protocols.

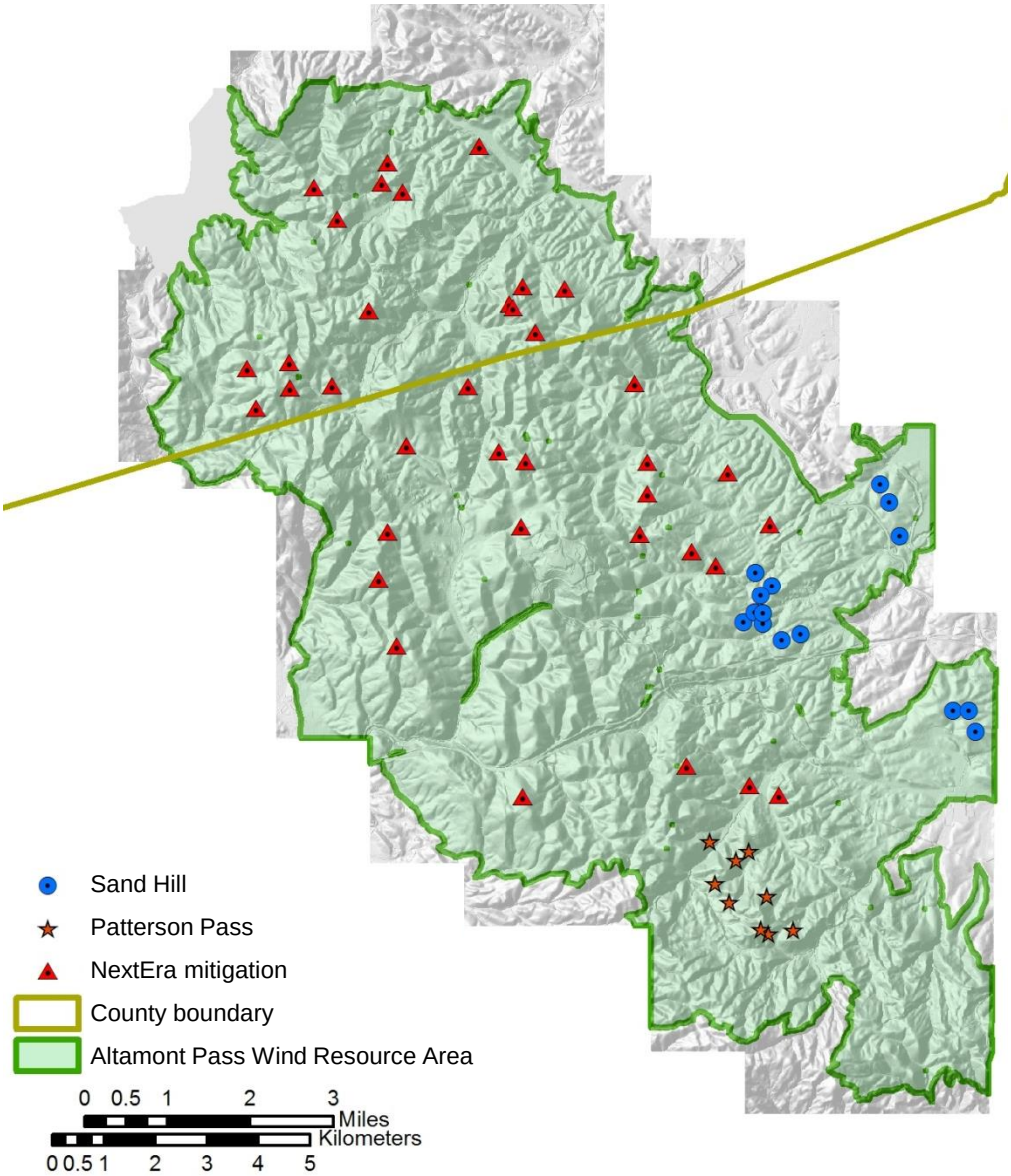

Figure 1. *Locations of behavior observation stations used for 30 min and 60 min visual scans to track individual birds and record behaviors and flight heights along the way*.

Another objective of the behavior surveys was to learn how birds interact with wind turbines when they approached the wind turbines. Special attention was given to the bird's flight whenever it flew within 50 m of a wind turbine and, in the opinion of the observer, faced the possibility of colliding with the wind turbine. During this time, the bird's approach angle to the

turbine was recorded, as well as any changes in flight direction, flight height, behavior, interactions with other birds, and the wind turbine's operating status. Whenever special attention was directed to such flights, the flight observation was termed an "event," or a wind turbine interaction event.

At the start of each behavior session, the observer identified which wind turbines in the survey area were operating, as well as temperature, wind direction, average and maximum wind speed, and percentage cloud cover. Behavior data were transcribed to electronic spreadsheets within 24 hours of collection. Mapped bird location points and line features representing the bird's flight path were then digitized into the GIS.

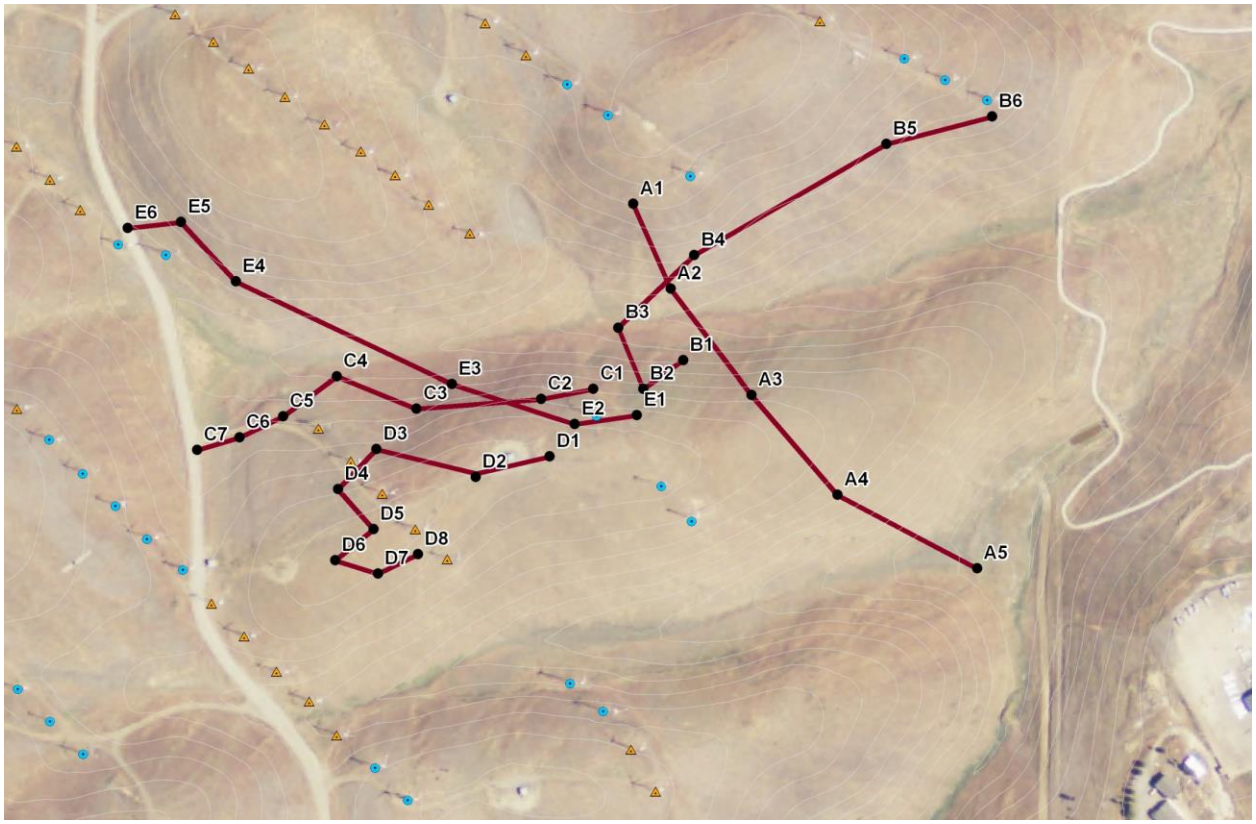

Figure 2. *Example of how birds were tracked visually during behavior surveys. Flight attributes were recorded at points, which were later connected by line segments representing a flight path. In this case 5 flight paths were recorded, A through E, and at each number associated with a point we also recorded behavior, height above ground, social group size and, when appropriate, wind turbine events. For example, D4 would likely have involved a wind turbine event.*

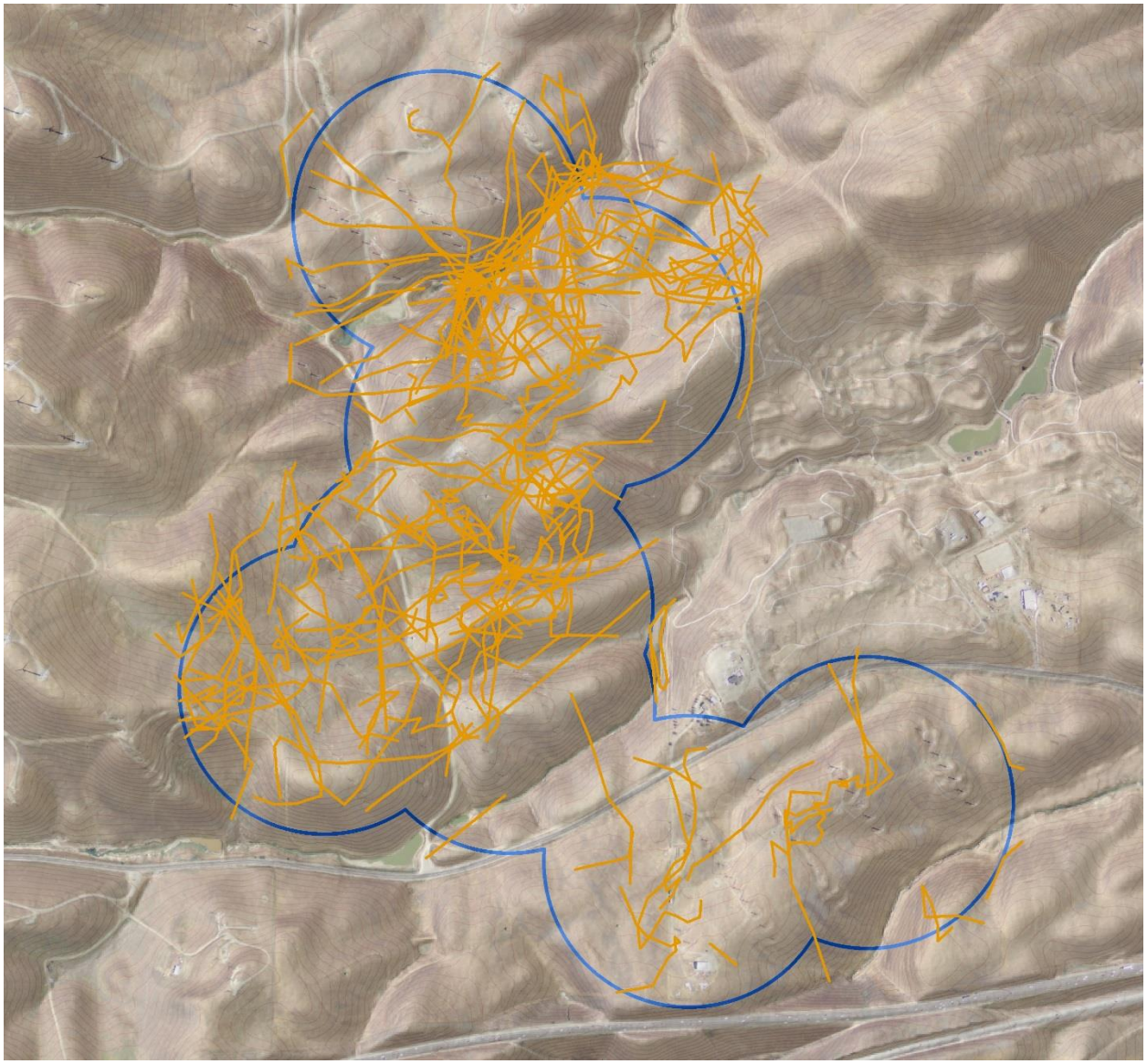

Figure 3. *Golden eagle flight paths recorded during 3 years of visual scans for behavior patterns within a portion of the Sand Hill project area, 2012-2015*.

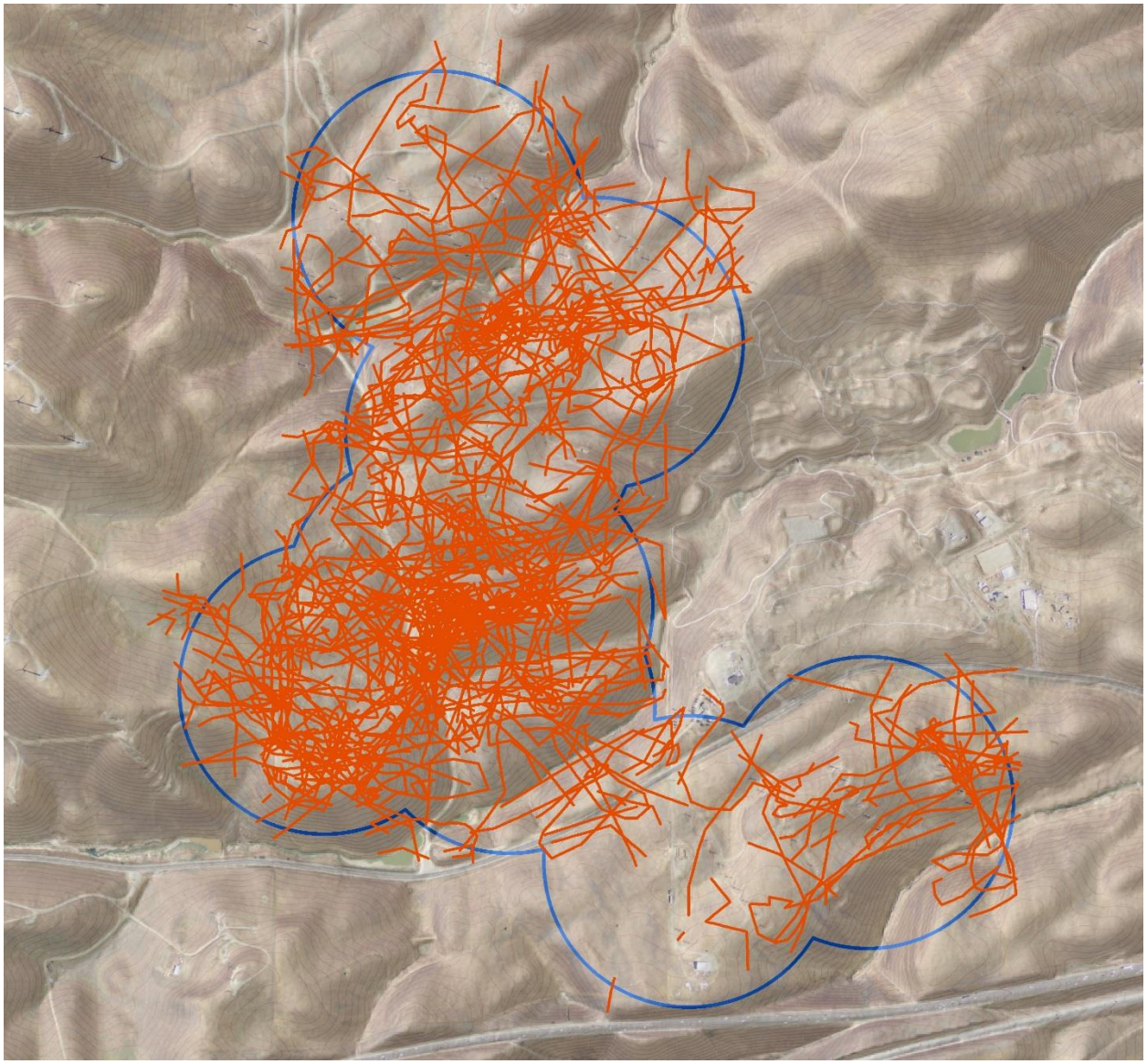

Figure 4. *Red-tailed hawk flight paths recorded during 3 years of visual scans for behavior patterns within a portion of the Sand Hill project area, 2012-2015.*

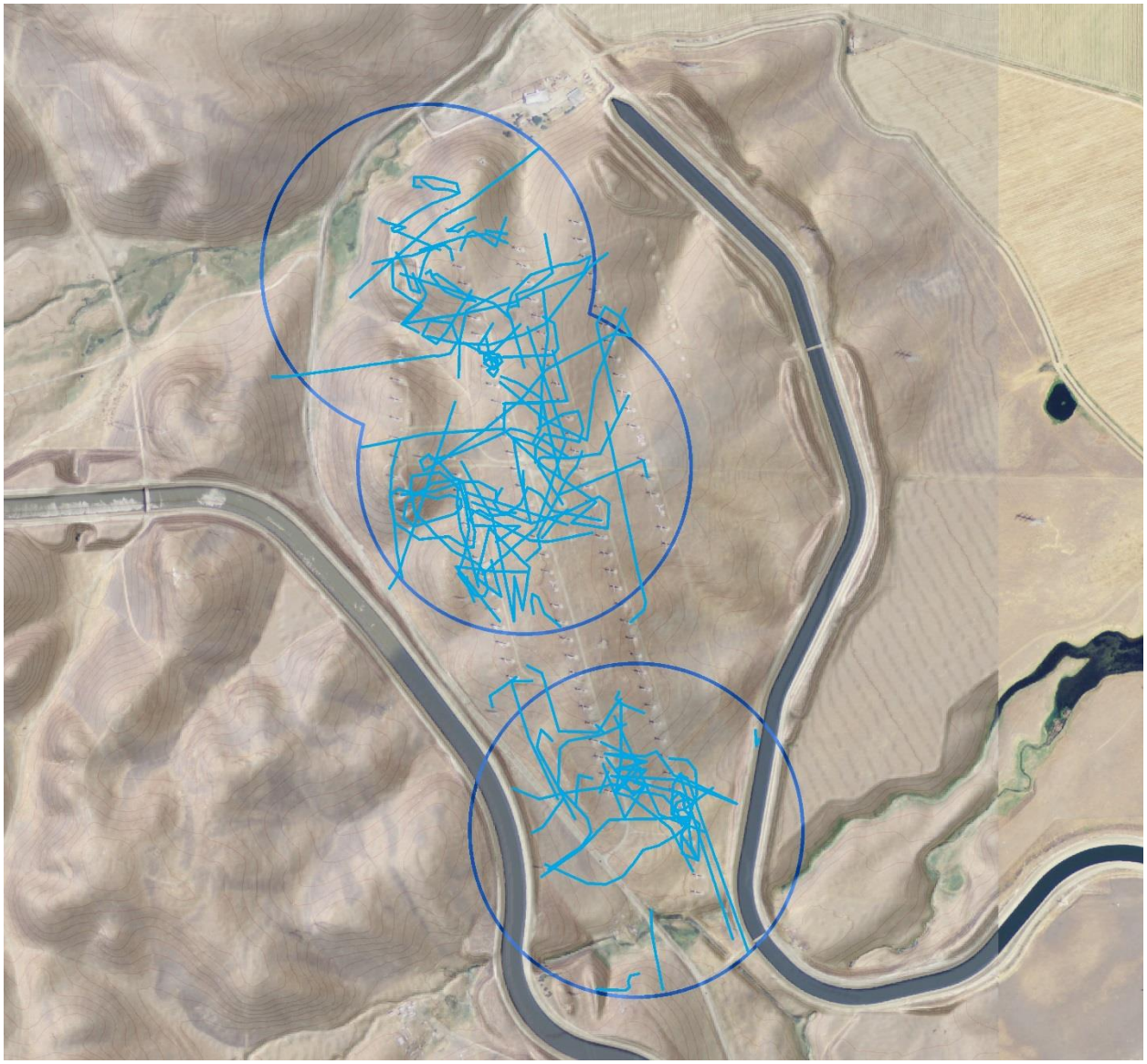

Figure 5. *American kestrel flight paths recorded during 3 years of visual scans for behavior patterns within a portion of the Sand Hill project area, 2012-2015.*

Burrowing owl burrows

Burrowing owl burrows (Figure 6) were mapped in sampling plots throughout the APWRA using a Trimble GeoXT GPS, both during the nesting season (Smallwood et al. 2013) and throughout the year in 2011 (Figure 7). Additional burrow mapping efforts were made in follow-up visits during breeding seasons of 2012-2015. Most of the burrows that were mapped were nest burrows, but refuge burrows were also included in the data pool. No satellite burrows (alternate nest burrows) were used in the analysis because satellite burrows are merely nearby extensions of nest burrows. The burrow location data were used to develop a predictive model of burrowing owl burrow sites, but for the micro-siting effort herein we discontinued using this model for anything other than gaining a better understanding of how burrowing owls distribute themselves across the APWRA.

Figure 6*. Example of a burrowing owl nest burrow, including an adult (top) and chicks.*

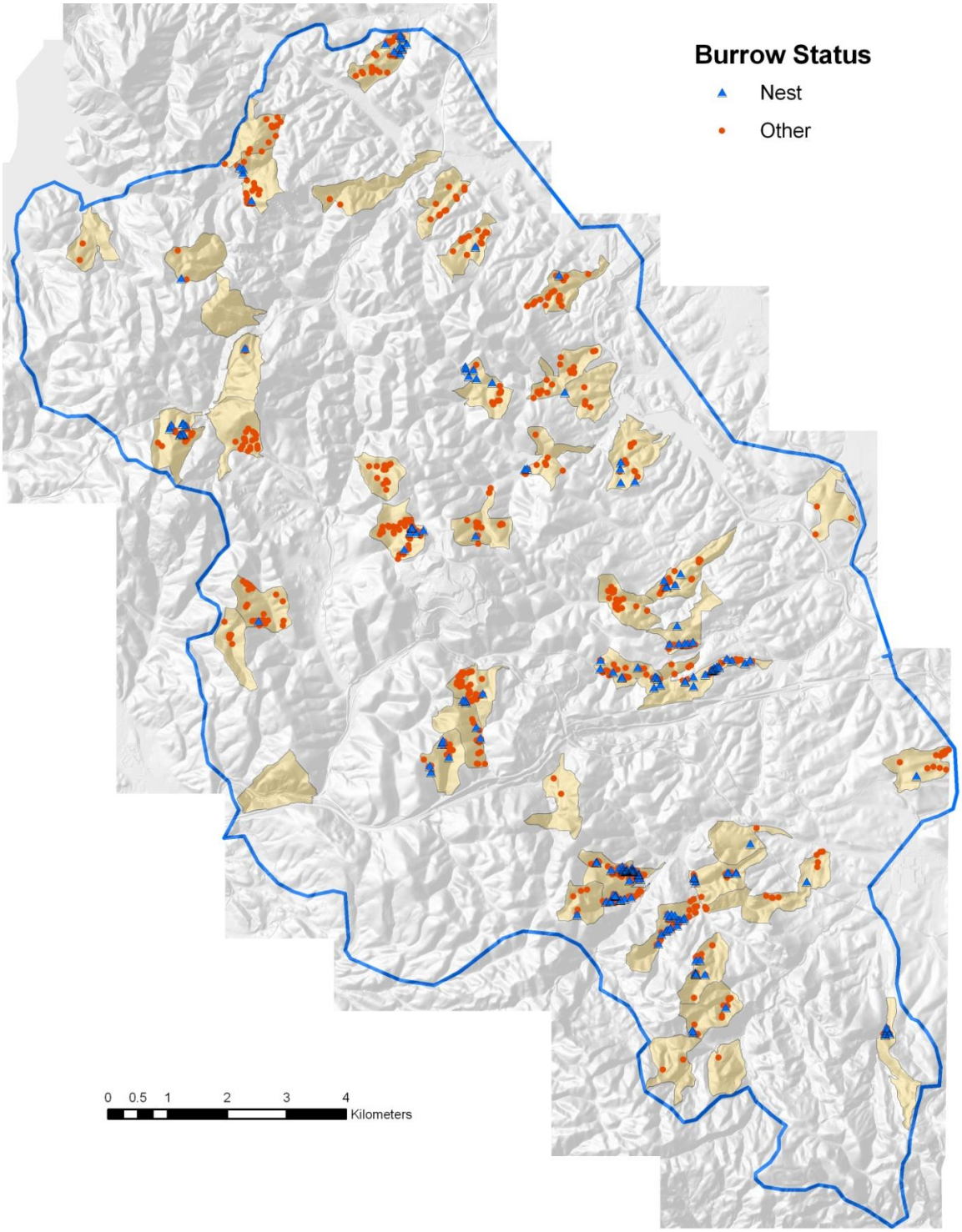

Figure 7. *Burrowing owl sampling plots (tan color) and 2011 nest and refuge burrow locations (as examples) within the Altamont Pass Wind Resource Area (blue polygon).*

Fatality rates

We estimated annual fatality rates at all old generation wind turbines that were searched at least one year between the years 1998 through 2011 in the APWRA. We also estimated annual fatality rates at modern wind turbines monitored 2012-2015 in the Vasco Winds project (Brown et al. 2016), 2008-2011 in the Buena Vista project (Insignia Environmental 2011), and 2005-2010 in the Diablo Winds project (ICF International 2016). All fatality rates at old-generation turbines were adjusted for search detection and carcass persistence rates that were averaged among wind projects where trials were performed in similar grassland environments as compared to the APWRA (see Smallwood 2013). Fatality rates were also adjusted for variation in the maximum search radius around wind turbines (Smallwood 2013). Finally, we adjusted fatality rates for monitoring duration to account for a potential bias warned about in Smallwood and Thelander (2004:App. A). This bias is actually two biases in one, and it applies more to comparing fatality rates among individual wind turbines than it does to wind projects. The adjustments are shown in Figure 8.

Going to the first portion of the bias, as the number of fatalities is averaged into more years of survey effort, the resulting ratio of fatalities to years will decrease inversely with increasing number of years at turbines where fatalities were found. This decrease is caused simply by a relatively constant numerator (number of fatalities) being divided by a constantly changing denominator (years). If an eagle fatality is found at a wind turbine monitored over one year, the fatality rate would be 1 eagle death per year, but if this turbine is monitored over 10 years and no more eagle fatalities are found, then the fatality rate would be 0.1 eagle deaths per year. At a wind turbine monitored over 10 years, the measured rate should be regarded as reasonably reliable. But a fatality rate of 1 eagle per year measured at a wind turbine monitored only over 1 year should be regard as much less reliable because it remains unknown whether additional eagle fatalities would be found at that turbine had it been monitored over more years. Monitored over 10 years, this turbine might yield a fatality rate of 1 or more eagle deaths per year or only 0.1 eagle deaths per year, an uncertainty range of 10-fold or greater.

Going to the second portion of the bias, some fatality rates will represent false zeros where wind turbines were monitored for only one or a few years and no fatalities were found. Assuming a golden eagle fatality rate of 0.1 deaths per MW per year and assuming for this example that fatality risk is equal among 100-KW wind turbines in a project area, then the monitoring duration sufficient to register a single golden eagle fatality at the average wind turbine would be 100 years. A reasonable assumption would be that false zeroes are common for golden eagle fatality rate estimates in the APWRA. This bias, or both biases together, was partially corrected by fitting an inverse function to the data, and then multiplying the ratio of observed to predicted values by the predicted value at 10 years of monitoring (Figure 8). In other words, all fatality rates at individual wind turbines were adjusted to a common 10-year period of monitoring, even if they had been monitored only one year, 4 years, or 10 years, etc. (We note that the fatality rate metric in this case excluded the turbine's rated capacity, MW.) Our adjustment reduces the magnitude of mathematical artefact caused by high fatality rates at wind turbines monitored briefly, but it does not adjust for false zeroes at wind turbines monitored briefly.

Fatality rates adjusted for duration of monitoring were related to terrain measurements and terrain features to identify associations useful for developing predictive collision hazard models. The terrain features and terrain measurements used were those associated with the wind turbines where fatality rates had been recorded (Figure 9).

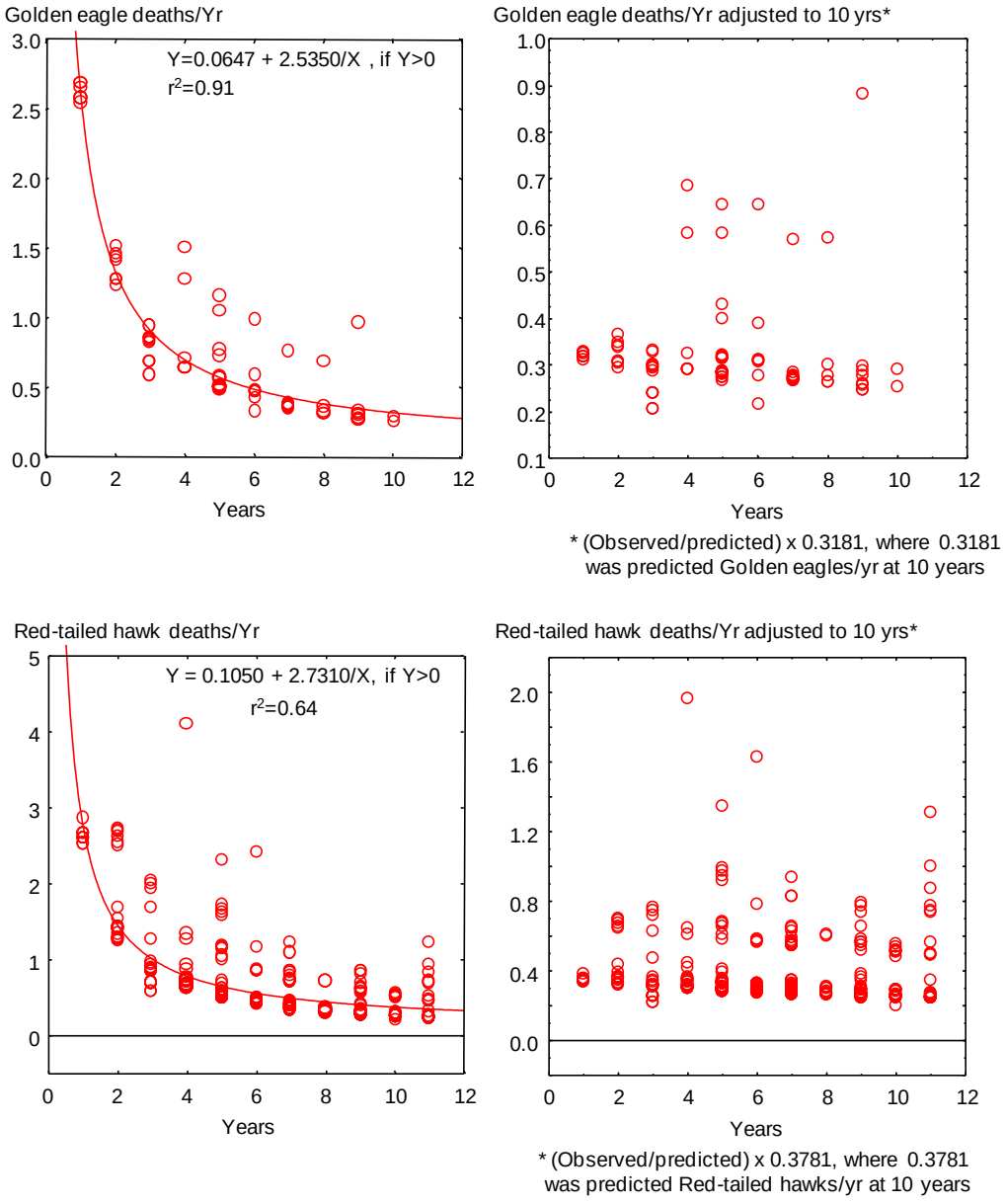

Figure 8a. *Mean annual fatalities/year at turbines where fatalities were found declined inversely with the number of years used in the denominator for golden eagle and red-tailed hawk (left graphs), so fitting inverse functions to the data removed the effect of number of years on the metric (right graphs).*

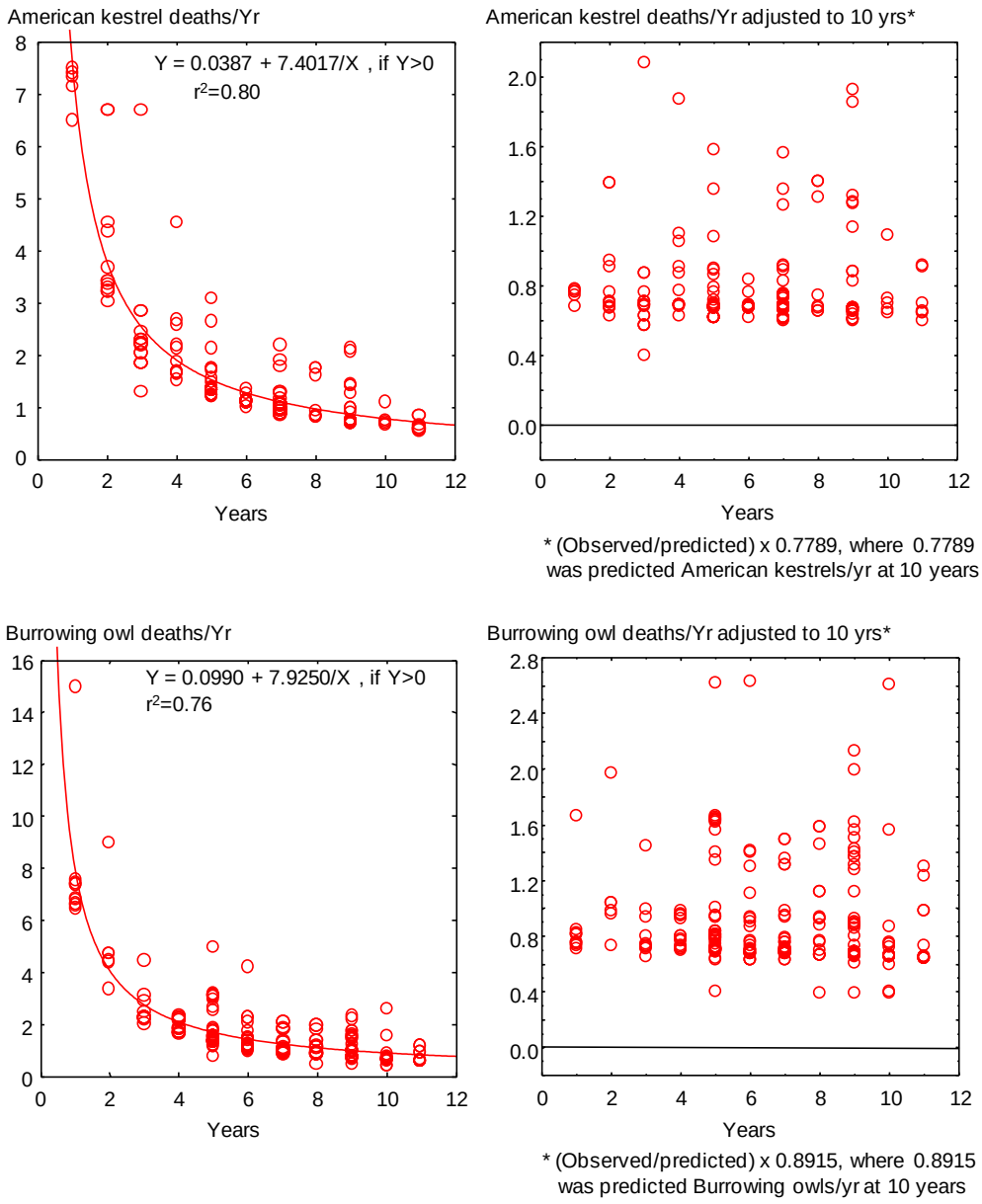

Figure 8b. *Mean annual fatalities/year at turbines where fatalities were found declined inversely with the number of years used in the denominator for American kestrel and burrowing owl (left graphs), so fitting inverse functions to the data removed the effect of number of years on the metric (right graphs).*

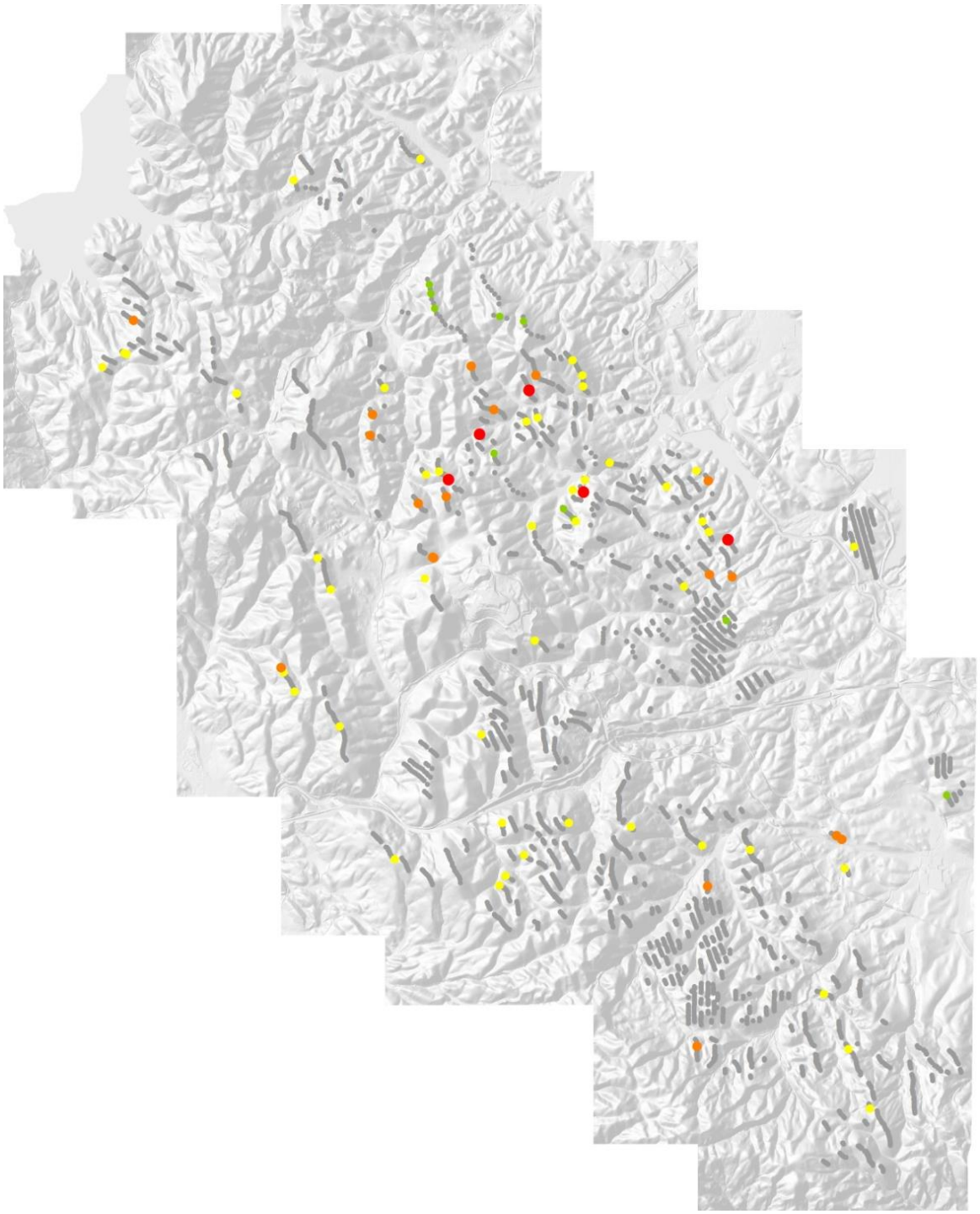

Figure 9. *Golden eagle fatality rates at Altamont Pass wind turbines, 1998 through 2010, adjusted for the duration of monitoring where gray circles represent monitored wind turbines where eagle fatalities were not found and colored circles represent adjusted fatality rates from lowest (yellow) to highest (red).*

Digital Elevation Model

Two separate digital elevation model (DEM) grids were utilized for this project. The geoprocessing tasks were performed using a 10 foot cell size DEM created by combining DEMs obtained from Contra Costa and Alameda Counties. These data sets were produced using LIDAR data and ARC TIN software by Mapcon Mapping Inc. during 2007-2008. The border of the APWRA was used as a mask to produce the APWRA DEM composed of 25,440,000 10x10-foot cells. This DEM was then converted to a cell centroid point feature class and each point assigned a unique membership number.

All derived parameters were calculated for the entire APWRA DEM and attributed into the cell centroid point feature class. An aggregated 792-m buffer served as our mask (limit) for analyzing previously collected bird data against the DEM parameters. The 792-m radius was converted to a 2,600 foot radius and an additional 200 feet was added to buffer modeling data for geoprocessing and to ensure that all bird observations would be covered.

The statistical analyses within the APWRA were limited (masked) to data within the areas searched for raptors within the behavior study areas, for burrowing owl burrows within the burrowing owl sampling plots, and for fatality rates among the wind turbines that were monitored at least one year (and the grid cells on which the turbines were located). The resulting analytical grids within the behavior survey areas were composed of a 7,548,578 (30%) subset of the 10x10-foot centroid point feature class serving as the study area for the behavior surveys, and a 393,555 subset serving as the study area for the behavior surveys restricted to 10-m buffered ridge-like features. These analytical grids were used to develop and test predictive models.

The same geoprocessing steps were used to characterize terrain attributes as reported in Smallwood and Neher (2010a,b) and in Smallwood et al. (2017). We used the Curvature function in the Spatial Analysis extension of ArcGIS 10.2 to calculate the curvature of a surface at each cell centroid. A positive curvature indicated the cell surface was upwardly convex, a negative curvature indicated the cell surface was upwardly concave, and zero indicated the cell surface was flat. Curvature data (-51 to 38) were classified using Natural Breaks (Jenks) with 3 classes of curvature – convex, concave and mid-range. Break values were visually adjusted to minimize the size of the mid-range class. A series of geoprocessing steps was used, called 'expand,' 'shrink,' and 'region group,' as well as 'majority filter tools' to enhance the primary slope curvature trend of a location. The result was a surface almost exclusively defined as either convex or concave (expressed as 1 or 0, respectively, for the variable *Curve*, and 2 and 1 respectively, for the variable *RidgeValley*, which will appear in the models below). Convex surface areas consisted primarily of ridge crests and peaks, hereafter referred to as ridges, and concave surface areas consisted primarily of valleys, ravines, ridge saddles and basins, hereafter referred to as valleys.

Line features representing the estimated average centers of ridge crests and valley bottoms were derived from the following steps. ESRI's Flow direction function was used to create a flow direction from each cell to its steepest down-slope neighbor, and then the Flow accumulation function was used to create a grid of accumulated flow through each cell by accumulating the weight of all cells flowing into each down-slope cell. A valley started where 50 upslope cells

had contributed to it in the Flow accumulation function, and a ridge started where 55 cells contributed to it. We applied flow direction and flow accumulation functions to ridges by multiplying the DEM by -2 to reverse the flow. Line features representing ridges and valley bottoms were derived from ESRI's gridline and thin functions, which feed a line through the centers of the cells composing the valley or ridge. Thinning put the line through the centers of groups of cells ≥40 in the case of valleys. Lines representing ridges and valleys were also clipped to identify the major valleys and major ridges, or the topographic features dominating the local skyline and local drainage systems (Figure 10).

We used the two-foot slope analysis grid to create polygons with relatively gentle slope. We used a Standard Deviation classification to identify areas with < 7.4 % slope. These areas were then converted to polygons and intersected with the ridge/valley lines to determine polygons associated with either ridge or valley descriptions. The borders of these polygons were converted to lines and combined with the ridge/valley line datasets, respectively, and polygons in valley features were termed *valley polygons* and polygons on ridge tops were termed *ridge polygons*.

Horizontal distances (m) were then measured between each DEM grid cell and the nearest valley bottom boundary (in the valley line combined data set) and the nearest ridge top boundary or ridgeline (in the ridgeline combined data set), referred to as *distance to valley* and *distance to ridge*, respectively. These distances were measured from the DEM grid cell to the closest grid cell of a valley bottom or ridgeline, respectively, not including vertical differences in position. The *total slope distance* was the sum of *distance to valley* and *distance to ridge*, and expressed the size of the slope. The DEM grid cell's position in the slope was also expressed as the ratio of *distance to valley* and *distance to ridge*, referred to as the *distance ratio*. This expression of the grid cell's position on the slope removed the size of the slope as a factor. The same measurements were made to major valleys and major ridges.

The vertical differences between each DEM grid cell and the nearest valley bottom boundary and nearest ridge top boundary or ridgeline were referred to as *elevation difference*, and this measure also expressed the size of the slope. In addition to the trend in slope grade at each DEM grid cell, the *gross slope* was measured as the ratio of *elevation difference* and *total slope distance*. The DEM grid cell's position on the slope was also expressed as the ratio of the elevation differences between the grid cell and the nearest valley and between the grid cell and the nearest ridge, referred to as *elevation ratio*. Additionally, the grid cell's position on the slope was measured as the average of the percentage distance and the percentage elevation to the ridge top. This mean percentage was named *percent up slope*, and provided a more robust expression of the grid cell's position on the slope (Figure 11). The same measurements were made to major valleys and major ridges, leading to the variable we named *percent up major terrain slope*. Thus, on a small hill adjacent to a major hill in the area, a grid cell could be 90% under *percent up slope* and only 30% under *percent up major terrain slope*.

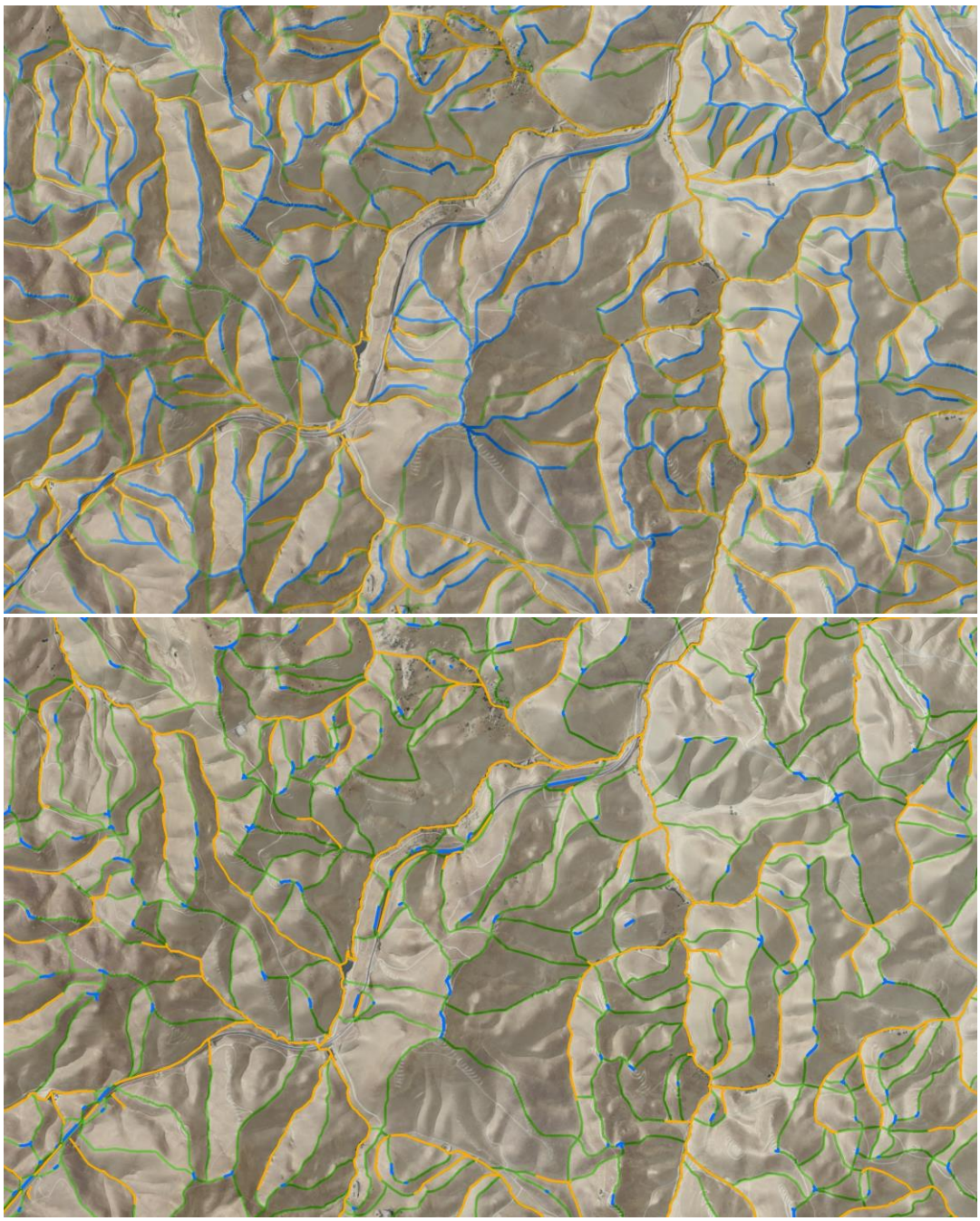

Figure 10. *Valley bottoms (gold) and ridge crests (blue) for all terrain (top) and major terrain (bottom) features*.

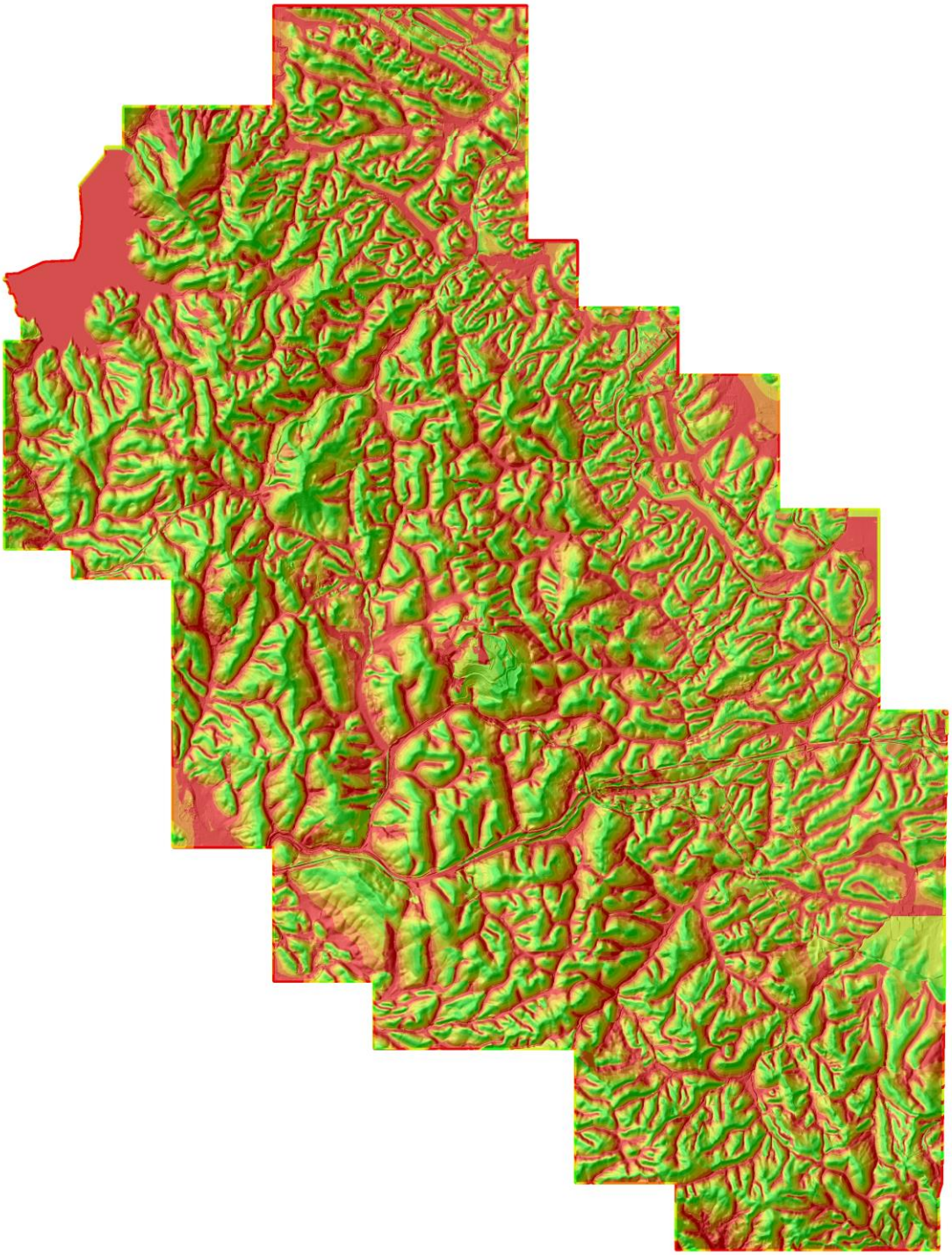

Figure 11. *Percent up slope across the Altamont Pass Wind Resource Area was derived from multiple terrain measurements to express a grid cell's position on the slope regardless of the size of the slope, where red was at the valley bottoms and dark green at the ridge crests*.

Percent up slope did not distinguish a grid cell's position between slopes on large hills versus medium or small-sized hills, so the local topographic influence of the feature where each cell was located was expressed by the variable *hill size*, which was the elevation difference between the nearest valley bottom polygon and nearest prominent ridge top polygon. *Major hill size* was the elevation difference between the nearest major valley bottom and nearest major ridge top.

Breaks in slope were characterized with the ratio of *slope to gross slope*, and the ratio *gross slope to major gross slope* was also calculated. Additional ratios included *local to major hill size*, *local to major ridge elevation*, and *local to major valley elevation*.

Each DEM grid cell was classified by *aspect* according to whether it faced north, northeast, east, southeast, south, southwest, west, northwest, or if it was on flat terrain. Each grid cell was also categorized as to whether its center on the landscape was windward, leeward or perpendicular to the prevailing southwest and northwest wind directions as recorded during the behavior observation sessions.

The study area was divided into smaller polygons of land with like aspect, creating a predictor variable termed *Subwatershed Orientation*. Existing sub-watershed polygons already had been created between ridgelines and valley bottom lines. These watershed polygons were further divided by reviewing the existing 2-foot hypsography (contour) data and then dividing them into orientation polygons where the overall orientation of the contours changed. An orientation line feature layer was digitized with a line for each new polygon following the best observed orientation of that polygon's contours. Python scripts attributed the new line with its compass orientation, e.g., N, NNE, NE. These lines were non-directional, so a compass value could be either the returned value or the direction 180 degrees opposite. These same scripts calculated a perpendicular compass direction to the returned orientation line direction. The perpendicular orientation direction had two possible values, differing by 180 degrees based on which side of the ridge the line described. A reference point within each orientation polygon was georeferenced by scripts to a generalized aspect grid of the study area. The scripts determined the correct perpendicular orientation and calculated the compass direction of the orientation polygon.

Using similar steps, a predictor variable termed *Ridge Orientation* was created. Ridgelines were buffered by 10 feet and the resulting ridgeline polygons classified by orientation: north to south, north-northwest to south-southeast, northwest to southeast, west-northwest to east-southeast, west to east, west-southwest to east-northeast, southwest to northeast, and south-southwest to north-northeast. Flight paths crossing ridgelines were related to these Ridge Orientation polygons in use and availability analysis.

We represented *ridgeline slope* as the difference between maximum and minimum elevation of grid cells within buffered ridgelines (as above) divided by the total length of the ridgeline polygon. We were hoping to characterize the slope of individual ridge features, but our ridgeline polygons often spanned multiple ridge features, often from one side of a hill across the top to the other side. Whereas we obtained a crude representation of change in elevation along ridge features, we did not measure the slope of individual ridge features.

We also derived a variable named *ridge context*, which was categorized ridge features by their elevation difference and distance from *major ridges* (see Figure 10). We subtracted the elevation of local ridges from the elevation of major ridges and we plotted the elevation differences against the distances between the local and major ridges. After fitting a regression line to the plot to isolate the data above the trend line, we rated *ridge context* as 1 for local ridges at least 790 m from major ridges, 2 for local ridges between 440 and 790 m distant and at least 40 m lower than major ridges, 3 for local ridges between 250 and 440 m distant and at least 26 m lower than major ridges, 4 for local ridges between 170 and 250 m distant and at least 18 m lower than major ridges, 5 for local ridges between 100 and 170 m distant and at least 10 m lower than major ridges, 6 for local ridges between 25 and 45 m distant and at least 4 m lower than major ridges or for local ridges between 45 and 75 m distant and at least 6 m lower than major ridges or for local ridges between 75 and 100 m distant and at least 8 m lower than major ridges. We related adjusted fatality rates to these categories of *ridge context* to identify disproportionate fatality rates.

Steps to identify saddles, notches, and benches

Because a large amount of evidence links disproportionate numbers of raptor fatalities to wind turbines located on aspects of the landscape that are lower than immediately surrounding terrain or that represent sudden changes in elevation (Figure 12), a special effort was directed toward identifying ridge saddles, notches in ridges, and benches of slopes. Benches of slopes are where ridge features emerge from hill slopes that extend above the emerging ridge. These types of locations are where winds often compress by the landscape to create stronger force, and where raptors typically cross hilly terrain or spend more time to forage for prey. Compared to surrounding terrain, these types of features are often relatively flatter or shallower in slope and sometimes include lower elevations (e.g., saddles). Geoprocessing steps were used to provide some objectively to the identification of these features, but judgment was also required because conditions varied widely in how such features were formed and situated (Figure 12).

The same procedures were used as used in the ridge/valley selection. The two foot slope analysis grid was used to create polygons with a relatively gentle slope. A Standard Deviation classification was used to identify areas with < 7.4 % slope. These areas were then converted to polygons. Those polygons not associated with ridge or valley polygons were examined manually. Where these polygons were visually associated with saddle and or step features, they were identified as *hazard sites* representing saddles, notches, or benches. Maps depicting contours of the variable *percent up slope* were also examined, because these contours readily revealed sudden breaks in slope typical of saddles, notches, and benches, which were then also represented with polygons.

Figure 12. *We delineated polygons where ridge saddles present opportunities for flying birds to conserve energy by flying through the relatively lower portions of ridge structures (yellow arrows denote popular flight routes).*

GPS/GSM Telemetry

Doug Bell (2015) caught 18 golden eagles using baited traps since 18 December 2012. To each eagle he affixed 70 g GPS/GSM units manufactured by Cellular Tracking Technologies, LLC (CTT; http://celltracktech.com/) via backpack harness. CTT units measure 100 mm x 40 mm x 23 mm and run on solar powered batteries during daylight hours (Figure 13). All units recorded positions at 15 min intervals, and a subset recorded positions at 30 sec intervals during 3 days of

every month. Actual times between position intervals varied, but were supposed to average 15 min or 30 sec. CTT Transmitters download data to cell towers daily during prescribed 1 hour windows, but if a transmitter is beyond cell tower coverage, it will store location data until it returns to an area with cell coverage. Eagle location data were down-loaded from the CTT website, and were password protected.

Figure 13*. A golden eagle fitted with a GPS/GSM telemetry unit as seen during a visual scan survey to record behavior patterns.*

GPS/GSM telemetry positions were collected from all telemetered golden eagles intersecting the boundary of the APWRA from the inception of telemetry monitoring through November 2015. Lines representing flight paths were derived by connecting sequential positions, so each line was associated with a distance and time interval summed among all line segments, where a line segment was the line connecting two sequential positions. New flight lines were initiated each day, as well as when time intervals between sequential positions exceeded 60 sec in the case of data collected at 30 sec intervals and 1,020 sec in the case of data collected at 15 min (900 sec) intervals. We also subsampled 15 min interval data from 30 sec data was when the accumulated time among sequential positions surpassed 900 sec. We included the subsampled 15 min data with the 15 min interval data.

To assess error in the GPS/GSM telemetry units, we placed the units on the ground for long periods next to a Trimble GeoXT GPS with sub-meter accuracy. We also mounted telemetry units in the back of Smallwood's truck (1.2 m above ground) and next to a Trimble GeoXT unit while driving throughout the APWRA on various dates from 22 October 2014 through 10 September 2015. Our visual examination of the GPS/GSM data indicated high lateral position accuracy relative to the Trimble GeoXT unit. However, we noticed high vertical error and a large vertical bias in the GPS/GSM data when examining simple statistics and histograms. Whereas the Trimble GeoXT unit generated positions that averaged about a meter above the 10-

foot DEM surface – where the average was supposed to be – the GPS/GSM data averaged 9 m below the 10-foot DEM surface. We therefore adjusted upward the vertical positions of the telemetered golden eagles by 9 m. We also generated a cumulative distribution curve of the vertical error in the truck-mounted telemetry data, and found that 95% of the recorded positions were within 27 m of their true positions above the 10-foot DEM surface (Figure 14). We therefore used 27 m as a threshold value for determining whether flight lines of golden eagles were above ground. Flight lines were assigned to the following height domains above our 10-foot DEM: **0 (ground)** was <0 m above the DEM surface, **1 (near ground)** = 0 to 27 m above the DEM, **2 (medium)** was >27 m and <200 m above the DEM, and **3 (high)** was >=200 m above the DEM.

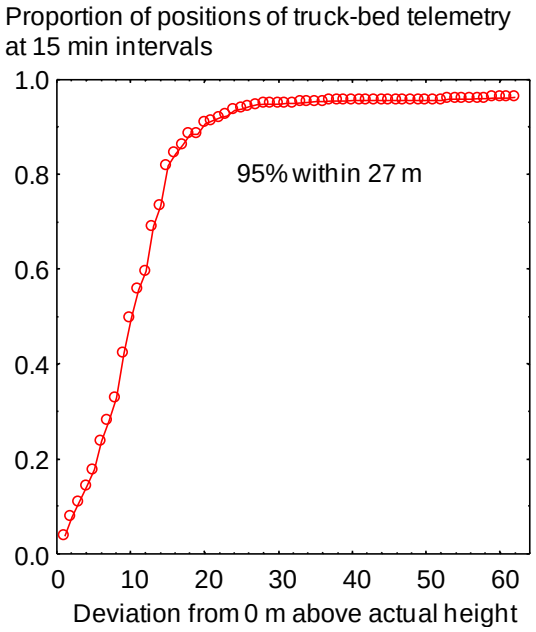

Figure 14. *Cumulative distribution of vertical error measured from 767 GPS/GSM telemetry positions between two units mounted in the back of Smallwood's truck at 1.2 m above ground while driving throughout the APWRA on various dates from 22 October 2014 through 10 September 2015*.

Examining data from GPS/GSM transmitters that we maintained at known locations (not affixed to eagles), we averaged false flight speeds caused by position scatter as 0.3 m/s (1.08 km/hr) for 30 second interval data, and 0.007 m/s (0.026 km/hr) for 15 min interval data. However, relying on speed alone was often insufficient for determining whether an eagle was flying because hovering or kiting golden eagles could have remained in the same locations over 30 sec intervals, and flying golden eagles could have returned to the same positions after flying out and back to another location or in a circle (these behaviors have been seen during visual surveys many times).

Whether an eagle was flying was determined as **possible (0)** if the flight line averaged slower than the speed of position scatter and ≤0 m above the DEM and intersected 1 subwatershed polygon, or it averaged slower than the speed of position scatter and <200 m above the DEM and

intersected 1 subwatershed polygon. Whether an eagle was flying was determined as **probable (1)** it the flight line averaged faster than position scatter and ≤27 m above the DEM and intersected ≥2 subwatershed polygons, or it averaged ≥3 km/hr and 0-27 m above the DEM and intersected ≥1 subwatershed polygon, or it averaged ≥1.08 km/hr and 27-200 m above the DEM and intersected ≥1 subwatershed polygon. Whether an eagle was flying was determined as **certain (2)** if the flight line averaged ≥2.5 km/hr or ≥100 m above the 10-foot DEM and intersected ≥4 subwatershed polygons, or it averaged ≥27 m above the DEM and intersected ≥3subwatershed polygons, or it averaged ≥2.3 km/hr and ≥27 m above the DEM and intersected ≥1subwatershed polygon. To prevent flight lines used in our association analysis from being falsely generated from position scatter around perched birds, we included lines determined to have been within height domains 1 or 2 and determined to have been certainly flying (2).

Associations between bird behaviors and terrain attributes

The location of each raptor was characterized by aspect, slope, rate of change in slope, direction of change in slope, and elevation. These variables were also used to generate raster layers of the study area, one raster expressing the aspect of the corresponding slope (hereafter referred to as *aspect*), and the other expressing whether the landscape feature was tending toward convex versus concave orientation (expressed in a variable named *curve*). These features were defined using geoprocessing.

Fuzzy logic (FL) modeling (Tanaka 1997) was used to predict the likelihood each grid cell would be used by golden eagle, red-tailed hawk, American kestrel, and burrowing owl. FL likelihood surfaces were first created by each selected predictor variable. The mean, standard deviation, and standard error were calculated for each predictor variable among the grid cells where each targeted bird species was observed during standard observation sessions. These statistics formed the basis from which FL membership was assigned to grid cells. Depending on the pattern in the data, FL membership was assigned values of 1 whenever the value of the predictor variable was within a certain prescribed distance in value from the mean, oftentimes within 1 SD, but sometimes within 1 or 2 SE. FL membership values of 1 expressed confidence that grid cells with the corresponding value range for the predictor variable are likely to be visited by the target species. FL membership values of 0 were assigned to grid cells that were far from the mean value, usually defined by prescribed distances from the mean such as >2 SD from the mean. FL membership values of 0 expressed confidence that grid cells with the corresponding value range for the predictor variable are unlikely to be visited by the target species. All other grid cells were assigned FL membership values according to the following formulae, assuming that the likelihood of occurrence of each species will grade gradually rather than abruptly across grid cells that vary in value of the predictor variable (Y):

$$0.5 \times (1 - \cos(\pi \times (Y - V_c) \div (V_f - V_c))) \text{ below the mean}$$
$$0.5 \times (1 + \cos(\pi \times (Y - V_c) \div (V_f - V_c))) \text{ above the mean,}$$

where V_c represented the variance term (SD or SE) closer to the mean and V_f represented the variance term farther from the mean.

FL likelihood values were then summed across predictor variables contributing to a species-specific model. In earlier efforts to develop FL models for golden eagle, red-tailed hawk, American kestrel and burrowing owl in other parts of the APWRA, natural breaks were used to divide the summed values into 4 classes, but the percentages of study area composing these classes remained fairly consistent despite use of natural breaks. Therefore, this time the class divides were established at 63.5%, 83.5%, and 95.5% when natural breaks were not evident; otherwise, we used natural breaks. Class 1, including FL likelihood values <63.5% (i.e., 63.5% of the study area), represented the suite of grid cells including fewer bird observations other than expected. Class 2, including FL likelihood values between 63.5% and 83.5% (i.e., 20% of the study area), represented the suite of grid cells including about equal or slightly greater than equal bird observations other than expected. Class 3, including FL likelihood values between 83.5% and 95.5% (i.e., 12% of the study area), represented the suite of grid cells including more bird observations other than expected. And class 4, including the upper 4.5% of FL likelihood values, represented the suite of grid cells including substantially more bird observations other than expected.

The performance of each model was assessed by the magnitude of the ratio of the observed number to the expected number of observations representing a dependent variable and occurring within the suite of conditions specified by each FL surface class. Dependent variables included fatality rates (except for American kestrel), flights <180 m above ground, flights across ridge features and <180 m above ground (Figure 15), social interactions while flying (Figure 16), wind turbine interaction events (Figures 17 and 18), and hovering or kiting or surfing behaviors (Figure 19). FL surface models were later projected across wind project areas.

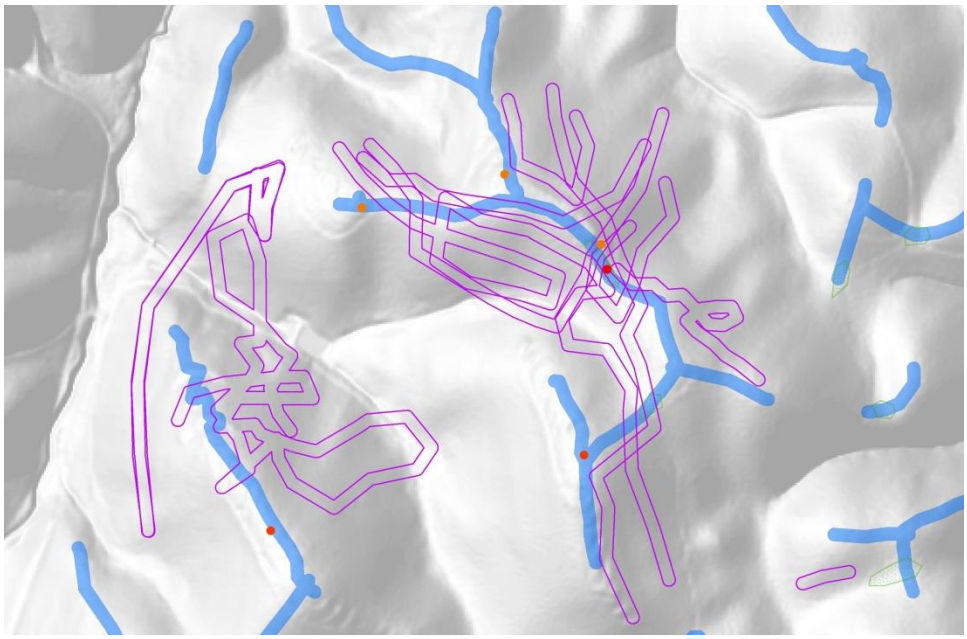

Figure 15. *Example of how golden eagle ridge crossings were quantified. WE buffered flights within 180 m of the ground by 10 m (purple polygons) and their overlap with 10-m buffered ridge crests (blue polygons) were counted for each ridge orientation: N-S, NNE-SSW, NE-SW,*

ENE-WSW, E-W, ESE-WNW, SE-NW, and SSE-NNW. Colored circles depict golden eagle fatality rates adjusted for monitoring duration, were red was the highest fatality rates.

Figure 16*. Social or competitive interactions between flying birds served as a dependent variable for collision hazard modeling, so associations were sought between interacting birds and terrain measurements and terrain features.*

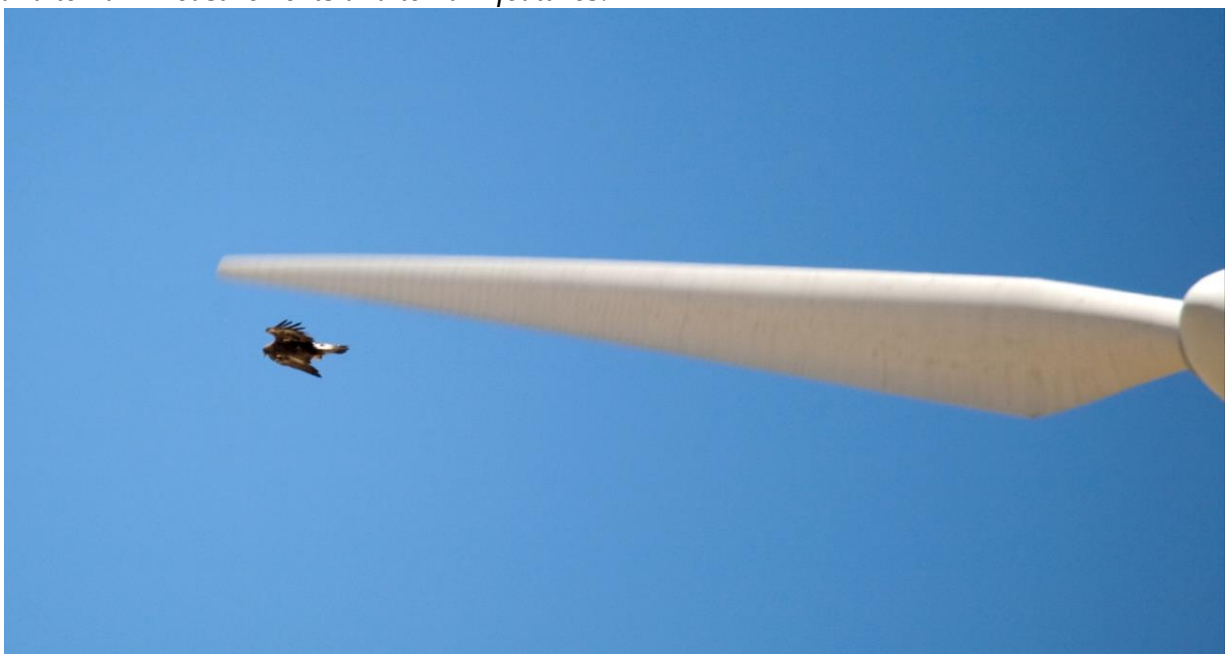

Figure 17*. Wind turbine events of birds adjudged by observers to have flown dangerously close to wind turbine blades were recorded and used for collision hazard modeling, so associations were sought between wind turbine events and terrain measurements and terrain features. In this case a golden eagle narrowly avoided a collision with a moving wind turbine blade.*

Figure 18. *Example of a social interaction between flying golden eagles that also happen to be near wind turbines. Where and under what conditions these combined social interactions and wind turbine events occur can assist with predicting collision hazard, but many hours of directed behavior surveys are needed to accumulate a sufficient number of these events to reliably associate them with environmental and terrain factors*.

Figure 19. *Red-tailed hawks kiting near the top of a slope. Red-tailed hawks, American kestrels and burrowing owls (at night) often perform this behavior just upwind of wind turbines. It is a known dangerous behavior, having preceded multiple eye-witness accounts of birds drifting with the wind or being pushed back by wind into operating wind turbine rotors. The behavior is also dangerous because kiting or hovering birds often break off from these behaviors to glide quickly with the wind before turning back into the wind to repeat the behaviors over another portion of the slope, but the glide with the wind often places them in sudden jeopardy of colliding with turbine blades*.

Burrowing owl model

Because burrowing owls tend to nest low on the slope, it would be rare for a predictive model of burrowing owl burrow locations to correspond with terrain where burrowing owls are killed by wind turbines. Therefore, we developed a burrowing owl fatality model. Previous attempts to develop reasonably predictive burrowing owl fatality models were frustrating. This time we examined earlier model predictions to learn where errors were accumulating. We discovered patterns that related to the size of the local terrain, with patterns of fatalities in shallower low-elevation terrain differing from those of larger high-elevation terrain (low and high elevation relative to the elevation range of the APWRA). Therefore, we divided the APWRA into four terrain regions based on ranges of analytical grid cell values representing *Valley elevation*, or elevation of the nearest valley bottom grid cell. Ranges of terrain size were Low (≤87 m), Mid-low (87-165 m), Mid-high (165-360 m), and High (>360 m). Candidate predictor variables were then related to fatality rates at monitored wind turbines within each terrain size category separately.

RESULTS

GPS/GSM Telemetry of Golden Eagles

All 18 of the golden eagles fitted with GPS/GSM telemetry units intersected the APWRA at some point during the study (Figure 20). Two of the eagles barely overlapped the APWRA with 3 positions each, so they did not contribute anything to the analysis. Another two eagles recorded only 15 and 16 positions within the APWRA, so they, too, contributed little if anything to the analysis. The other 14 eagles contributed hundreds or thousands of positions within the APWRA.

Our examination of associations between eagle positions and terrain variables indicated no difference between eagles tracked at 30 sec intervals and those tracked at 15 min intervals. Therefore, we combined the data from the two position intervals for quantifying associations with terrain variables. We found high variation in terrain associations between gender and age classes of eagles, but none of this variation appeared meaningful. However, we noticed strong differences in terrain associations between the 3 eagles that collided with wind turbines versus those that have not yet collided with wind turbines. Therefore, we relied mostly on terrain associations of the 3 eagles that collided with wind turbines to develop a collision hazard model.

After combining data sets based on 30 sec and 15 min intervals, golden eagle telemetry positions adjusted for vertical bias and intersecting the APWRA numbered 17,025 (14%) at or below ground (of course, these birds were not truly below ground, but recorded below ground due to position errors), 79,757 (66%) near ground, 18,396 (15%) within the hazardous height zone of 27 m to 200 m above ground, and 6,079 (5%) high above ground. Of the golden eagle positions intersecting the APWRA, 1.39% were possibly of flying eagles, 12.88% were probably of flying eagles, and 85.73% were certainly of flying eagles.

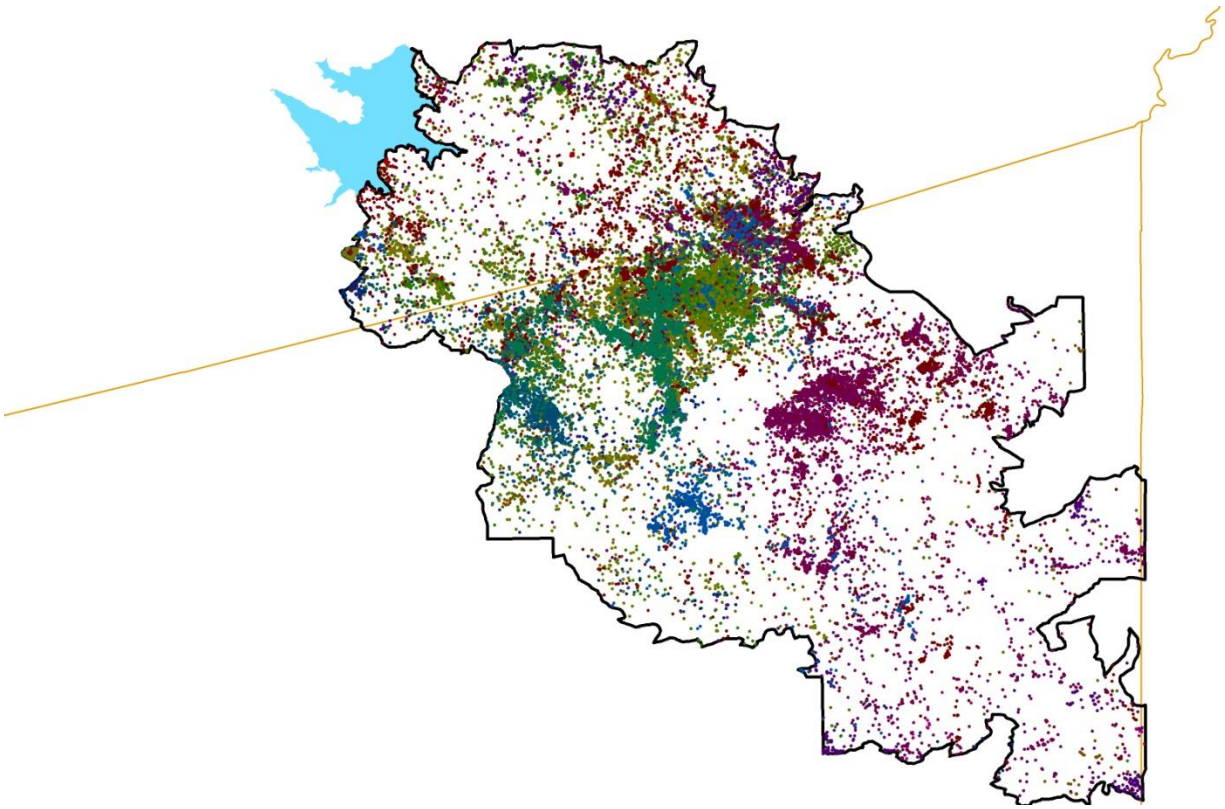

Figure 20. *GPS/GSM telemetry positions of golden eagles (each color represents a different eagle) within the boundary of the Altamont Pass Wind Resource Area, December 2012 through September 2015. Orange lines represent County boundaries, and the blue polygon at the upper left is Los Vaqueros Reservoir. As a cautionary note, the numbers and densities of telemetry positions represent those of tracked eagles and not of all the eagles that otherwise could have used the APWRA; in other words, the densities of positions do not represent densities of eagle activity in the APWRA.*

Visual Surveys

Behavior surveys performed at Sand Hill through 5 April 2015 numbered 2,002 30-min surveys and across the rest of the APWRA through 29 October 2015 numbered 1,095 1-hr surveys elsewhere in the APWRA for a combined 2,096 hours. APWRA-wide observation rates were 0.6115 golden eagles/hour, 1.3597 red-tailed hawks/hour, and 0.4054 American kestrels/hour. We recorded wind turbine interaction events, including 86 golden eagle events, 156 red-tailed hawk events, and 98 American kestrel events.

Hazard Models

The FL models of golden eagle were composed of 7 predictor variables based on telemetry data (Table 1), 3 predictor variables based on behavior data (Table 2), and 9 predictor variables based on fatality rates (Table 3). The FL models of red-tailed hawk were composed of 3 predictor variables based on behavior data (Table 4), and 6 predictor variables based on fatality rates (Table 5). The FL models of American kestrel were composed of 5 predictor variables based on behavior data (Table 6), and 7 predictor variables based on fatality rates (Table 7). The FL

models of burrowing owl were composed of 2 predictor variables based on burrow location data (Table 8), and 5 predictor variables based on fatality rates and conditional to size categories of terrain (Table 9). How the models were weighted and combined for each species is summarized in Table 10.

Telemetered golden eagles were recorded flying disproportionately over the upper portions of slopes, even more so for the colliders (Figure 21). Colliders were also disproportionately recorded flying higher up the slopes of major terrain features, as well as over ridges oriented east to west and east-southeast to west-northwest and over slopes facing north-northwest, south-southwest and south (Figure 22). Colliders were disproportionately recorded flying farther from the major valley bottoms and over steeper-than-average slopes.

Golden eagle flights and wind turbine interactions occurred disproportionately over ridges oriented generally west-east. Associations were also strong with subwatershed slopes facing westerly directions, especially west and northwest. Golden eagles flew and interacted with wind turbines disproportionately at 91% to 100% up the slope (Figure 23).

Red-tailed hawks hovered and kited disproportionately over slopes oriented north-northeast, west, and northwest. Red-tailed hawks hovered and kited disproportionately over ground that was between 85% and 100% to the top of the slope (Figure 24). Red-tailed hawk kiting and hovering was broader across major terrain features, with peak activity ranging between 53% and 83% to the top of the feature (Figure 24).

American kestrels flew most disproportionately over slopes oriented west and southwest, ranging mostly between three-quarters to the peak of the slope and midway to just below the peaks of major terrain features. American kestrel wind turbine interaction events were observed disproportionately on relatively small hills.

Burrowing owl burrows were located disproportionately between 5% and 30% of the way up south-facing slopes (Figure 25). Burrowing owl fatality rates were disproportionately higher at low to moderate elevations and between 35% and 42% of the way up the slopes of major terrain features and in hazard sites (Figure 25).

Based on the data used to develop the models, the models performed well (Figure 26). Of course, it should be remembered that model performance tends to be higher when validation is based on the data underlying the models.

Map-based collision hazard models were used to recommend shifts in the initially proposed wind turbine layout at Sand Hill (Figures 27-46). The models for golden eagle, red-tailed hawk and American kestrel were combined from other models as described in the Methods section and Table 10, and the burrowing owl model was based solely on fatality data. Addresses with letters indicate alternative sites under consideration with respect to the address number, so 15, 15-A and 15-B are three sites from which one wind turbine might be installed.

Table 1. *Golden eagle fuzzy logic membership functions of DEM grid cells based on GPS telemetry positions primarily of 3 study birds that collided with wind turbines.*

Value of variable Y for *i*th grid cell (type of event)	**Membership function of grid cell (Values >1 include weightings)**
Ridge orientation	
Y = W-E	3
Y = WNW-ESE	2
Y = NW-SE,	1
Y = Other orientation	0
Subwatershed orientation	
Y = S, SSW, NNW	2
Y = N, NE, SW, WNW	1
Y = Other orientation	0
Percent up slope	
$85.70 < Y \leq 100$	1
$71.56 \leq Y \leq 85.70$	$0.5 \times (1 - \cos(\pi \times (Y - 71.56) / (85.70 - 71.56)))$
$Y < 71.56$	0
Percent up major terrain slope	
$59.0 < Y \leq 98.0$	1
$39.5 \leq Y \leq 59.0$	$0.5 \times (1 - \cos(\pi \times (Y - 39.5) / (59.0 - 39.5)))$
$98.0 < Y \leq 100.0$	$0.5 \times (1 + \cos(\pi \times (Y - 98.0) / (100.0 - 98.0)))$
$Y < 39.5$	0
Distance to major valley	
$168.81 < Y \leq 538.34$	1
$117.25 \leq Y \leq 168.81$	$0.5 \times (1 - \cos(\pi \times (Y - 117.25) / (168.81 - 117.25)))$
$538.34 < Y < 684.44$	$0.5 \times (1 + \cos(\pi \times (Y - 538.34) / (684.44 - 538.34)))$
$Y < 117.25$ or $Y > 684.44$	0
Gross slope	
$19.56 < Y \leq 33.10$	1
$15.04 \leq Y \leq 19.56$	$0.5 \times (1 - \cos(\pi \times (Y - 15.04) / (19.56 - 15.04)))$
$33.10 < Y < 42.13$	$0.5 \times (1 + \cos(\pi \times (Y - 33.10) / (42.13 - 33.10)))$
$Y < 15.04$ or $Y > 42.13$	0
Hazard site	
Y = Within polygon	1
Y = Outside polygon	0

Table 2. *Golden eagle fuzzy logic membership functions of DEM grid cells based on flights involving ridge crossings, interactions with other birds, and wind turbine interaction events.*

Value of variable Y for *i*th grid cell (type of event)	**Membership function of grid cell (Values >1 include weightings)**
Ridge orientation (ridge crossings, social interactions, turbine events, behavior)	
Y = W-E	2
Y = N-S, NE-SW, WNW-ESE, NNW-SSE	1
Y = Other orientation	0
Subwatershed orientation (social interactions, turbine events, behavior)	
Y = WSW, W, NW	3
Y = SSE, WNW, SSW, NNW	2
Y = N, NNE, NE, SW	1
Y = Other orientation	0
Percent up slope (turbine events, social interactions)	
$91 < Y \leq 100$	1
$15 \leq Y \leq 91$	$0.5 \times (1 - \text{COS}(\pi \times (Y - 15) / (91 - 15)))$
$Y < 15$	0

Table 3. *Golden eagle fuzzy logic membership functions of DEM grid cells based on fatality rates at wind turbine locations.*

Value of variable Y for *i*th grid cell (type of event)	**Membership function of grid cell (Values >1 include weightings)**
Ridge orientation	
Y = WNW-ESE	2
Y = WSW-ENE, W-E	1
Slope orientation (for percent upslope <90)	
Y = WNW	3
Y = WSW, NW	2
Y = SSW, SW	1
Ridge context (relative to major ridges)	
Y = 2 (low & far), 6 (low & very near)	2
Y = 5 (low & near)	1
Ridge elevation	
$207.70 < Y \leq 251.48$	1
$69.09 \leq Y \leq 207.70$	$0.5 \times (1 - COS(\pi \times (Y - 69.09) / (207.70 - 69.09)))$
$251.48 < Y \leq 360.91$	$0.5 \times (1 + COS(\pi \times (Y - 251.48) / (360.91 - 251.48)))$
$Y < 69.09$ or $Y > 360.91$	0
Hill size (for percent upslope <90)	
$66.76 < Y < 75.24$	1
$49.80 \leq Y \leq 66.76$	$0.5 \times (1 - COS(\pi \times (Y - 49.80) / (66.76 - 49.80)))$
$75.24 < Y \leq 92.20$	$0.5 \times (1 + COS(\pi \times (Y - 75.24) / (92.20 - 75.24)))$
$Y < 49.80$ or $Y > 92.20$	0
Ridgeline slope	
$Y > 10$	1
$Y \leq 10$	0
Percent upslope	
$30.65 < Y \leq 51.35$	1
$15.13 \leq Y \leq 30.65$	$0.5 \times (1 - COS(\pi \times (Y - 15.13) / (30.65 - 15.13)))$
$51.35 < Y \leq 66.87$	$0.5 \times (1 + COS(\pi \times (Y - 51.35) / (66.87 - 51.35)))$
$Y < 15.13$ or $Y > 66.87$	0
Percent up major terrain slope	
$15.29 < Y \leq 36.71$	1
$9.30 \leq Y \leq 15.29$	$0.5 \times (1 - COS(\pi \times (Y - 9.30) / (15.29 - 9.30)))$
$36.71 < Y < 42.07$	$0.5 \times (1 + COS(\pi \times (Y - 36.71) / (42.07 - 36.71)))$
$Y < 9.30$ or $Y > 42.07$	0
Hazard site	
Y = Within polygon	1
Y = Outside polygon	0

Table 4. *Red-tailed hawk fuzzy logic membership functions of DEM grid cells based on flights involving ridge crossings, interactions with other birds, behavior, and wind turbine interaction events.*

Value of variable Y for *i*th grid cell (type of event)	**Membership function of grid cell (Values >1 include weightings)**
Subwatershed orientation (ridge crossings, social interactions, turbine events, hovering/kiting)	
Y = NNE, W, NW	3
Y = SW, N	2
Y = WSW, WNW, NNW	1
Y = Other orientation	0
Percent up slope (hovering/kiting)	
$85.43 < Y \leq 100$	1
$43.84 \leq Y \leq 85.43$	$0.5 \times (1 - \text{COS}(\pi \times (Y - 43.84) / (85.43 - 43.84)))$
$Y < 43.84$	0
Percent up major terrain slope (hovering/kiting)	
$52.98 < Y \leq 82.66$	1
$29.24 \leq Y \leq 52.98$	$0.5 \times (1 - \text{COS}(\pi \times (Y - 29.24) / (52.98 - 29.24)))$
$82.66 < Y \leq 100$	$0.5 \times (1 + \text{COS}(\pi \times (Y - 82.66) / (100 - 82.66)))$
$Y < 29.24$	0

Table 5. *Red-tailed hawk fuzzy logic membership functions of DEM grid cells based on fatality rates at wind turbine locations.*

Value of variable Y for *i*th grid cell (type of event)	**Membership function of grid cell (Values >1 include weightings)**
Ridge orientation	
Y = N-S, NW-SE, WNW-ESE, W-E, WSW-ENE	1
Y = NNW-SSE, SW-NE, SSW-NNE	0
Subwatershed orientation (percent upslope <90)	
Y = SSW, NW	1.5
Y = SW, WNW, NNW	1
Ridge context (relative to major ridges)	
Y = 6 (low & very near)	1
Ridge elevation	
$195.68 < Y \leq 222.32$	1
$80.24 \leq Y \leq 195.68$	$0.5 \times (1 - COS(\pi \times (Y - 80.24) / (195.68 - 80.24)))$
$222.32 < Y \leq 320$	$0.5 \times (1 + COS(\pi \times (Y - 222.32) / (320 - 222.32)))$
$Y < 80.24$ or $Y > 320$	0
Percent up major terrain slope	
$22.18 < Y \leq 27.82$	1
$13.71 \leq Y \leq 22.18$	$0.5 \times (1 - COS(\pi \times (Y - 13.71) / (22.18 - 13.71)))$
$27.82 < Y < 36.29$	$0.5 \times (1 + COS(\pi \times (Y - 27.82) / (36.29 - 27.82)))$
$Y < 13.71$ or $Y > 36.29$	0
Hazard site	
Y = Within polygon	1
Y = Outside polygon	0

Table 6. *American kestrel fuzzy logic membership functions of DEM grid cells based on flights involving ridge crossings, interactions with other birds, behavior, and wind turbine interaction events.*

Value of variable Y for *i*th grid cell (type of event)	**Membership function of grid cell (Values >1 include weightings)**
Subwatershed orientation (ridge crossings, social interactions, turbine events, hovering/kiting)	
Y = SE, SSW, SW, W, NNW	3
Y = WSW, NW	2
Y = N, NNE, SSE, S	1
Y = Other orientation	0
Percent up slope (hovering/kiting)	
$85.43 < Y \leq 100$	1
$43.84 \leq Y \leq 85.43$	$0.5 \times (1 - COS(\pi \times (Y - 43.84) / (85.43 - 43.84)))$
$Y < 43.84$	0
Percent up major terrain slope (hovering/kiting)	
$66.36 < Y \leq 92.55$	1
$40.15 \leq Y \leq 66.36$	$0.5 \times (1 - COS(\pi \times (Y - 40.15) / (66.36 - 40.15)))$
$92.55 < Y \leq 100$	$0.5 \times (1 + COS(\pi \times (Y - 92.55) / (100 - 92.55)))$
$Y < 40.15$	
Hill size (turbine events)	
$20.73 < Y \leq 25.03$	1
$9.98 \leq Y \leq 20.73$	$0.5 \times (1 - COS(\pi \times (Y - 9.98) / (20.73 - 9.98)))$
$25.03 < Y \leq 44.38$	$0.5 \times (1 + COS(\pi \times (Y - 25.03) / (44.38 - 25.03)))$
$Y < 9.98$ or $Y > 44.38$	0
Hazard site	
Y = Within polygon	1
Y = Outside polygon	0

Table 7. *American kestrel fuzzy logic membership functions of DEM grid cells based on fatality rates at wind turbine locations.*

Value of variable Y for *i*th grid cell (type of event)	**Membership function of grid cell (Values >1 include weightings)**
Subwatershed orientation	
Y = NNE, SW	2
Y = SE, SSW	1
Y = Other orientation	0
Ridge orientation	
Y = WSW-ENE	2
Y = NW-SE, NNW-SSE	1
Ridge context (relative to major ridges)	
Y = 4 (low & close), 5 (low & near)	1
Valley elevation (percent upslope < 90)	
66.75 < Y < 91.25 or 135.88 < Y < 148.12	1
54.50 ≤ Y ≤ 66.75 or 129.75 ≤ Y ≤ 135.88	0.5 × (1 - COS(π × (Y – 54.50) / (66.75 – 54.50)))
	0.5 × (1 - COS(π × (Y – 129.75) / (135.88– 129.75)))
91.25 < Y ≤ 103.5 or 148.12 < Y < 154.25	0.5 × (1 + COS(π × (Y – 91.25) / (103.5 – 91.25)))
	0.5 × (1 + COS(π × (Y –148.12) / (154.25 – 148.12)))
54.5 < Y > 154.25	0
Slope to gross slope ratio (percent upslope < 90)	
0.79 < Y ≤ 1.20	1
0.69 ≤ Y ≤ 0.79	0.5 × (1 - COS(π × (Y – 0.69) / (0.79 – 0.69)))
1.20 < Y ≤ 1.31	0.5 × (1 + COS(π × (Y – 1.2) / (1.31 – 1.2)))
Y < 0.69 or Y > 1.31	0
Distance to major ridge (percent upslope ≥90)	
155 < Y ≤ 195	1
75 ≤ Y ≤ 155	0.5 × (1 - COS(π × (Y – 75) / (155 – 75)))
195 < Y ≤ 275	0.5 × (1 + COS(π × (Y – 195) / (275 – 195)))
Y < 75 or Y > 275	0
Hazard site	
Y = Within polygon	1
Y = Outside polygon	0

Table 8. *Burrowing owl fuzzy logic membership functions of DEM grid cells for burrow sites.*

Value of variable Y for *i*th grid cell (type of event)	**Membership function of grid cell (Values >1 include weightings)**
Subwatershed orientation	
Y = S	2.5
Y = ESE, SE, SSE	1.5
Y = ENE, E	1
Y = Other orientation	0
Percent up slope	
$5.56 < Y \leq 20.83$	1
$0.47 \leq Y \leq 5.56$	$0.5 \times (1 - \text{COS}(\pi \times (Y - 0.47) / (5.56 - 0.47)))$
$20.83 \leq Y \leq 51.37$	$0.5 \times (1 + \text{COS}(\pi \times (Y - 20.83) / (51.37 - 20.83)))$
$Y < 0.47$ or $Y > 51.37$	0

Table 9. *Burrowing owl fuzzy logic membership functions of DEM grid cells based on fatality rates at wind turbine locations.*

Value of variable Y for *i*th grid cell (type of event)	**Membership function of grid cell (Values >1 include weightings)**
Low: Valley elevation ≤ 87 m	
Ridge orientation	
Y = N-S, NNE-SSW, NE-SW, ENE-WSW, W-E, NNW-SSE	1
Y = SNW-ESE, NW-SE, or not on ridge	2
Mid-low: 87 m < Valley elevation ≤ 165 m	
Not on Ridge: Slope orientation	
Y = SSW, SW, WSW, W	0
Y = WNW, NW, NNW, E	1
Y = N, NNE, NE. ENE, SE	2
Ridge orientation	
Y = WNW-ESE, NW-SE, NNW-SSE	0
Y = NNE-SSW, NE-SW, ENE-WSW, W-E	1
Y = N-S	2
Percent up slope	$Y = (3.153\text{-}0.0242 \times \text{Slope})/3.153$
Mid-high: 165 m < Valley elevation ≤ 360 m	
Ridge orientation	
Y = On ridge	1
Y = Not on ridge	2
Slope	$Y = (0.27 + 0.02 \times \text{Slope})/0.76503$
High: Valley elevation > 360 m	
Ridge orientation	
Y = N-S	1
Y = NNE-SSW or not on ridge	2
Slope	
Y > 6.5	1
Hill size	
$15 \leq Y \leq 30$	1

Table 10. *Fuzzy logic models developed for Sand Hill, where Low, Mid-low, Mid-high, and High VE represent nearest Valley elevation ranges of ≤87 m, 87-165 m, 165-360 m, and >360 m, respectively.*

Dependent variable	**Model**	**Max score possible**
Golden eagle telemetry	Distance to major valley + 2×Percent up slope + 2× Percent up major terrain slope + Gross slope + 2×Subwatershed orientation + 3×Ridge orientation + 10×Hazard site	29
Golden eagle flights	Ridge orientation + 2×Subwatershed orientation + 2×Percent up slope + 10×Hazard site + Ridge orientation + 2×Subwatershed orientation + 2×Ridge context + Ridge elevation + 2×Hill size + Ridgeline slope + Percent upslope + Major terrain upslope	10
Golden eagle fatalities		28
Golden eagle combined	((Telemetry score/29)×2 + Behavior score/10 + (Fatality score/28)×3)/6	1
Red-tailed hawk kiting	2×(Percent up slope + Percent up major terrain slope) + Subwatershed orientation	7
Red-tailed hawk fatalities	6×Hazard site + Ridge orientation + 3×Subwatershed orientation + Ridge context + Ridge elevation + Percent up major terrain slope	14.5
Red-tailed hawk combined	((Behavior score/7) + (Fatality score/14.5))/2	1
American kestrel kiting	7×Hazard site + Ridge orientation + 3×Subwatershed orientation + 3×Percent up slope + Percent up major terrain slope + Hill size	21
American kestrel fatalities	8×Hazard site + 2×Ridge orientation + 2×Subwatershed orientation + 2×Ridge context + Valley elevation + Slope to grosslope ratio + Major ridge distance	21
American kestrel combined	((Behavior score/21)×3 + (Fatality score/21))/4	1
Burrowing owl fatalities	4×Hazard site + Ridge orientation $_{\text{Low VE}}$ + ((Ridge orientation $_{\text{Mid-low VE}}$ or Slope orientation not on ridge $_{\text{Mid-low VE}}$) + 3×Percent up slope $_{\text{Mid-low VE}}$)×3 + (Ridge orientation $_{\text{Mid-high VE}}$ × Slope $_{\text{Mid-high VE}}$)×2 + (Ridge orientation $_{\text{High VE}}$ + Slope $_{\text{High VE}}$ + Hill size $_{\text{High VE}}$)	31

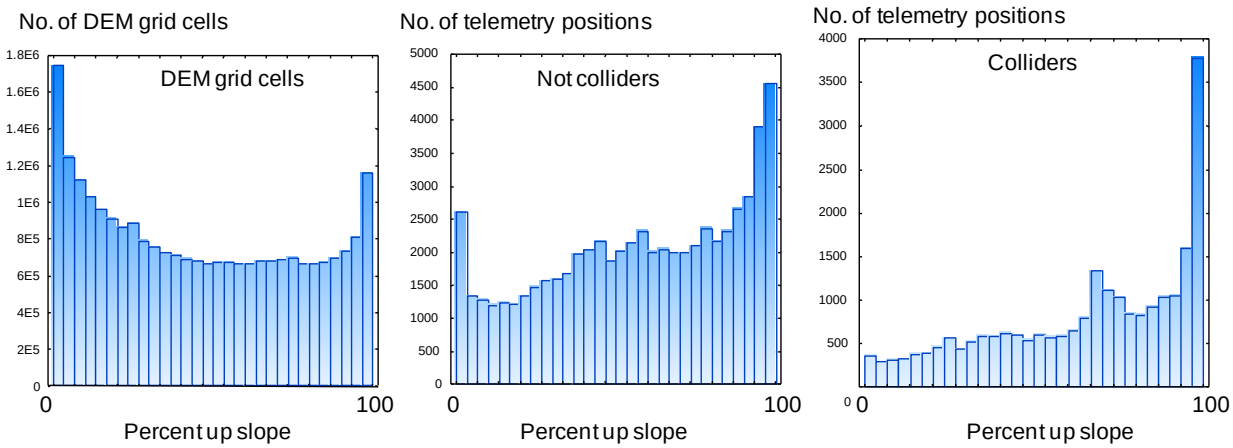

Figure 21. The distributions of telemetered eagle positions were shifted up the slopes (middle and right graphs) compared to the distribution of DEM grid cells in the APWRA (left graph).

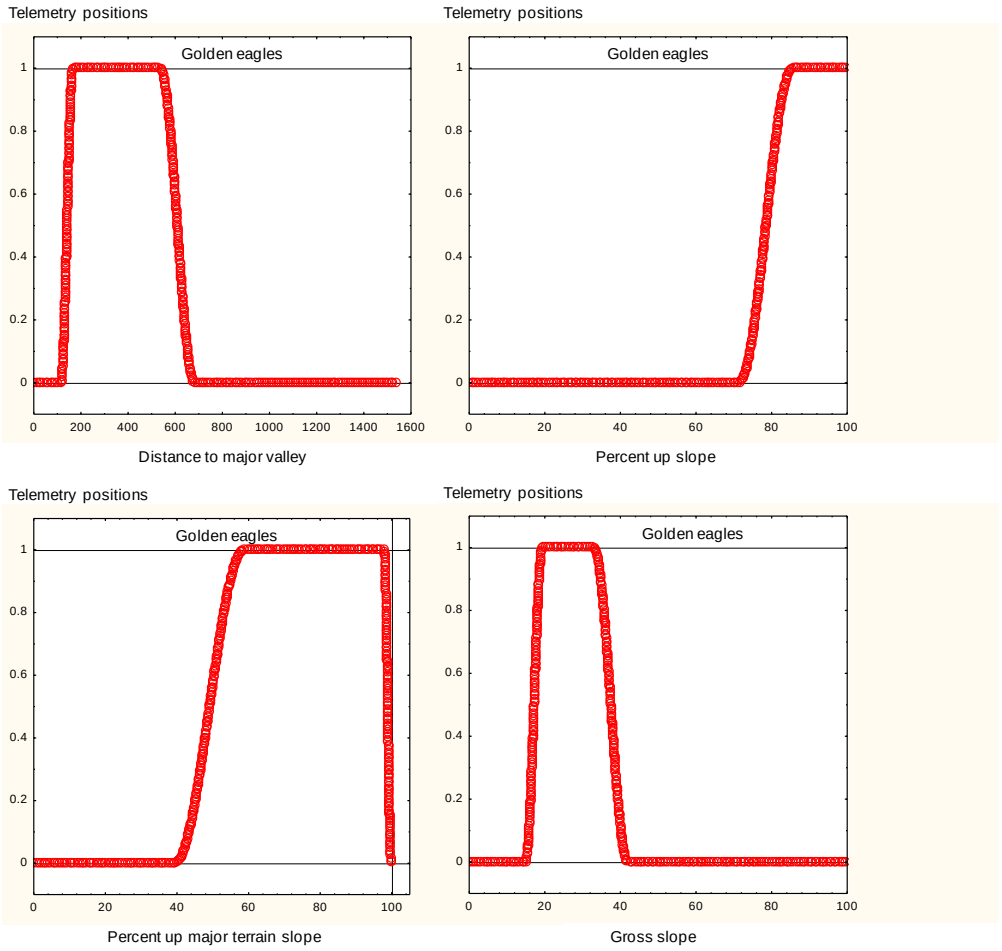

Figure 22. *Examples of grid cell membership values in respective fuzzy logic sets for telemetry positions related to four predictor variables.*

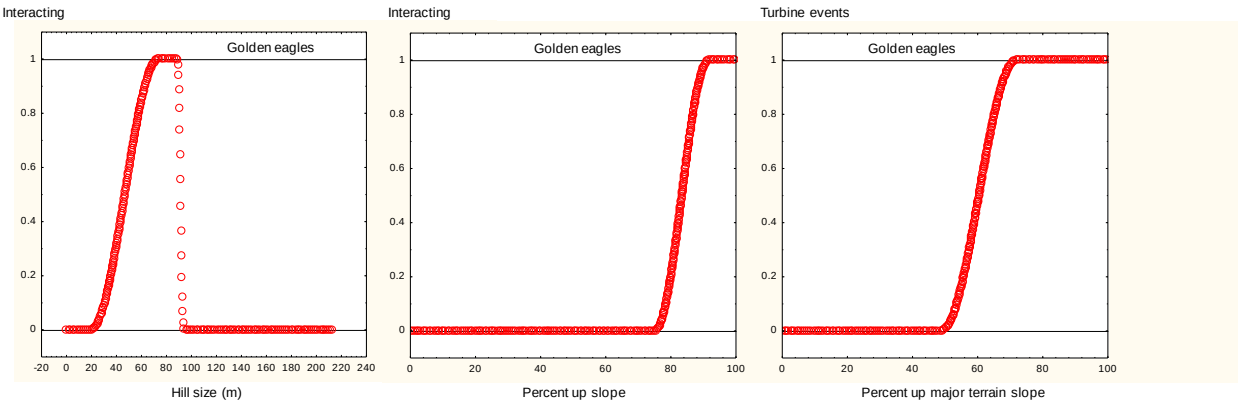

Figure 23. *Examples of grid cell membership values in respective fuzzy logic sets for three predictor variables, including of golden eagle interactions with other birds (left and middle) and wind turbine events (right).*

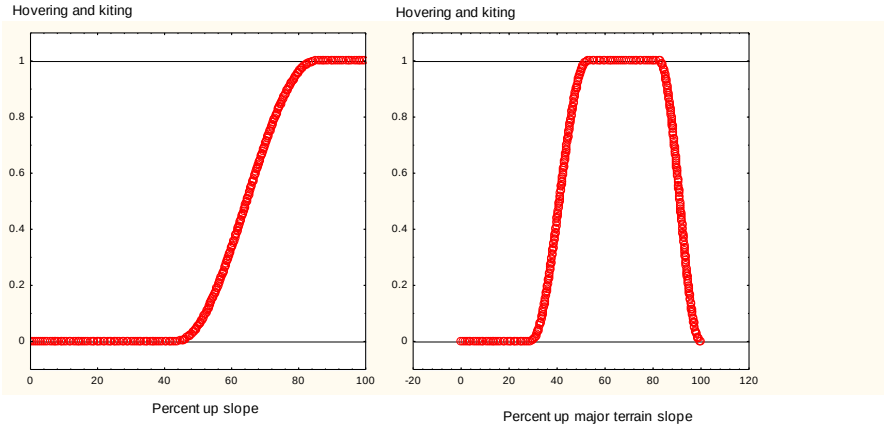

Figure 24. *Examples of grid cell membership values of red-tailed hawk hovering and kiting in respective fuzzy logic sets for percent upslope (left) and percent upslope of major terrain (right).*

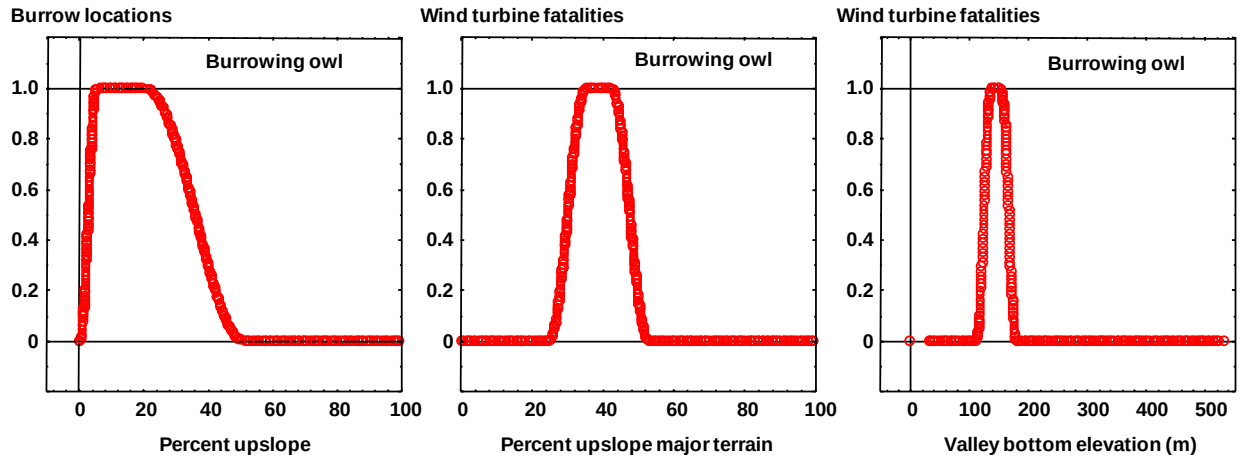

Figure 25. *Examples of grid cell membership values in respective fuzzy logic sets for three predictor variables, including of burrowing owl burrow locations (left) and burrowing owl fatalities at wind turbines (middle and right) in the study area.*

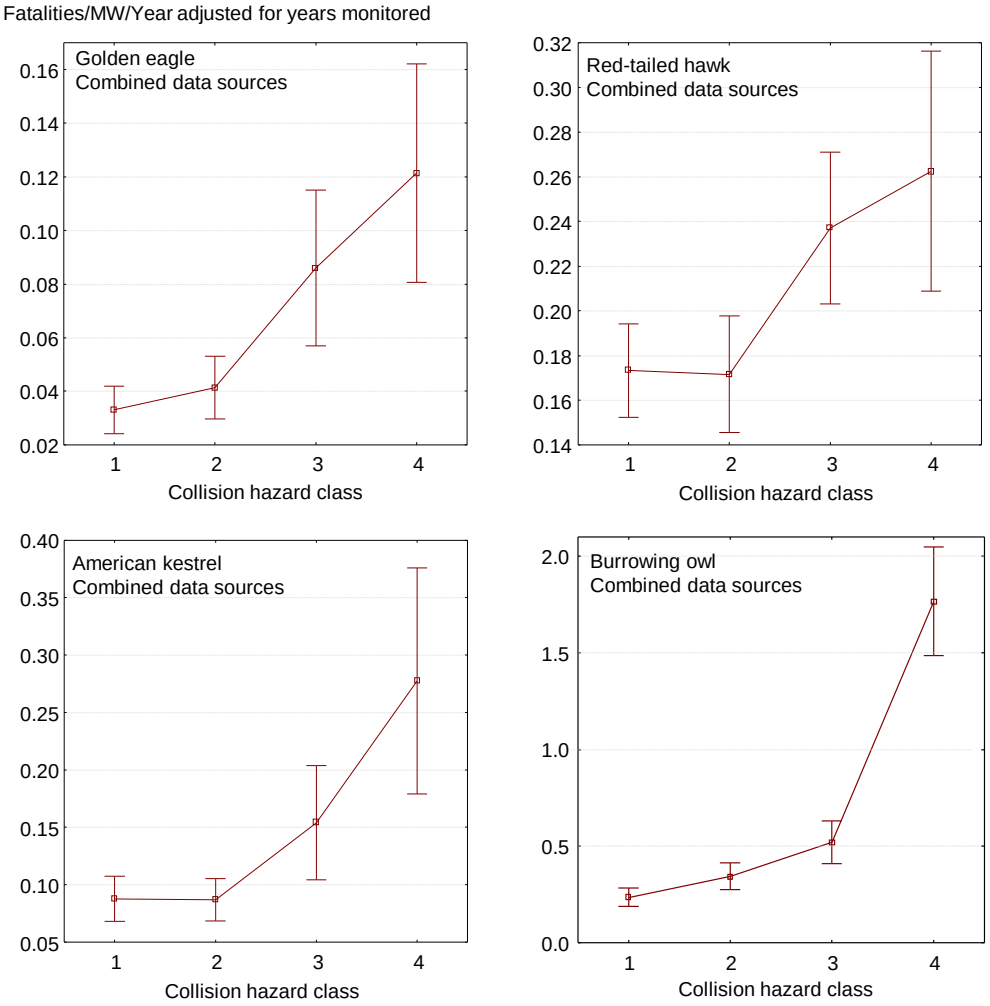

Figure 26. *Performance of collision hazard models based on data used to generate the models.*

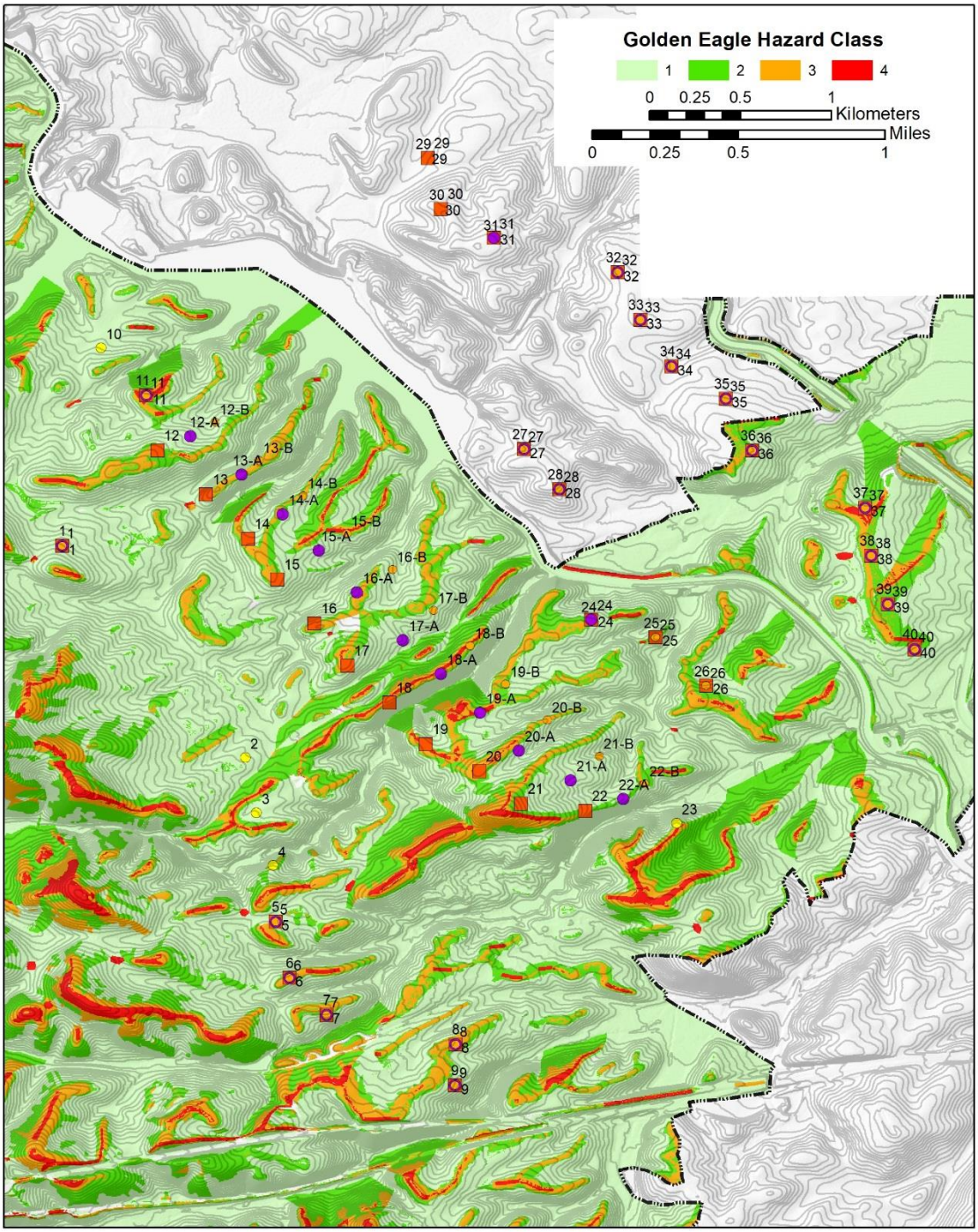

Figure 27. *Fuzzy Logic likelihood surface classes of golden eagle telemetry, flight behavior and fatality locations across the Sand Hill project area, Altamont Pass Wind Resources Area, California, where red corresponds with the highest likelihood of golden eagle collision, orange corresponds with the second highest likelihood, yellow corresponds with the third highest likelihood, and dark green corresponds with the least likelihood.*

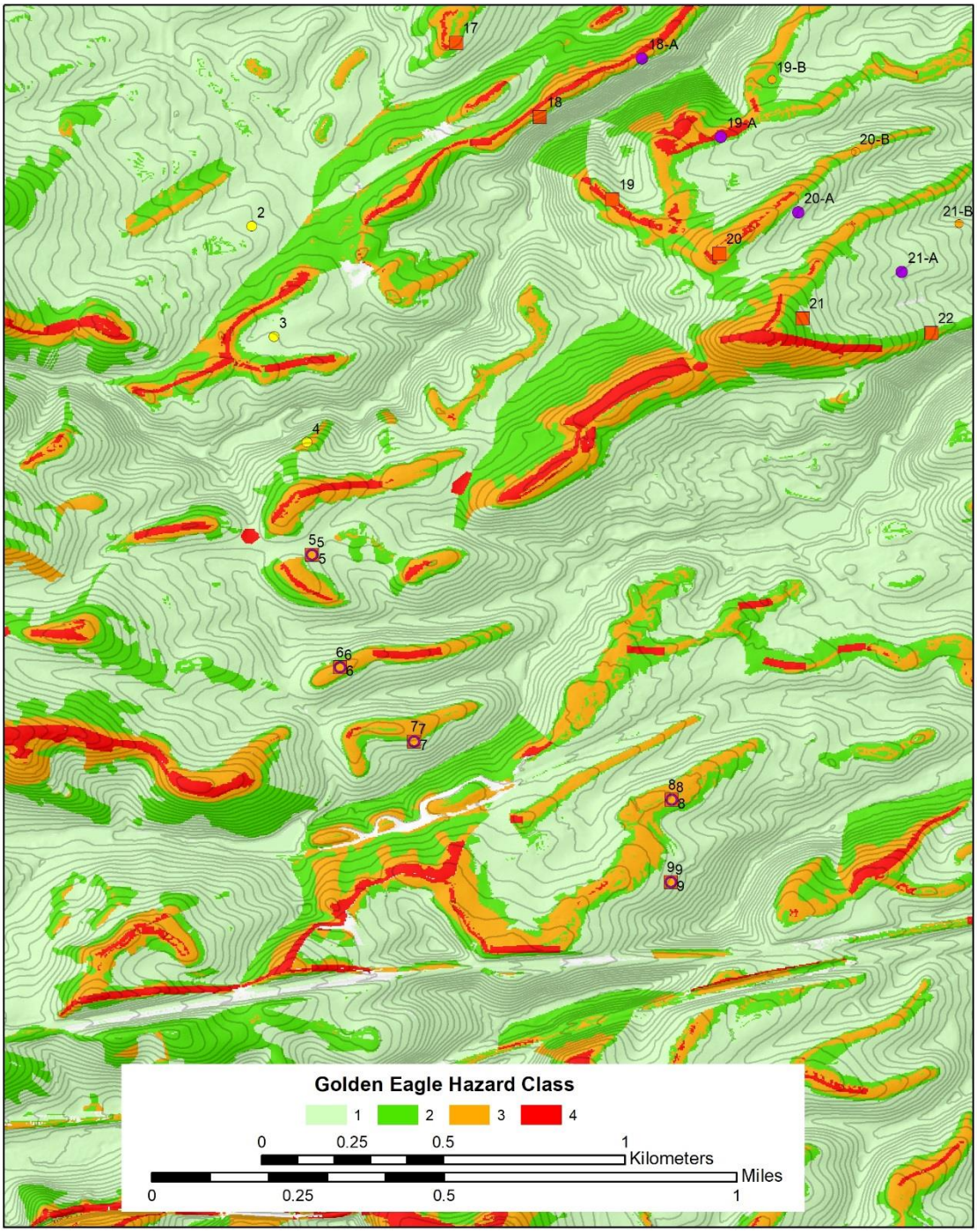

Figure 28. *Fuzzy Logic likelihood surface classes of golden eagle telemetry, flight behavior and fatality locations across the southwest portion of the Sand Hill project area, Altamont Pass Wind Resources Area, California, where red corresponds with the highest likelihood of golden eagle collision, orange corresponds with the second highest likelihood, yellow corresponds with the third highest likelihood, and dark green corresponds with the least likelihood.*

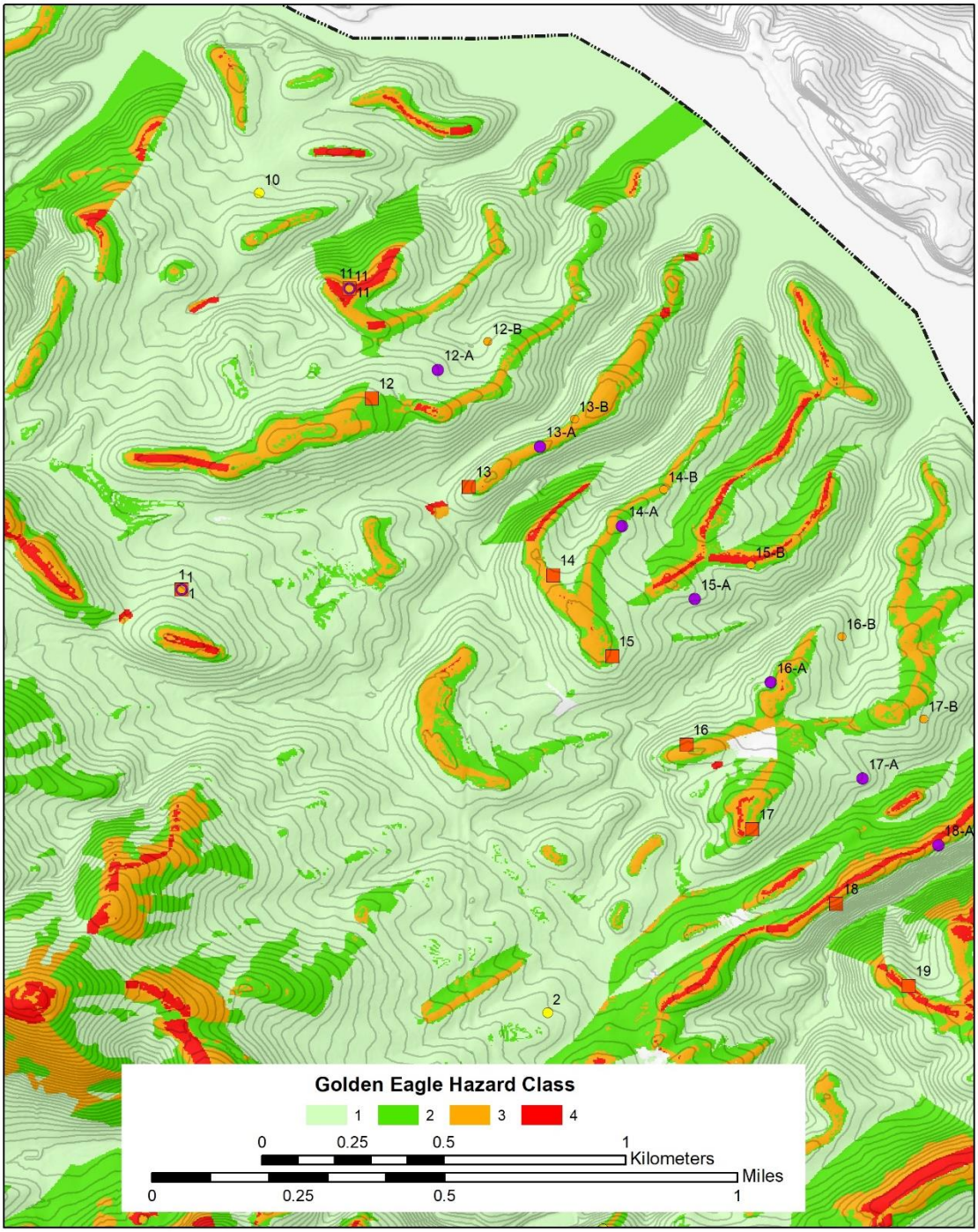

Figure 29. *Fuzzy Logic likelihood surface classes of golden eagle telemetry, flight behavior and fatality locations across the northcentral portion of the Sand Hill project area, Altamont Pass Wind Resources Area, California, where red corresponds with the highest likelihood of golden eagle collision, orange corresponds with the second highest likelihood, yellow corresponds with the third highest likelihood, and dark green corresponds with the least likelihood.*

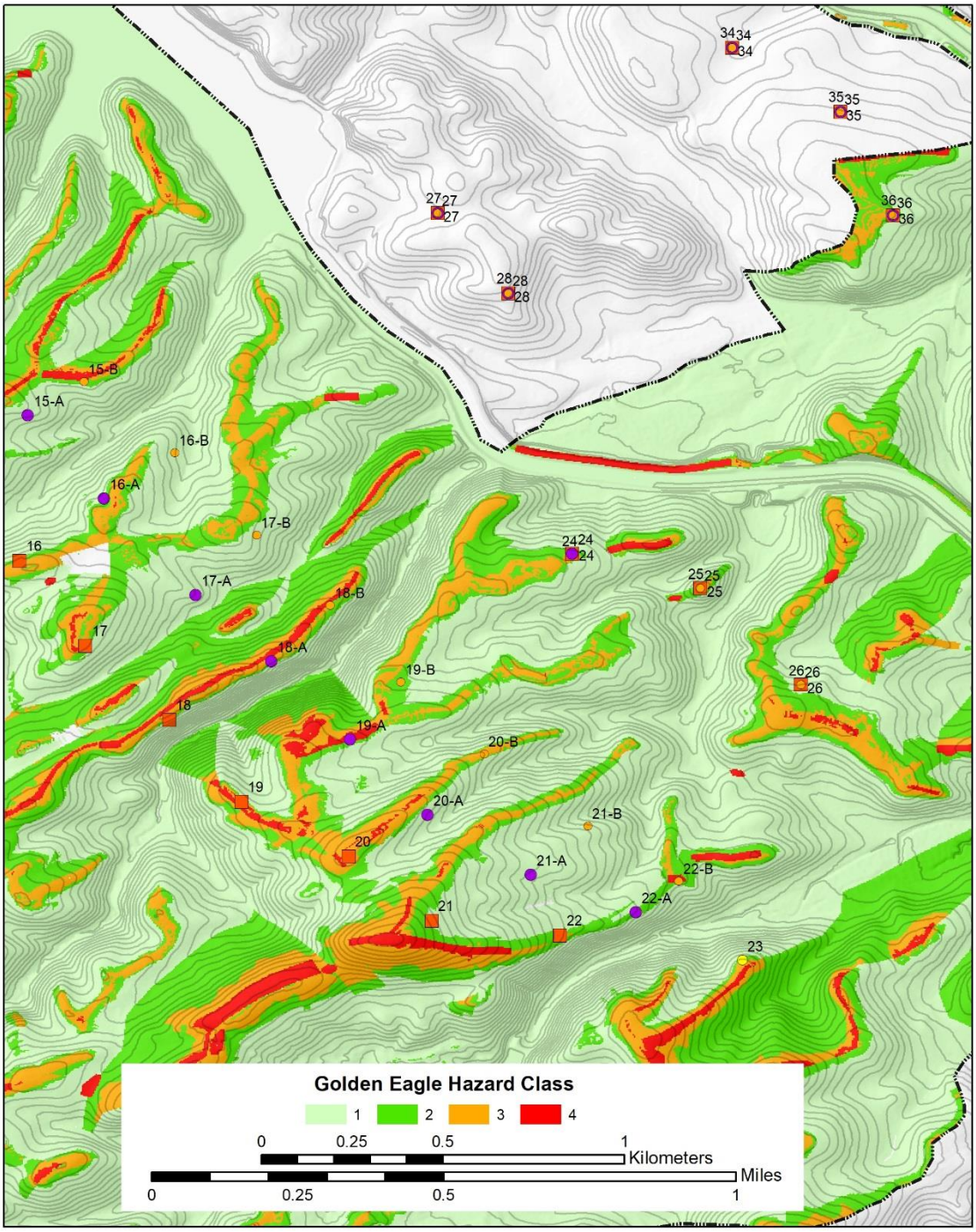

Figure 30. *Fuzzy Logic likelihood surface classes of golden eagle telemetry, flight behavior and fatality locations across the central portion of the Sand Hill project area, Altamont Pass Wind Resources Area, California, where red corresponds with the highest likelihood of golden eagle collision, orange corresponds with the second highest likelihood, yellow corresponds with the third highest likelihood, and dark green corresponds with the least likelihood.*

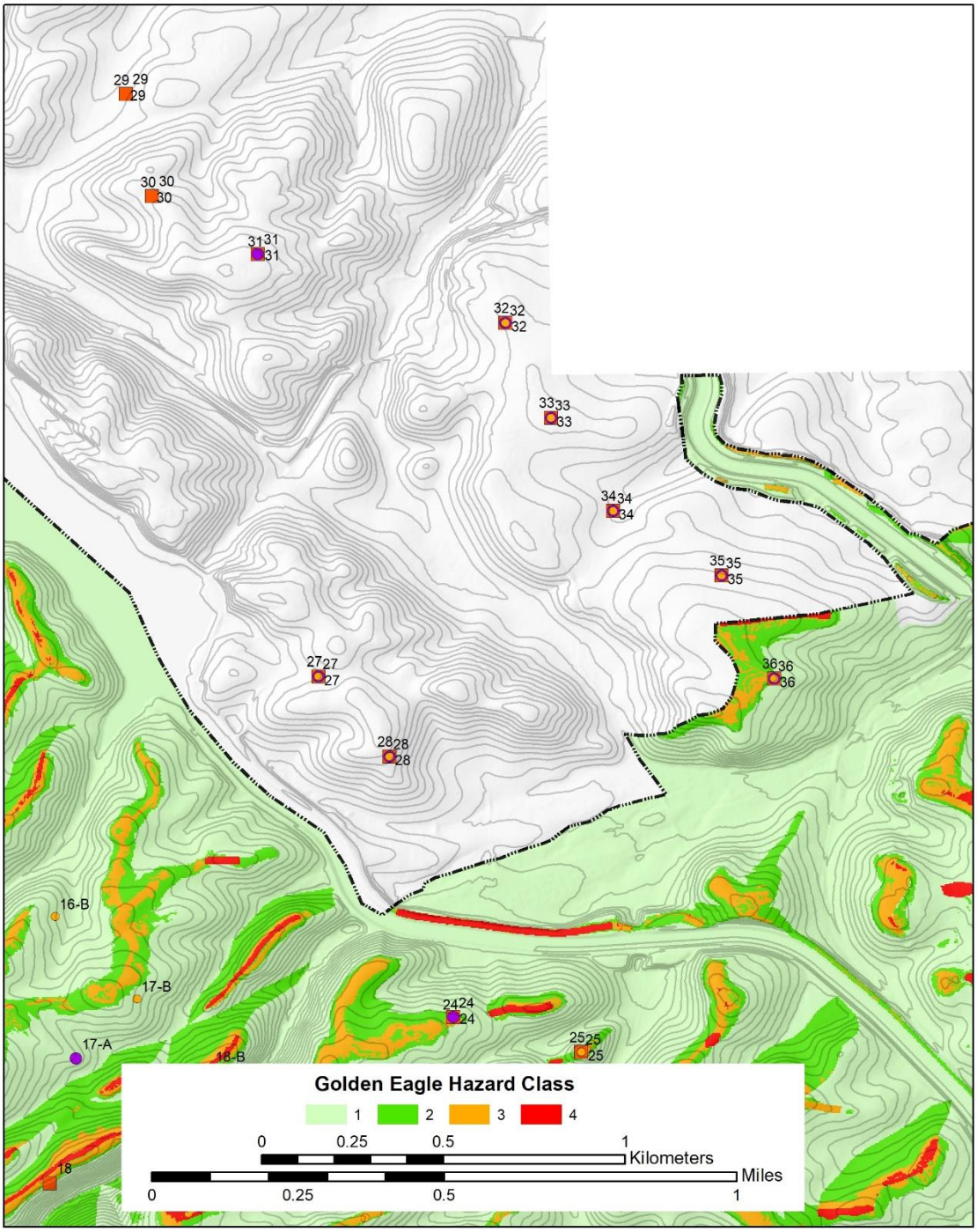

Figure 31. *Fuzzy Logic likelihood surface classes of golden eagle telemetry, flight behavior and fatality locations across the northeastern portion of the Sand Hill project area, Altamont Pass Wind Resources Area, California, where red corresponds with the highest likelihood of golden eagle collision, orange corresponds with the second highest likelihood, yellow corresponds with the third highest likelihood, and dark green corresponds with the least likelihood.*

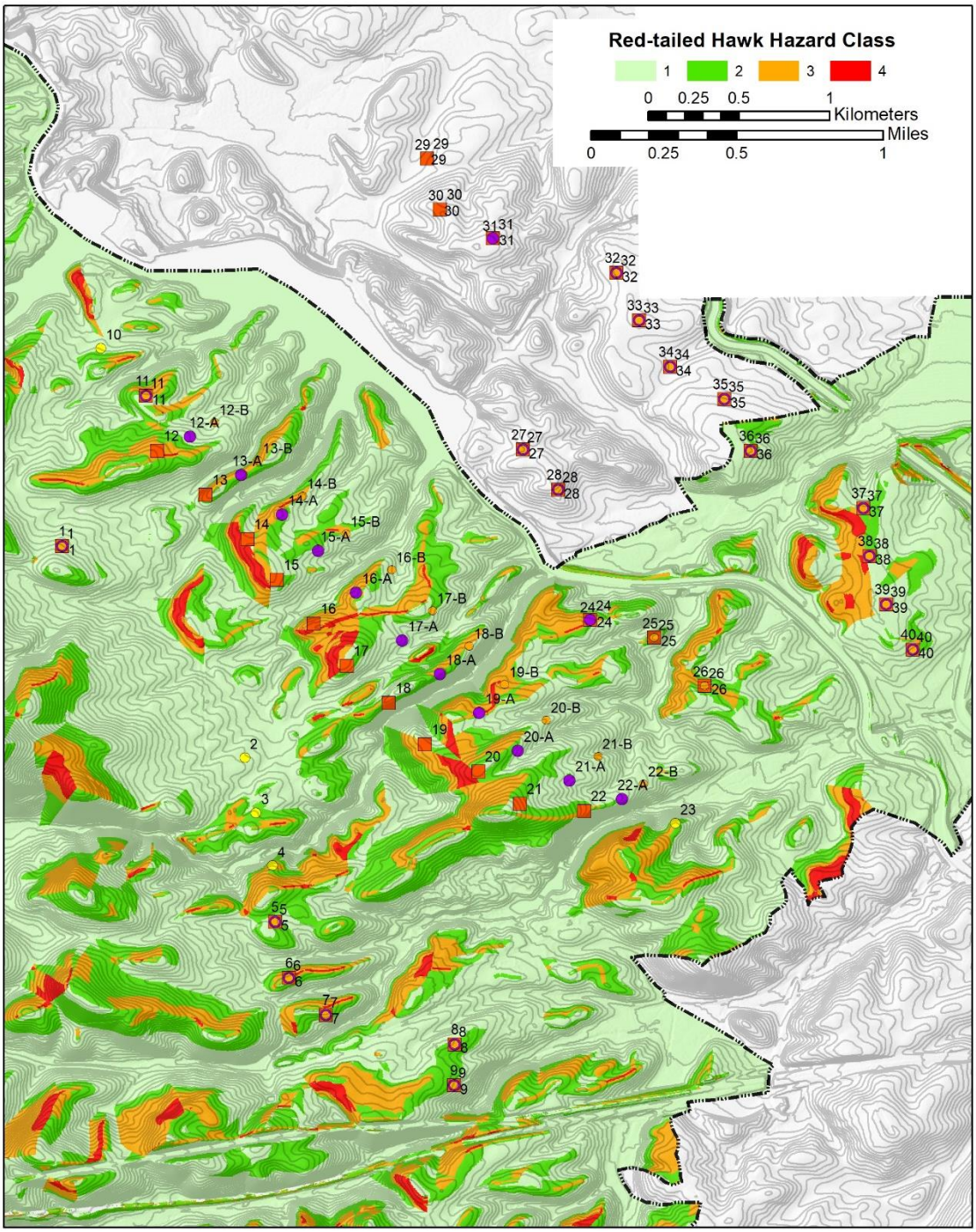

Figure 32. *Fuzzy Logic likelihood surface classes of red-tailed hawk flight behavior and fatality locations across the Sand Hill project area, Altamont Pass Wind Resources Area, California, where red corresponds with the highest likelihood of golden eagle collision, orange corresponds with the second highest likelihood, yellow corresponds with the third highest likelihood, and dark green corresponds with the least likelihood.*

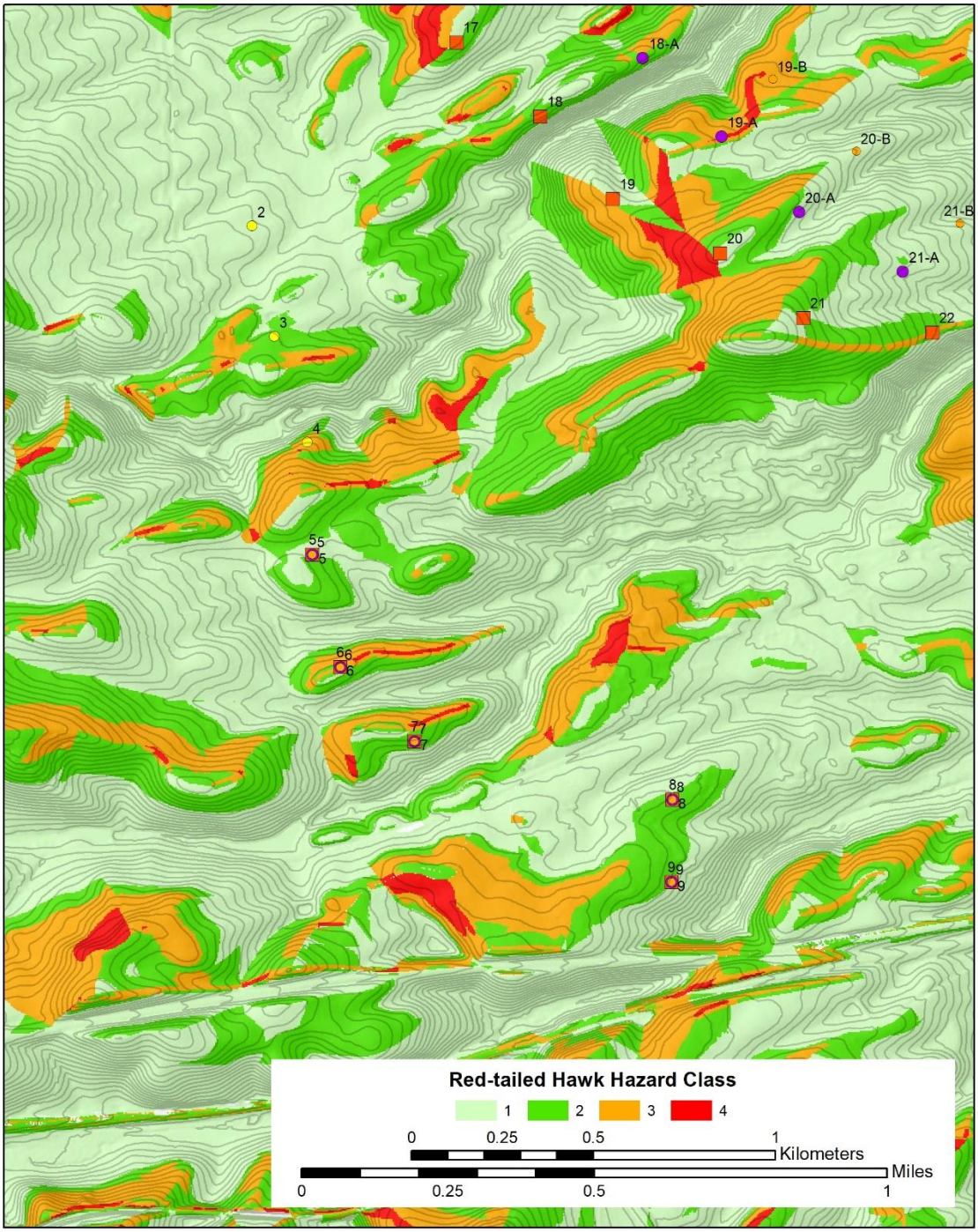

Figure 33. *Fuzzy Logic likelihood surface classes of red-tailed hawk flight behavior and fatality locations across the southwest portion of the Sand Hill project area, Altamont Pass Wind Resources Area, California, where red corresponds with the highest likelihood of golden eagle collision, orange corresponds with the second highest likelihood, yellow corresponds with the third highest likelihood, and dark green corresponds with the least likelihood.*

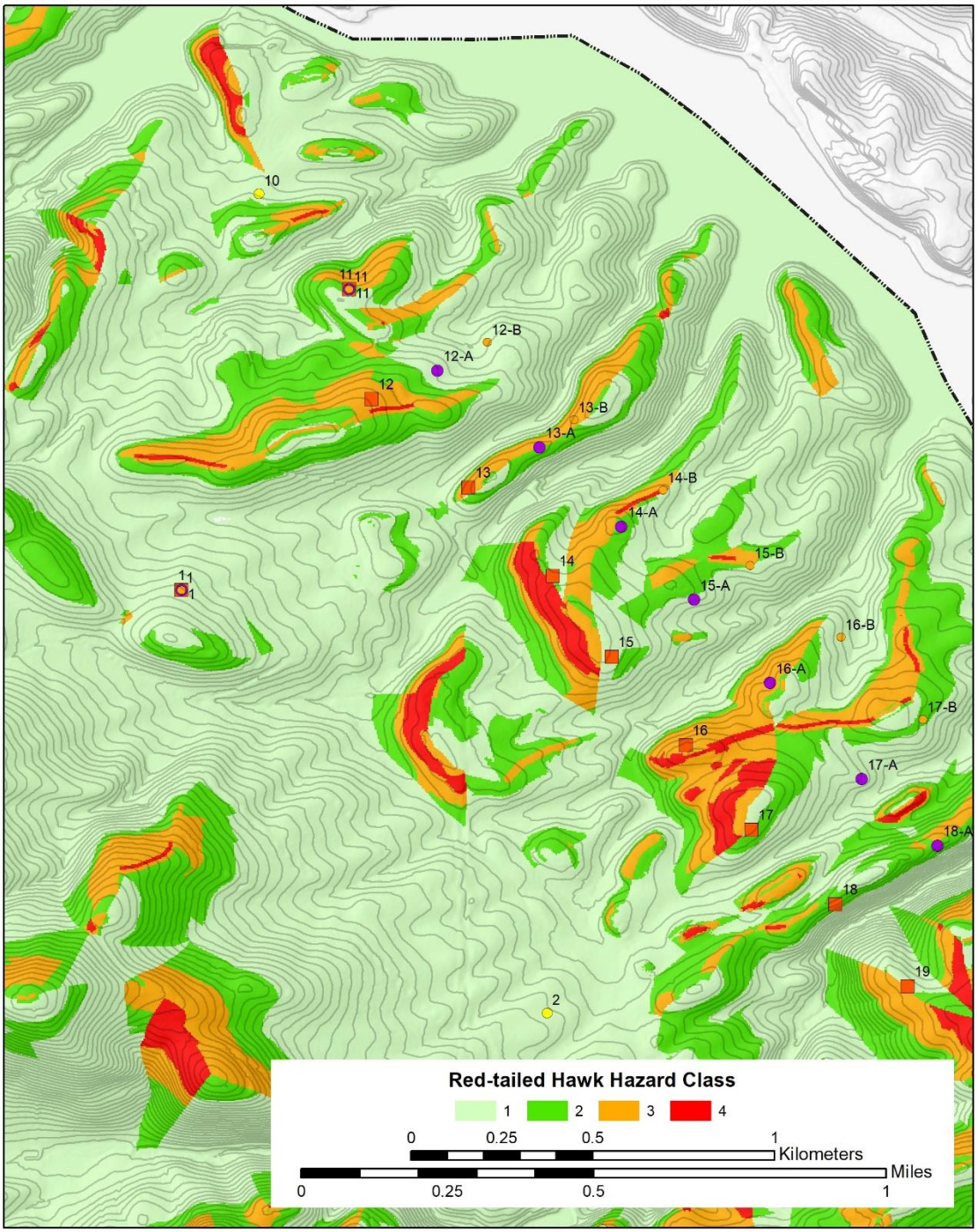

Figure 34. *Fuzzy Logic likelihood surface classes of red-tailed hawk flight behavior and fatality locations across the northcentral portion of the Sand Hill project area, Altamont Pass Wind Resources Area, California, where red corresponds with the highest likelihood of golden eagle collision, orange corresponds with the second highest likelihood, yellow corresponds with the third highest likelihood, and dark green corresponds with the least likelihood.*

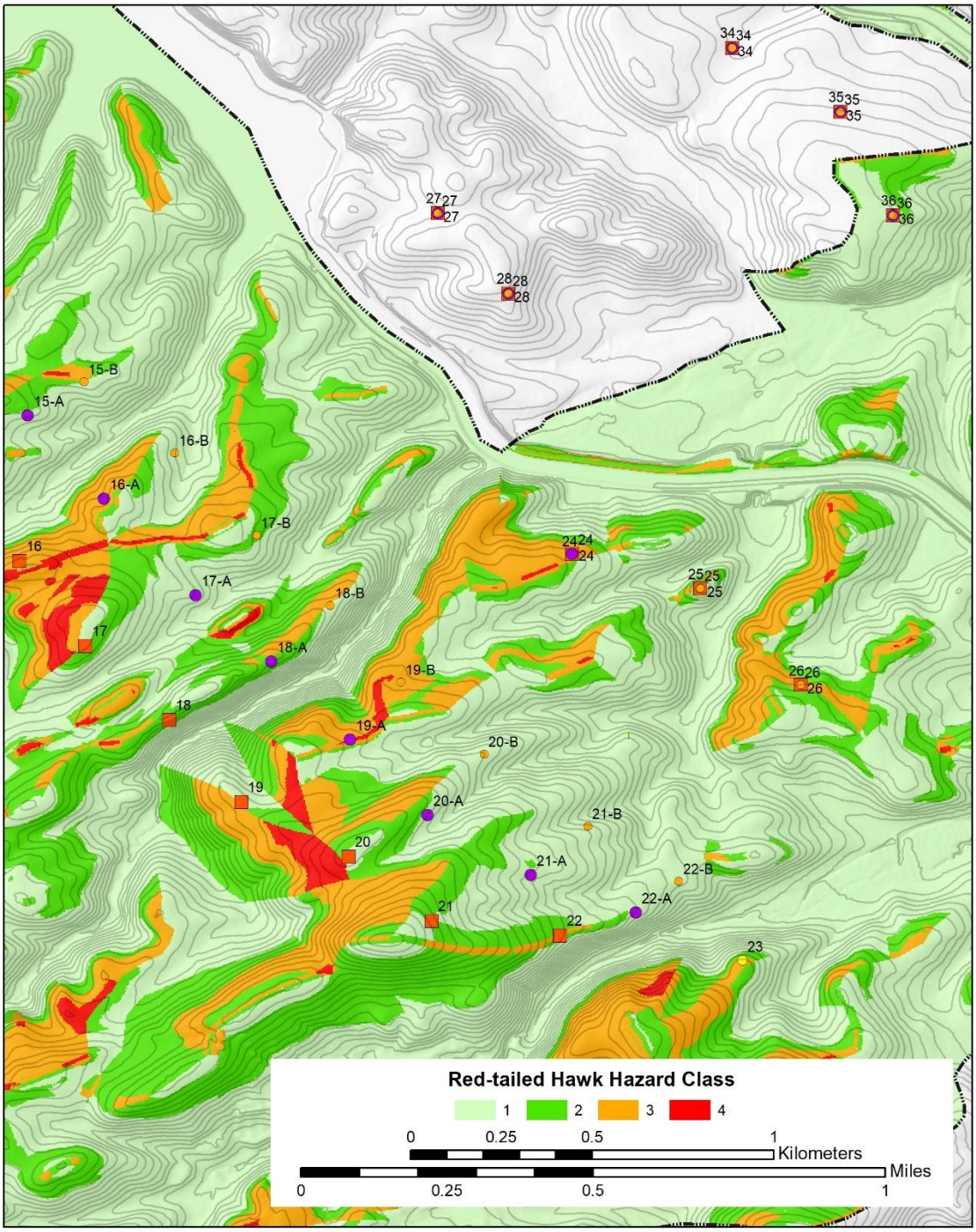

Figure 35. *Fuzzy Logic likelihood surface classes of red-tailed hawk flight behavior and fatality locations across the central portion of the Sand Hill project area, Altamont Pass Wind Resources Area, California, where red corresponds with the highest likelihood of golden eagle collision, orange corresponds with the second highest likelihood, yellow corresponds with the third highest likelihood, and dark green corresponds with the least likelihood.*

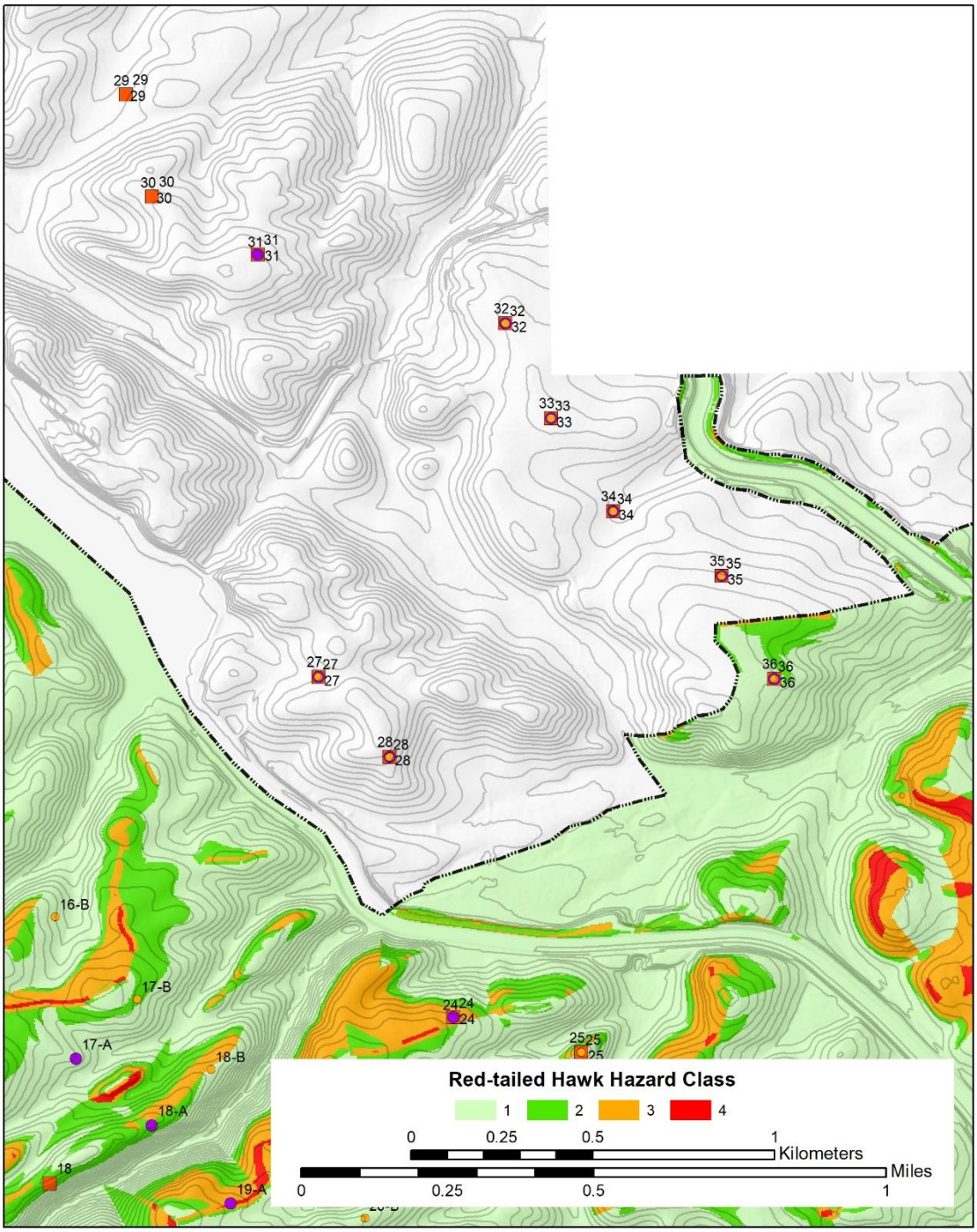

Figure 36. *Fuzzy Logic likelihood surface classes of red-tailed hawk flight behavior and fatality locations across the northeastern portion of the Sand Hill project area, Altamont Pass Wind Resources Area, California, where red corresponds with the highest likelihood of golden eagle collision, orange corresponds with the second highest likelihood, yellow corresponds with the third highest likelihood, and dark green corresponds with the least likelihood.*

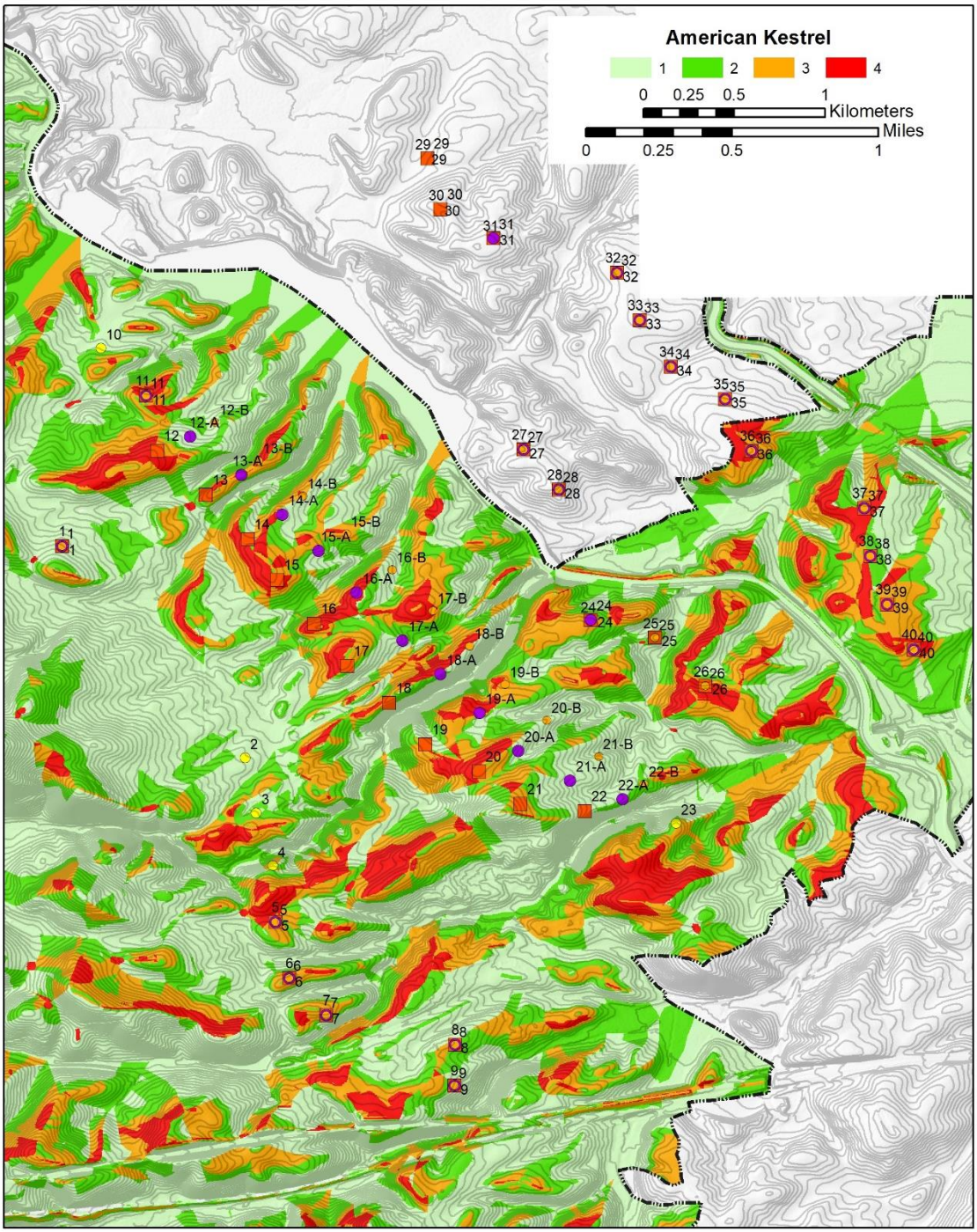

Figure 37. *Fuzzy Logic likelihood surface classes of American kestrel flight behavior and fatality locations across the Sand Hill project area, Altamont Pass Wind Resources Area, California, where red corresponds with the highest likelihood of golden eagle collision, orange corresponds with the second highest likelihood, yellow corresponds with the third highest likelihood, and dark green corresponds with the least likelihood.*

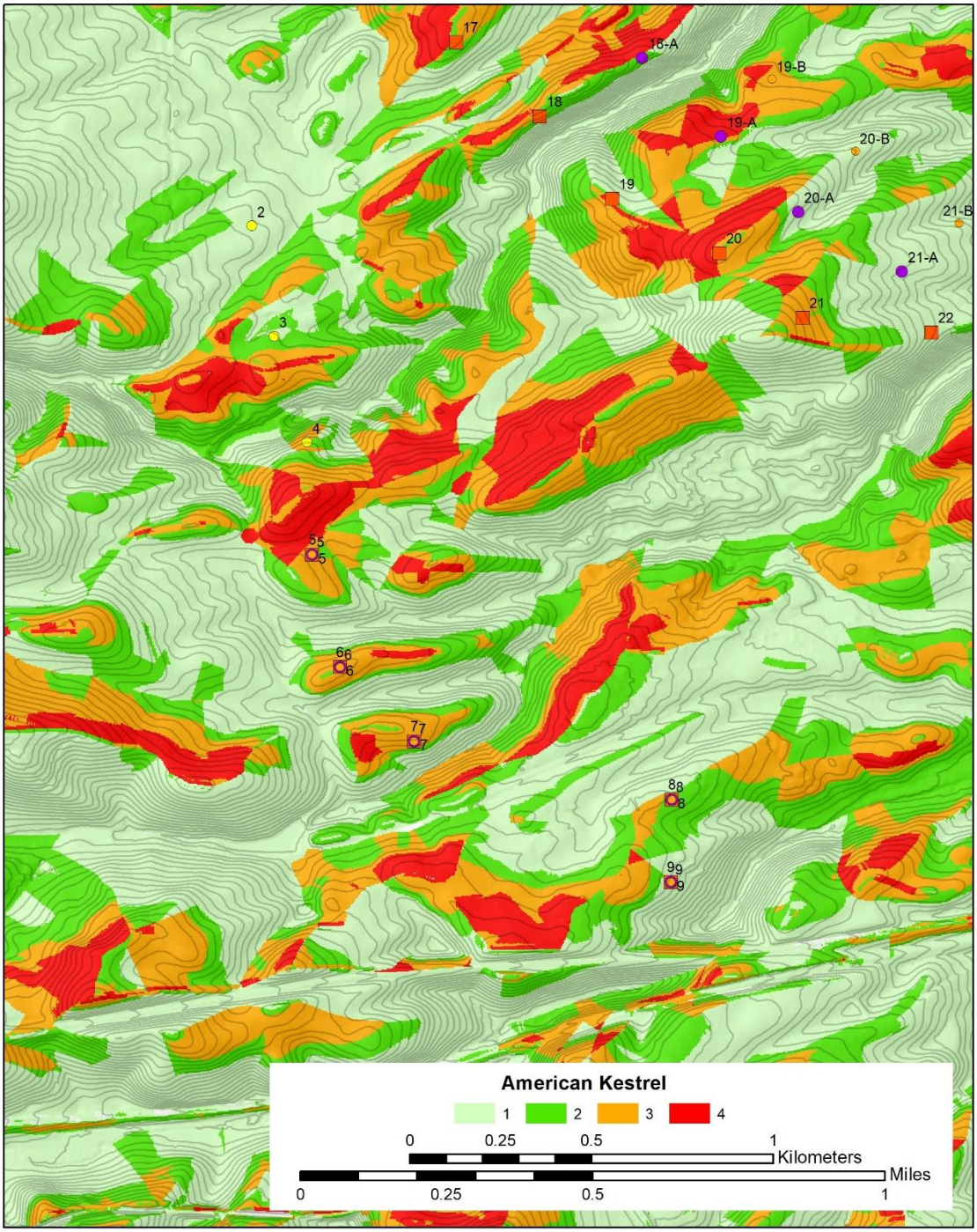

Figure 38. *Fuzzy Logic likelihood surface classes of American kestrel flight behavior and fatality locations across the southwest portion of the Sand Hill project area, Altamont Pass Wind Resources Area, California, where red corresponds with the highest likelihood of golden eagle collision, orange corresponds with the second highest likelihood, yellow corresponds with the third highest likelihood, and dark green corresponds with the least likelihood.*

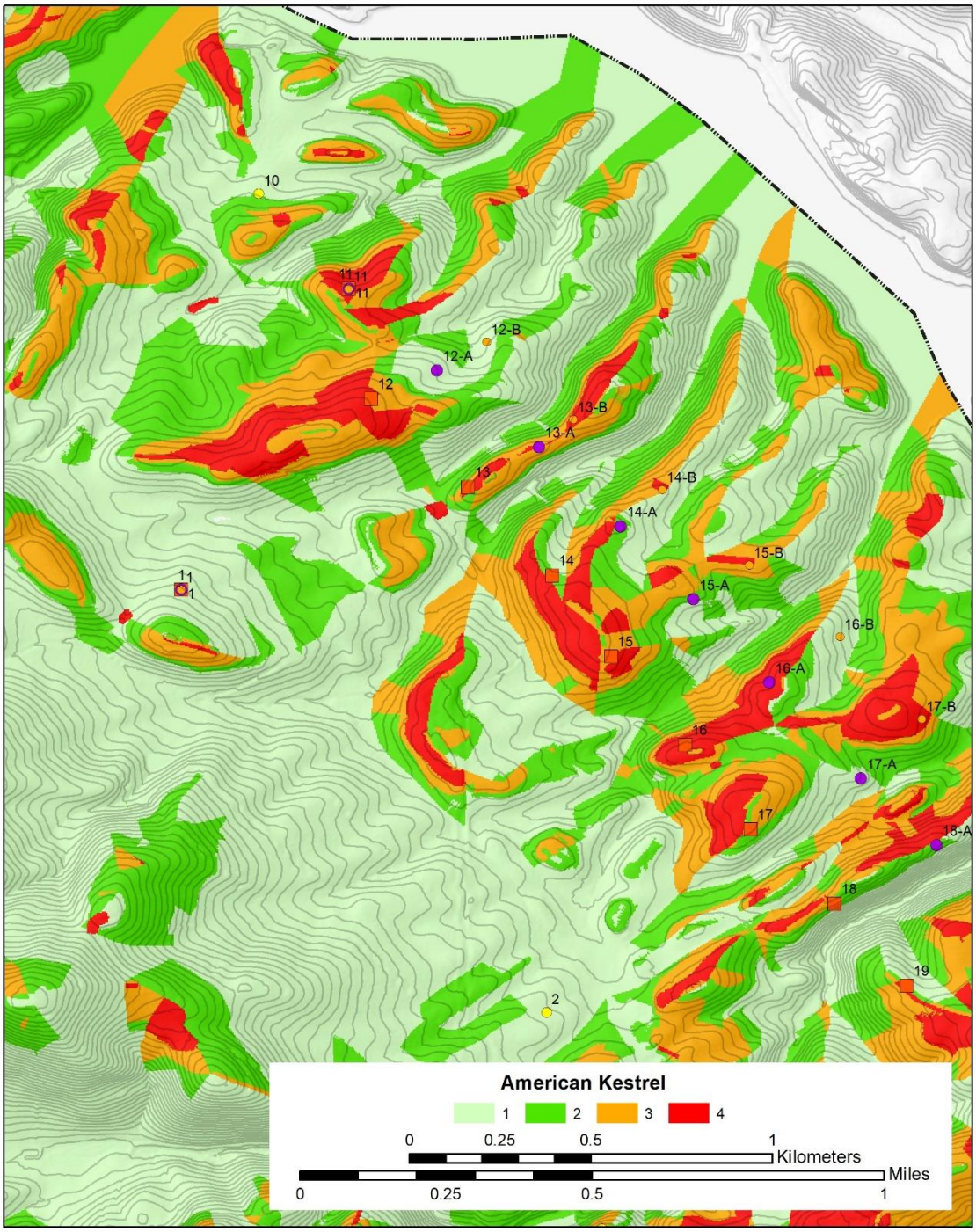

Figure 39. *Fuzzy Logic likelihood surface classes of American kestrel flight behavior and fatality locations across the northcentral portion of the Sand Hill project area, Altamont Pass Wind Resources Area, California, where red corresponds with the highest likelihood of golden eagle collision, orange corresponds with the second highest likelihood, yellow corresponds with the third highest likelihood, and dark green corresponds with the least likelihood.*

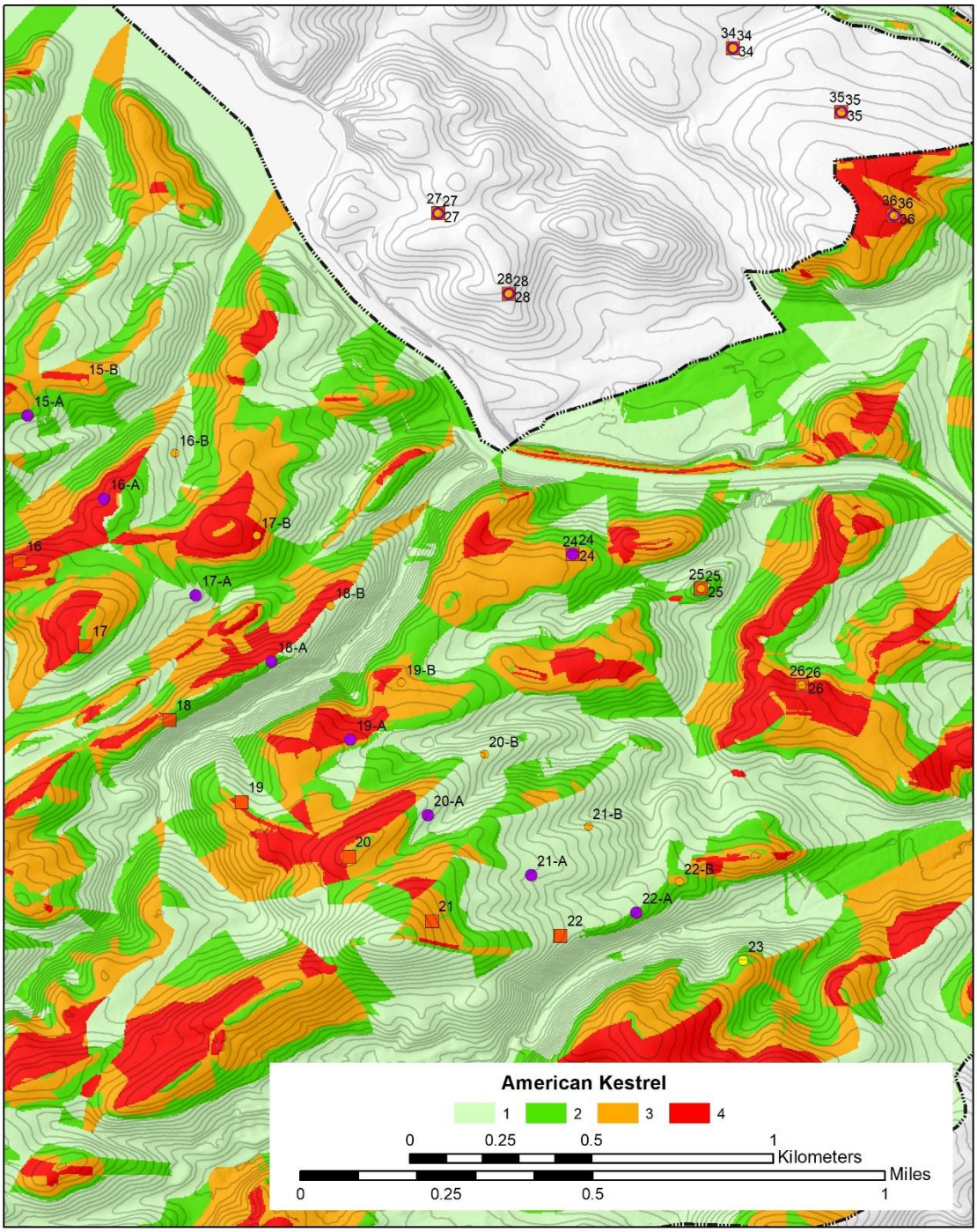

Figure 40. *Fuzzy Logic likelihood surface classes of American kestrel flight behavior and fatality locations across the central portion of the Sand Hill project area, Altamont Pass Wind Resources Area, California, where red corresponds with the highest likelihood of golden eagle collision, orange corresponds with the second highest likelihood, yellow corresponds with the third highest likelihood, and dark green corresponds with the least likelihood.*

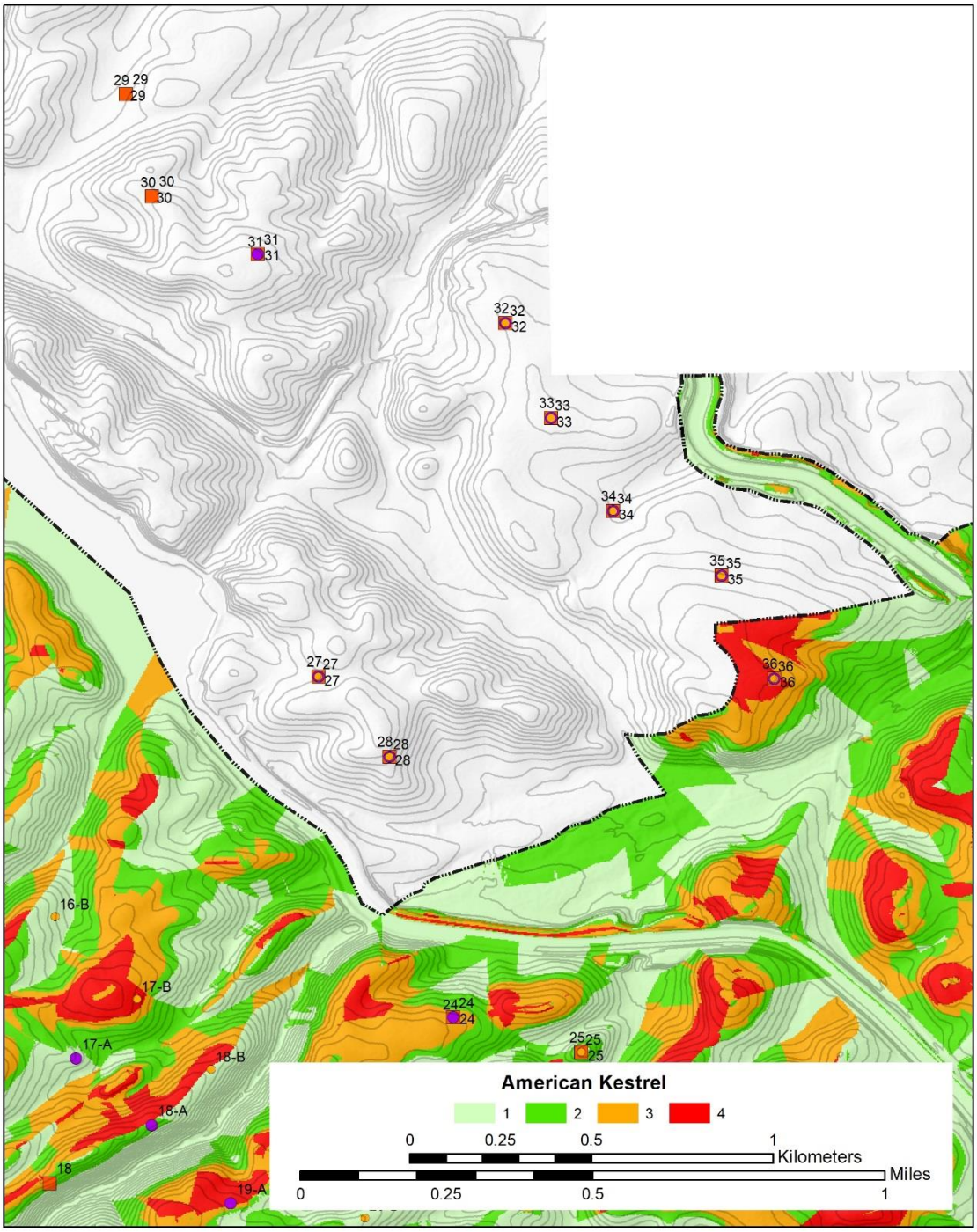

Figure 41. *Fuzzy Logic likelihood surface classes of American kestrel flight behavior and fatality locations across the northeastern portion of the Sand Hill project area, Altamont Pass Wind Resources Area, California, where red corresponds with the highest likelihood of golden eagle collision, orange corresponds with the second highest likelihood, yellow corresponds with the third highest likelihood, and dark green corresponds with the least likelihood.*

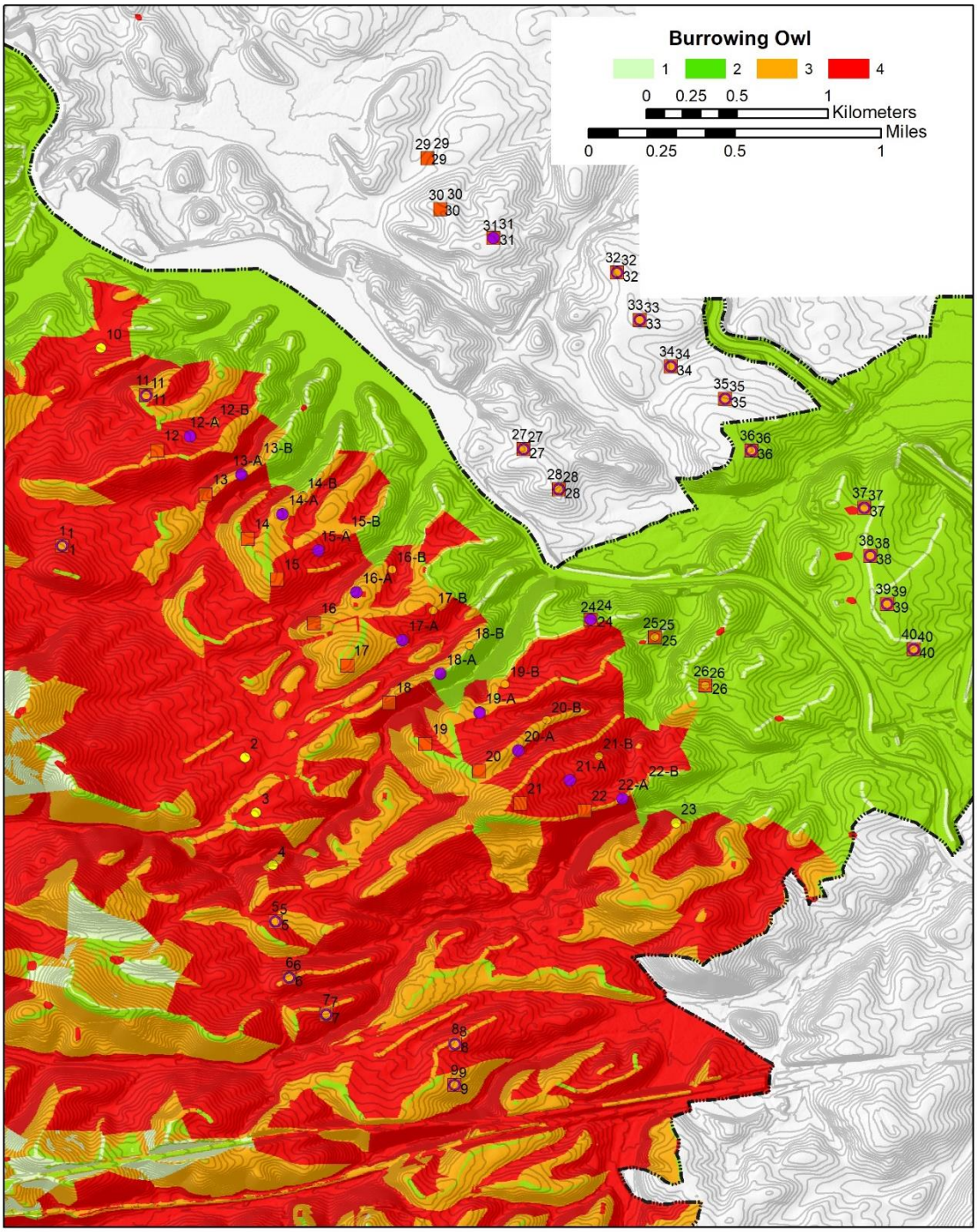

Figure 42. *Fuzzy Logic likelihood surface classes of burrowing owl fatality locations across the Sand Hill project area, Altamont Pass Wind Resources Area, California, where red corresponds with the highest likelihood of golden eagle collision, orange corresponds with the second highest likelihood, yellow corresponds with the third highest likelihood, and dark green corresponds with the least likelihood.*

Figure 43. *Fuzzy Logic likelihood surface classes of burrowing owl fatality locations across the northcentral portion of the Sand Hill project area, Altamont Pass Wind Resources Area, California, where red corresponds with the highest likelihood of golden eagle collision, orange corresponds with the second highest likelihood, yellow corresponds with the third highest likelihood, and dark green corresponds with the least likelihood.*

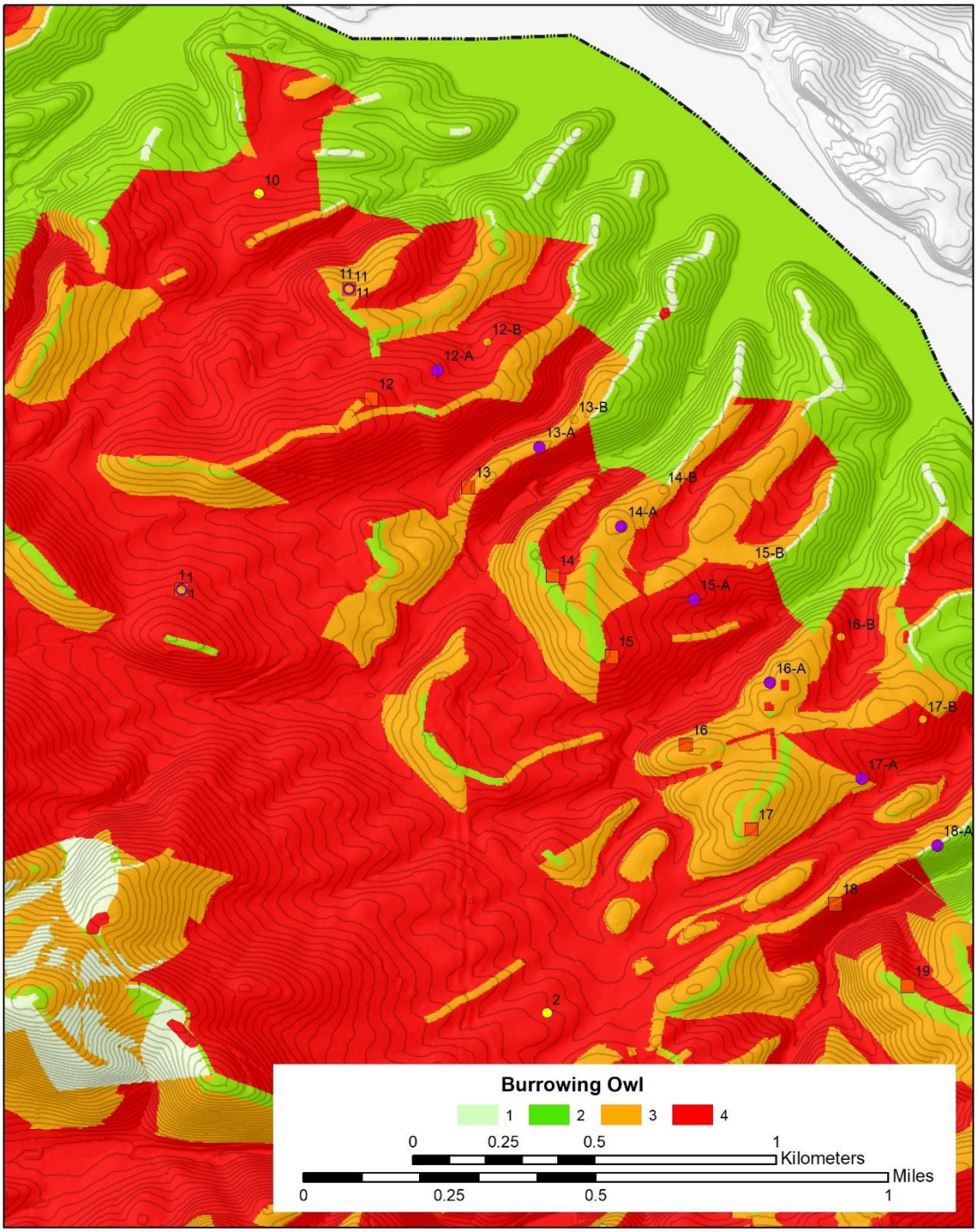

Figure 44. *Fuzzy Logic likelihood surface classes of burrowing owl fatality locations across the central portion of the Sand Hill project area, Altamont Pass Wind Resources Area, California, where red corresponds with the highest likelihood of golden eagle collision, orange corresponds with the second highest likelihood, yellow corresponds with the third highest likelihood, and dark green corresponds with the least likelihood.*

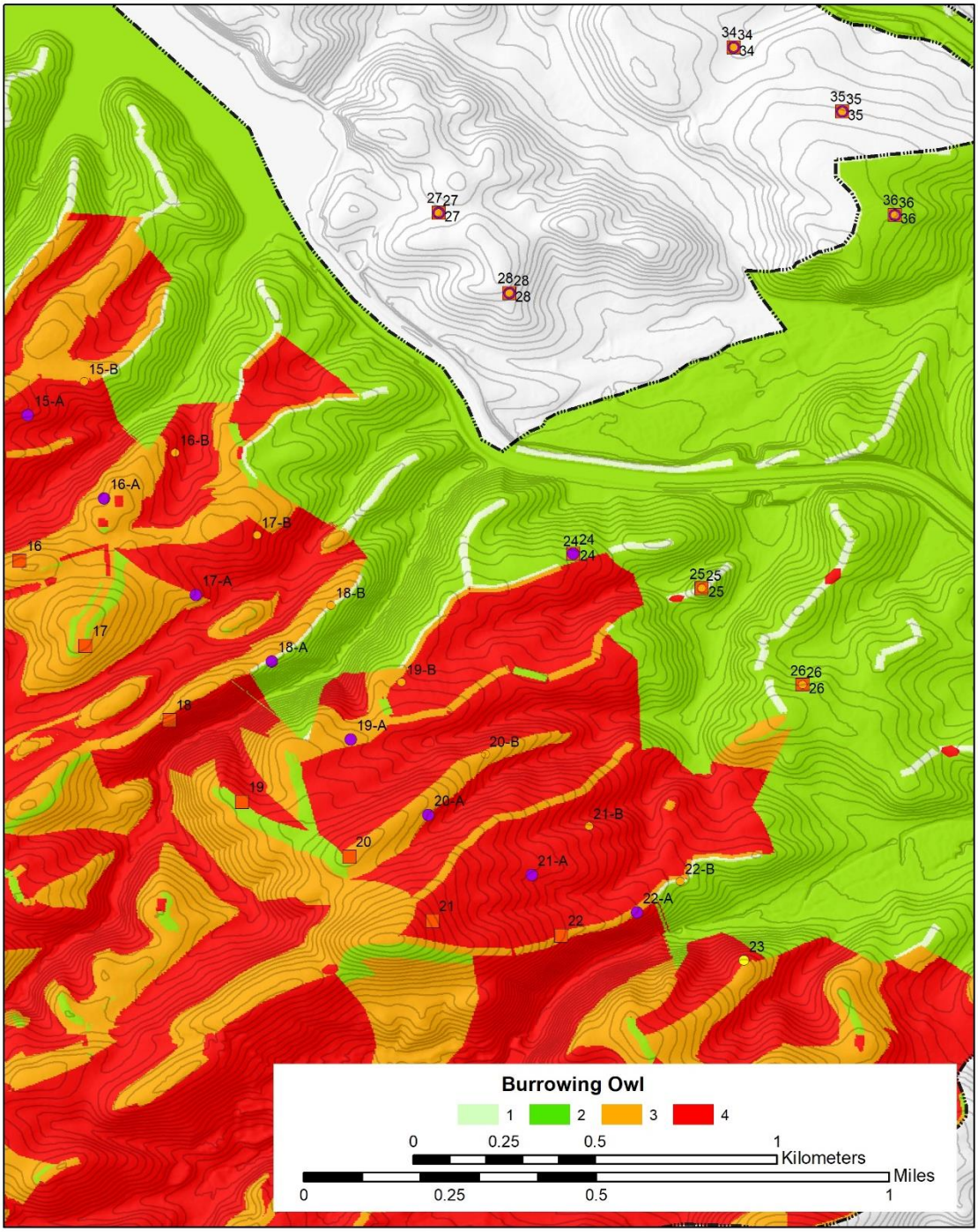

Figure 45. *Fuzzy Logic likelihood surface classes of burrowing owl fatality locations across the northeastern portion of the Sand Hill project area, Altamont Pass Wind Resources Area, California, where red corresponds with the highest likelihood of golden eagle collision, orange corresponds with the second highest likelihood, yellow corresponds with the third highest likelihood, and dark green corresponds with the least likelihood.*

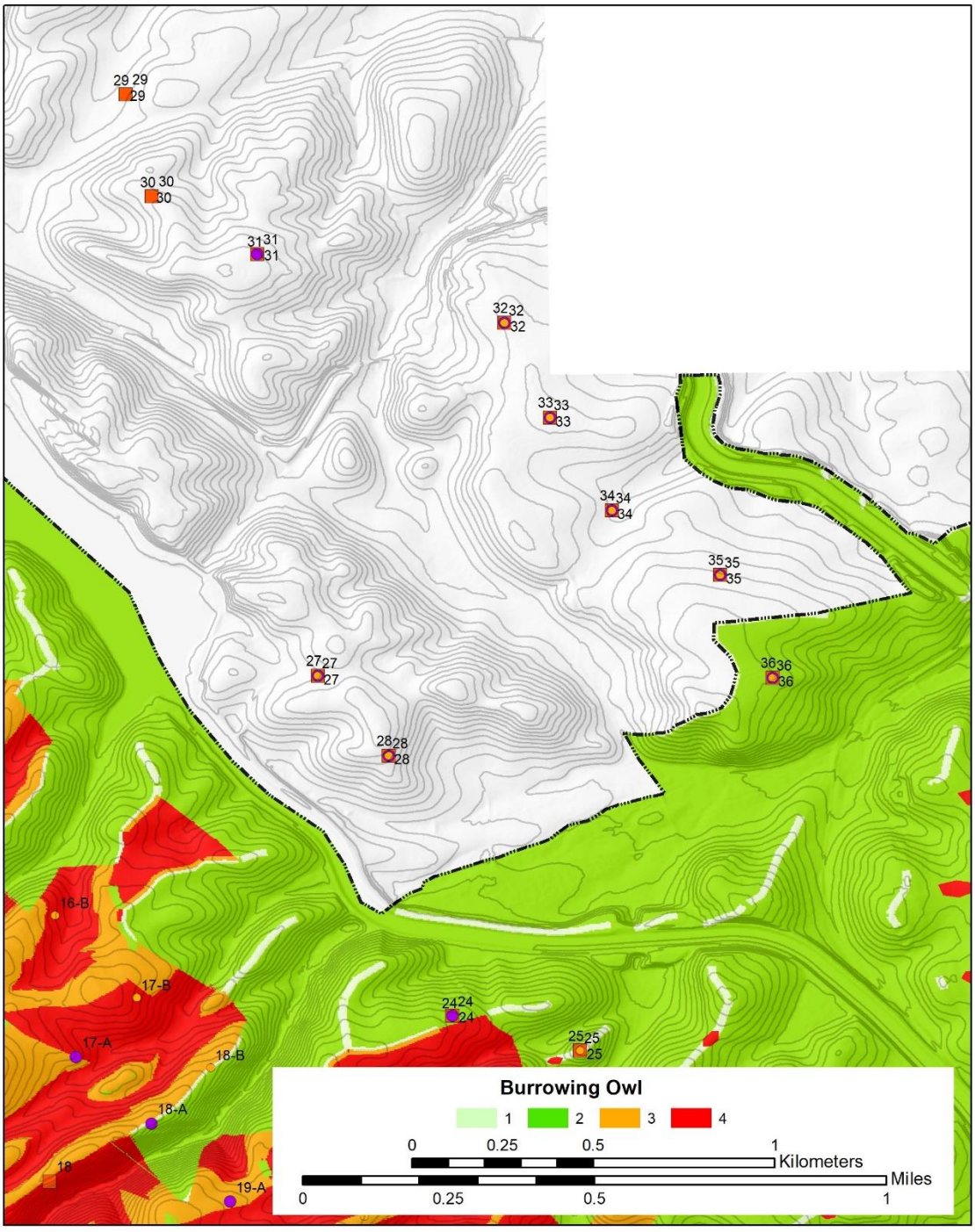

Figure 46. *Fuzzy Logic likelihood surface classes of burrowing owl fatality locations across the northeastern portion of the Sand Hill project area, Altamont Pass Wind Resources Area, California, where red corresponds with the highest likelihood of golden eagle collision, orange corresponds with the second highest likelihood, yellow corresponds with the third highest likelihood, and dark green corresponds with the least likelihood.*

DISCUSSION

We produced simple map-based collision hazard models of golden eagle telemetry positions, ridge crossing flights, wind turbine events, and wind turbine fatalities, as well as of red-tailed hawk and American kestrel flight behaviors and fatalities in the Altamont Pass Wind Resource Area. We also produced a simple collision hazard model of burrowing owls based on fatalities at wind turbines and further informed by burrow locations. We extended these models to the Sand Hill project area for which we had developed a DEM and terrain measurements. Most of these areas also included stations where flight behavior data were collected and sampling plots where burrowing owl burrow data were collected for developing the collision hazard models. Micro-siting according to these models and expert opinion should generally achieve the levels of fatality reductions observed at the repowered Vasco Winds project, although it is likely that fatality reductions will not be as great for burrowing owl. After three years of operations at Vasco Winds, and compared to the old-generation wind project that preceded it, Brown et al. (2016) estimated fatality rate reductions of 75% to 82% for golden eagle, 34% to 47% for red-tailed hawk, and 48% to 57% for American kestrel, and 45% to 59% for burrowing owl.

Table 11 summarizes the coincidences of proposed wind turbine locations with Smallwood's SRC-style hazard rating made upon site inspections, predicted fuzzy logic collision hazard classes, and fatality monitoring histories for golden eagle, red-tailed hawk, American kestrel and burrowing owl. Proposed turbine sites where Smallwood made SRC-style hazard ratings of 8 or greater should be reconsidered, and Table 12 should be consulted for recommended relocations. Ratings of 6.5 to 7.5 were worrying to Smallwood, but sufficient uncertainty remains that relocations are not always warranted. Some terrain settings posed collision hazard risks that were difficult to predict or outside our experience, such as turbine sites on very narrow east-west ridge structures such as sites 20B or 18 to 18-B. Another example of an uncertain site was site 10, where several valley-like structures come together in low terrain. Site 25 – a small hill surrounded by larger hill and ridge structures – will not be predicted as particularly hazardous by our models, but based on all that we have experienced in the APWRA, we judged it to be high risk. Golden eagles approaching site 25 will be at altitudes established by the surrounding higher-elevation terrain, thereby putting them at rotor-height when encountering site 25. Table 12 also warns of many situations where in our experience the grading for turbine pads will likely leave berms or cut slopes located between the tower base and the prevailing upwind direction. Golden eagles or other birds approaching the turbine from the prevailing wind direction will need to clear the ground just upwind of the turbine, putting the bird into the rotor. Such berms or cut slopes shorten the effective height above ground of the low reach of the turbine blades – from the bird's perspective, an 8-m berm might shorten the low reach of the blades from 28 m to 20 m, thereby lessening the room to negotiate the blade sweeps.

Map-based collision hazard maps need to be interpreted carefully, meaning the hazards of specific terrain and wind situations – ridge saddles, apices of southwest and northwest-facing concave slopes, and breaks in slope – should always trump model predictions. The turbine sites causing us the greatest concern at Sand Hill include 4, 16-A, 16-B, 17-A, 20-A, 21, 25, and 34 (Table 12). In Table 12 we also recommend using particular alternative sites over others, and we recommend numerous relocations to avoid hazardous situations.

At some sites we know from experience that golden eagle traffic has been intense, or that social interactions are common. At these locations we are inclined to rely more on experience in the field than on model predictions. As examples, we know that golden eagles often fly through a certain canyon, exiting east toward proposed Sand Hill sites 3 and 4. As these eagles exist east they are moving fast as they glide downhill through the canyon with the wind, so when they reach the area of sites 3 and 4 they might have less time to negotiate the turbines, especially in cloudy conditions. In another example, Sand Hill site 1 is located east of a ridge saddle often used by eagles to cross the ridge structure west of site 1. Our models were unable to predict collision hazard posed by some associations between terrain features affecting flight patterns at coarse resolutions, such as flight trajectories set by canyons, long ravines or nearby ridge saddles used as crossing points.

As earlier discussed, the effects of grading for turbine access roads and tower pads also need to be considered, because they are not anticipated in the collision hazard models. Changes in the shape of the hills due to grading can transform the location to a more hazardous situation than was assessed herein. It would be safer to avoid enhancing ridge saddles or breaks in slope due to grading. It would also be safer to not leave earthen berms upwind of turbine towers, because doing so decreases the effective vertical space between the low reach of turbine blades and the ground that birds need to clear.

Whereas we focused on four target raptor species, Sand Hill could have adverse impacts on bats and small birds. We developed no collision hazard maps for bats or small birds. Recent research has revealed that modern wind turbines in the AWPRA take many small birds and bats (Brown et al. 2016, Smallwood 2017c, Smallwood et al. 2017 unpublished data). Bats might be attracted to modern wind turbines, thereby increasing collision risk (Smallwood 2016b).

We also found cause to support many of the proposed wind turbine locations from a micro-siting perspective. As much as we worry about every proposed location due to the inherent risk to birds and bats, our working philosophy is that once the project capacity has been decided upon, the wind turbines to meet that capacity must go someplace. We make our recommendations on micro-siting based on the wind company's proposed capacity, and nothing more. Proposed turbine sites that we believe pose the least collision risk, including as recommended for slight relocations in Table 12, were sites 2, 3, 5, 6, 7, 11, 12-A, 12-B, 14-A, 15, 16, 17, 18, 19-B, 21-A, 24, 30, 32, 33, 35, 38, 39.

Grading for pads in complex terrain has created unsafe situations for golden eagles and other raptors by leaving berms or cut slopes in the prevailing upwind direction (Smallwood 2018, attached). We recommend avoiding pad excavations that create or enhance ridge saddles or breaks in slope, because eagles use them for passage, they alter winds at the interface between the cut slope and natural slope, and eagles approaching a rotor just above grade-level will have less room to maneuver when crossing into the airspace between the pad and rotor.

Table 11. *Micro-siting recommendations directed to Sand Hill wind turbine layout, where GOEA = golden eagle, RTHA = red-tailed hawk, AMKE = American kestrel, and BUOW = burrowing owl. Additional acronyms are BNOW = barn owl, GHOW = great-horned owl, and TUVU = turkey vulture. Birds represent species other than raptors. Values in parentheses represented hazard classes very close to the proposed turbine site. 'Yrs' represented the number of years of monitoring.*

Site	SRC hazard rating	Predicted hazard class				Nearest old turbines	SRC ratings old turbines	Collision history
		GOEA	RTHA	AMKE	BUOW			
1	8.5	1	1	1	4	Far away		No history available
2	6	1	1	1	4	Far away		No history available
3	6	1	2	2	4	VK-16, VK-17	7, 7.5	1 BUOW, 1 GHOW, 9 birds – 10 yrs
4	10	3	3	3	3	M-1, M-2	8.5, 7.5	2 RTHA, 2 BUOW, 6 birds – 10 yrs
5	6	1	1	3	4	K-11	<7	1 bird – 10 yrs
6	7	3	3	3	3 (4)	J-10, J-9	--, --	4 birds – 8 yrs
7	6.5	1	2	3	4	F-5, F-4	<7, <7	1 BUOW, 5 birds – 9 yrs
8	8	3	2	2	3	PO-27, PO-28	<7, <7	1 RTHA, 1 BUOW, 38 birds – 9 yrs
9	7	1	2	1	3	WM-24	--	1 TUVU, 1 bird – 6 yrs
10	7.5	1	1	1 (2)	4	Far away		No history available
11	4	4	2 (3)	4	3	6363, 6364	<7, <7	2 birds – 6 yrs
12	7	2	3	4	4	6375	7	3 birds – 6 yrs
12A	6	1	1	1	4	6375	7	3 birds – 6 yrs
12B	6	1	1	1	4	6357	7	7 birds – 5 yrs
13	7	1	3	4	3	6393, 6394	7, 7	1 GOEA, 1 RTHA, 8 birds – 3.5 yrs
13A	8	3	2 (3)	3	3	6392	<7	No birds – 0 yrs
13B	8.5	3	3	4	3	6392	<7	No birds – 0 yrs
14	7.5	3	2 (4)	2 (4)	4	6441-6443	8, 7, 7	1 GOEA, 1 Buteo, 3 birds – 3.5 yrs
14A	6.5	2	2	2	3	6427, 6428	--, --	1 RTHA, 2 birds – 1 yr
14B	7	3	4	4	3	6410, 6411	<7, <7	No birds – 0 yrs
15	6	2 (3)	1	3(4)	4	6453, 6452	<7, --	3 birds – 3.5 yrs
15A	6.5	1	1	2	4	6434	<7	No birds – 0 yrs
15B	6.5	2 (4)	3	4	4	6422, 6421	<7, <7	No birds – 0 yrs
16	7	3	3	4	3	6489, 6490	<7, 7.5	1 RTHA, 1 AMKE, 4 birds – 3.5 yrs

Site	SRC hazard rating	Predicted hazard class				Nearest old turbines	SRC ratings old turbines	Collision history
		GOEA	RTHA	AMKE	BUOW			
16A	7	2	3	4	3	6477-6479	7.5, <7, <7	2 GOEA, 5 RTHA, 1 Buteo, 1 Raptor, 1 GHOW, 1 TUVU, 17 birds – 7.5 yrs
16B	8.5	1	1	1	4	Far away		No history available
17	6	3	1	2 (3/4)	3	6498	<7	1 BUOW, 3 birds – 3.5 yrs
17A	8	1	1	1	3 (4)	Far away		No history available
17B	7.5	1	2	4	4	Far away		No history available
18	7	3	2	2 (3)	3 (4)	Far away		No history available
18A	7	3 (4)	2	2	3	Far away		No history available
18B	7	2 (4)	1 (3)	1 (4)	3	Far away		No history available
19	6	4	1 (3)	2 (4)	2 (4)	Far away		No history available
19A	6	4	4	4	3	Far away		No history available
19B	5	2	3	3	4	Far away		No history available
20	8	3 (4)	1	3 (4)	3	Far away		No history available
20A	9.5	1	1	1	3 (4)	Far away		No history available
20B	8	3	1	1	3 (4)	Far away		No history available
21	8	2	1	3	4	Far away		No history available
21A	6	1	1	1	4	Far away		No history available
21B	6	1	1	1	4	Far away		No history available
22	8.5	2	3	1	3 (4)	Far away		No history available
22A	7.5	2	1	2	3 (4)	Far away		No history available
22B	7.5	4	1	3	3 (4)	Far away		No history available
23	8	2 (3)	3	2	4	Far away		No history available
24	6	2	3	3	2	Far away		No history available
25	9	3	3	2	2	Far away		No history available
26	8	1	3	4	2	Far away		No history available
27	8	--	--	--	--	Far away		No history available
28	8	--	--	--	--	Far away		No history available
29	8	--	--	--	--	Far away		No history available
30	6	--	--	--	--	Far away		No history available

Site	SRC hazard rating	Predicted hazard class				Nearest old turbines	SRC ratings old turbines	Collision history
		GOEA	RTHA	AMKE	BUOW			
31	4	--	--	--	--	Far away		No history available
32	3	--	--	--	--	Far away		No history available
33	4	--	--	--	--	Far away		No history available
34	8	--	--	--	--	Far away		No history available
35	5	--	--	--	--	Far away		No history available
36	7	3	1	4	2	Far away		No history available
37	8	4	3	4	4	CD-13	<7	1 BUOW, 13 birds – 11 yrs
38	6	2	2	2	2	CC-2	<7	1 bird – 11 yrs
39	6	2	1	3	2	AC-8, AC-9	<7, <7	1 RTHA, 1 bird – 8.5 yrs
40	7	1	1	3 (4)	2	AD-13, AD-14	<7, <7	15 birds – 11 yrs

Table 12. *Micro-siting recommendations directed to Sand Hill wind turbine layout, where GOEA = golden eagle, RTHA = red-tailed hawk, AMKE = American kestrel, and BUOW = burrowing owl, and E =east, W = west, and so on.*

Site	Concern	Suggested move/Recommendation
1	Near Vestas & near upwind saddle	Maybe move ENE 60 m
2	None	None
3	East of major E-W canyon, so likely more flight traffic here	No better options locally
4	In ravine on steep slope; documented RTHA hazard site	We recommend avoiding this site
5	None	Shift SW to hill peak
6	E-W ridge	Likely safest site on ridge
7	Low on slope of E-W ravine	Move to N ridge crest
8	E-W ridge; record of many bird collisions, but mostly rock pigeons	Likely safest local option
9	Low on slope	Shift west and uphill
10	Low spot where shallow valleys meet; model predictions safe except for BUOW	Uncertain about likely impacts here
11	Conflicts with model prediction	Safest place in area
12	Near N-S saddle	move 25 m west
12A	None	Safest place in area
12B	None	Safest place in area
13	Low terrain; documented eagle fatality	Move east to ridge crest
13A	Shallow saddle on E-W ridge; no monitoring history	Use modified site 13 or 13B
13B	Shallow saddle on E-W ridge; no monitoring history	Move east to peak of hill
14	West edge of E-W concave slope; documented eagle fatality	Use site 14A
14A	E-W ridge	Probably safest site on this ridge
14B	Low along E-W ridge	Use site 14A
15	Next to model-predicted class 3 hazard level and long ravine	Shift north 25 m
15A	On concave slope	Use site 15
15B	E-W ridge close to golden eagle hazard class 4	Use site 15
16	E-W ridge; edge of deep ravine	Avoid leaving berm
16A	Side of deep ravine; documented 2 golden eagle & 5 RTHA fatalities	We recommend avoiding this site
16B	Side of ravine; too low on slope	We recommend avoiding this site
17	Edge of ravine	Move north to ridge crest

Site	Concern	Suggested move/Recommendation
17A	Shallow saddle	We recommend avoiding this site
17B	Edge of ravine; low on slope	Move north to ridge crest
18	Long E-W ridge	Best option on this ridge
18A	Long E-W ridge	Use site 18
18B	Long E-W ridge	Use site 18
19	Conflicts with model prediction	Might be safer 30 m south
19A	Conflicts with model prediction	Use either site 19 or 19B
19B	W side of long E-W concave slope	Safest local option except for burrowing owls
20	Near saddle/bench; Conflicts with model prediction	move N to crest
20A	Ravine	We recommend avoiding this site
20B	Very narrow E-W ridge	Relatively unsafe for eagles
21	Below & downwind of ridge crest	We recommend avoiding this site
21A	None	Safest place in area
21B	In small ravine	Use site 21A
22	Edge of canyon	Move N away from canyon edge or use 22A
22A	Edge of deep ravine	Move N away from edge of deep ravine
22B	Declining E-W ridge next to canyon; conflicts with model prediction	Use modified site 22A
23	E-W ridge into deep canyon	No safer local option
24	E-W ridge	No safer local option
25	On knoll lower than surrounding ridges; surrounded by valleys	No solution here; We recommend avoiding this site
26	In shallow trough/saddle	Move SW to crest or south to higher ground
27	No model; In saddle (also on pipeline)	Move north to hill peak
28	No model; Break in slope near saddle (also on pipeline)	Move north to hill peak
29	No model; Low near valley	Move east to high ground
30	No model; Trough to E; edge of deep ravine to S	No better local options
31	No model; Pad grading will leave upwind berm	Avoid berm by moving west
32	None but no model	Safest place in area
33	None but no model	Safest place in area
34	No model; Saddle with concave slopes to NE, SW – crossover point	We recommend avoiding this site

Site	Concern	Suggested move/Recommendation
35	None but no model	Safest place in area
36	Edge of canyon	Move NNW away from canyon edge
37	Complex saddle; known crossing point; conflicts with model prediction	Move west to higher ground
38	None	Safest place in area
39	None	Safest place in area
40	Known crossing point on descending ridge	No local option to recommend

ACKOWLEDGEMENTS

We thank S-Power for the opportunity to develop map-based wind turbine micro-siting recommendations. We also thank East Bay Regional Park District, California Energy Commission's Public Interest Energy Research program, NextEra Renewables, Ogin Inc. and EDF Renewables for earlier funding of research that prepared us for this project. We thank Mulqueeny Ranch, Leeward Renewable Energy LLC, Salka Energy, NextEra Renewables and others for property access. Directed behavior surveys were performed since 2012 by K. S. Smallwood, H. Wilson, E. Walther, B. Karas, J. Mount, S. Standish, and E. Leyvas, and breeding season burrowing owl surveys by K. S. Smallwood and Noriko Smallwood. We thank D. Funderburg, S. Michehl, Leah Neher, and S. Neher for digitizing bird locations from hard-copy maps. We thank D. Bell for use of GPS/GSM telemetry data of golden eagles.

REFERENCES CITED

Alameda County SRC (Smallwood, K. S., S. Orloff, J. Estep, J. Burger, and J. Yee). December 11, 2007. SRC selection of dangerous wind turbines. Alameda County SRC document P-67. 8 pp.

Alameda County SRC (Smallwood, K. S., S. Orloff, J. Estep, J. Burger, and J. Yee). 2010. Guidelines for siting wind turbines recommended for relocation to minimize potential collision-related mortality of four focal raptor species in the Altamont Pass Wind Resource Area. Alameda County SRC document P-70.

Bell, D. A. and C. Nowell. 2015. GPS Satellite Tracking of Golden Eagles (*Aquila chrysaetos*) in the Altamont Pass Wind Resource Area (APWRA) and the Diablo Range. Main Report-Active Birds for the Quarters ending in March and June 2015. Report to Parties to Repowering Agreement with California Attorney General, Oakland, California.

Brown, K., K. S. Smallwood, J. Szewczak, and B. Karas. 2016. Final 2012-2015 Annual Report Avian and Bat Monitoring Project Vasco Winds, LLC. Prepared for NextEra Energy Resources, Livermore, California.

Brown, K., K. S. Smallwood, J. Szewczak, and B. Karas. 2014. Final 2013-2014 Annual Report Avian and Bat Monitoring Project Vasco Winds, LLC. Prepared for NextEra Energy Resources, Livermore, California.

Brown, K., K. S. Smallwood, and B. Karas. 2013. Final 2012-2013 Annual Report Avian and Bat Monitoring Project Vasco Winds, LLC. Prepared for NextEra Energy Resources, Livermore, California.
http://www.altamontsrc.org/alt_doc/p274_ventus_vasco_winds_2012_ 13_avian_ bat_monitoring_report_year_1.pdf

ICF International. 2011. Altamont Pass Wind Resource Area Bird Fatality Study, Bird Years 2005–2009. Report # ICF 00904.08, to Alameda County Community Development Agency, Hayward, California.

http://www.altamontsrc.org/alt_doc/m73_altamont_pass_wind_resource_area_bird_fatality_study_bird_years_2005_2009.pdf

ICF International. 2016. Final Report Altamont Pass Wind Resource Area bird fatality study, monitoring years 2005–2013. Report to Alameda County Community Development Agency, Hayward, California.

Insignia Environmental. 2011. Draft Final Report for the Buena Vista Avian and Bat Monitoring Project. Report to County of Contra Costa, Martinez, California.

Orloff, S., and A. Flannery. 1992. Wind turbine effects on avian activity, habitat use, and mortality in Altamont Pass and Solano County Wind Resource Areas: 1989-1991. Report to California Energy Commission, Sacramento, California.

Smallwood, K. S. 2010a. Inter-turbine Comparisons of Fatality Rates in the Altamont Pass Wind Resource Area. http://www.altamontsrc.org/alt_doc/p189_smallwood_report_of_apwra_fatality_rate_patterns.pdf

Smallwood, S. 2010b. Old-generation wind turbines rated for raptor collision hazard by Alameda County Scientific Review Committee in 2010, an Update on those Rated in 2007, and an Update on Tier Rankings. http://www.altamontsrc.org/alt_doc/p155_smallwood_src_turbine_ratings_and_status.pdf

Smallwood, K. S. 2013. Comparing bird and bat fatality-rate estimates among North American wind-energy projects. Wildlife Society Bulletin 37: 19-33.

Smallwood, K. S. 2016a. Bird and bat impacts and behaviors at old wind turbines at Forebay, Altamont Pass Wind Resource Area. Report CEC-500-2016-066, California Energy Commission Public Interest Energy Research program, Sacramento, California. http://www.energy.ca.gov/2016publications/CEC-500-2016-066/CEC-500-2016-066.pdf

Smallwood, K. S. 2016b. Report of Altamont Pass research as Vasco Winds mitigation. Report to NextEra Energy Resources, Inc., Office of the California Attorney General, Audubon Society, East Bay Regional Park District.

Smallwood, K. S. 2017a. The challenges of addressing wildlife impacts when repowering wind energy projects. Pages 175-187 in Köppel, J., Editor, Wind Energy and Wildlife Impacts: Proceedings from the CWW2015 Conference. Springer. Cham, Switzerland.

Smallwood, K. S. 2017b. Monitoring birds. M. Perrow, Ed., Wildlife and Wind Farms - Conflicts and Solutions, Volume 2. Pelagic Publishing, Exeter, United Kingdom. www.bit.ly/2v3cR9Q

Smallwood, K. S. 2017c. Long search intervals under-estimate bird and bat fatalities caused by wind turbines. Wildlife Society Bulletin 41:224-230.

Smallwood, K. S. 2018. Addendum to Comparison of Wind Turbine Collision Hazard Model Performance: One-year Post-construction Assessment of Golden Eagle Fatalities at Golden Hills. Report to Audubon Society, NextEra Energy, and the California Attorney General.

Smallwood, K. S. and J. Estep. 2010. Report of additional wind turbine hazard ratings in the Altamont Pass Wind Resource Area by Two Members of the Alameda County Scientific Review Committee. http://www.altamontsrc.org/alt_doc/p153_smallwood_estep_additional_hazard_ratings.pdf

Smallwood, K. S. and B. Karas. 2009. Avian and Bat Fatality Rates at Old-Generation and Repowered Wind Turbines in California. Journal of Wildlife Management 73:1062-1071.

Smallwood, K. S. and L. Neher. 2010a. Siting Repowered Wind Turbines to Minimize Raptor Collisions at the Tres Vaqueros Wind Project, Contra Costa County, California. Draft Report to the East Bay Regional Park District, Oakland, California.

Smallwood, K. S. and L. Neher. 2010b. Siting Repowered Wind Turbines to Minimize Raptor Collisions at Vasco Winds. Unpublished report to NextEra Energy Resources, LLC, Livermore, California.

Smallwood, K. S., and L. Neher. 2016. Siting Wind Turbines to Minimize Raptor collisions at Sand Hill Repowering Project, Altamont Pass Wind Resource Area. Report to Ogin, Inc., Waltham, Massachusetts.

Smallwood, K. S., and L. Neher. 2017a. Comparing bird and bat use data for siting new wind power generation. Report CEC-500-2017-019, California Energy Commission Public Interest Energy Research program, Sacramento, California. http://www.energy.ca.gov/2017publications/CEC-500-2017-019/CEC-500-2017-019.pdf and http://www.energy.ca.gov/ 2017publications/CEC-500-2017-019/CEC-500-2017-019-APA-F.pdf

Smallwood, K. S., and L. Neher. 2017b. Comparison of wind turbine collision hazard model performance prepared for repowering projects in the Altamont Pass Wind Resources Area. Report to NextEra Energy Resources, Inc., Office of the California Attorney General, Audubon Society, East Bay Regional Park District.

Smallwood, K. S. and C. Thelander. 2004. Developing methods to reduce bird mortality in the Altamont Pass Wind Resource Area. Final Report to the California Energy Commission, Public Interest Energy Research – Environmental Area, Contract No. 500-01-019. Sacramento, California.

Smallwood, K. S. and C. Thelander. 2005. Bird mortality in the Altamont Pass Wind Resource Area, March 1998 – September 2001 Final Report. National Renewable Energy Laboratory, NREL/SR-500-36973. Golden, Colorado.

Smallwood, K. S., C. G. Thelander. 2008. Bird Mortality in the Altamont Pass Wind Resource Area, California. Journal of Wildlife Management 72:215-223.

Smallwood, K. S., L. Neher, and D. A. Bell. 2009. Map-based repowering and reorganization of a wind resource area to minimize burrowing owl and other bird fatalities. Energies 2009(2):915-943. http://www.mdpi.com/1996-1073/2/4/915

Smallwood, K. S., L. Neher, and D. A. Bell. 2017a. Mitigating golden eagle impacts from repowering Altamont Pass Wind Resource Area and expanding Los Vaqueros Reservoir. Report to East Contra Costa County Habitat Conservation Plan Conservancy and Contra Costa Water District.

Smallwood, K.S., L. Neher, and D.A. Bell. 2017b. Siting to Minimize Raptor Collisions: an example from the Repowering Altamont Pass Wind Resource Area. M. Perrow, Ed., Wildlife and Wind Farms - Conflicts and Solutions, Volume 2. Pelagic Publishing, Exeter, United Kingdom. www.bit.ly/2v3cR9Q

Smallwood, K. S., L. Rugge, and M. L. Morrison. 2009b. Influence of Behavior on Bird Mortality in Wind Energy Developments: The Altamont Pass Wind Resource Area, California. Journal of Wildlife Management 73:1082-1098.

Smallwood, K. S., L. Neher, J. Mount, and R. C. E. Culver. 2013. Nesting burrowing owl abundance in the Altamont Pass Wind Resource Area, California. Wildlife Society Bulletin: 37:787-795.

Smallwood, K. S., L. Neher, D. Bell, J. DiDonato, B. Karas, S. Snyder, and S. Lopez. 2009c. Range Management Practices to Reduce Wind Turbine Impacts on Burrowing Owls and Other Raptors in the Altamont Pass Wind Resource Area, California. Final Report to the California Energy Commission, Public Interest Energy Research – Environmental Area, Contract No. CEC-500-2008-080. Sacramento, California. 183 pp. http://www.energy.ca.gov/ 2008publications/CEC-500-2008-080/CEC-500-2008-080.PDF

Tanaka, K. 1997. An Introduction to Fuzzy Logic for Practical Applications. Springer-Verlag, New York.